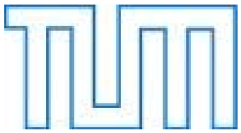

Wissenschaftszentrum Weihenstephan für Ernährung, Landnutzung und Umwelt

Lehrstuhl für Waldwachstumskunde

Laboratoire de Mathématiques et Informatique pour la Complexité et les Systèmes

Digiplante

Spatial Leaf Density-based Modelling of Teleonomic Crown Dynamics of Crops and Trees

Robert Maria Beyer

Vollständiger Abdruck der vom Wissenschaftszentrum für Ernährung, Landnutzung und Umwelt der Technischen Universität München zur Erlangung des akademischen Grades eines

Doktors der Naturwissenschaften (Dr. rer. nat.)

genehmigten Dissertation.

Vorsitzender:	Priv.-Doz. Dr. Thomas Rötzer
Prüfende:	1. Prof. Dr. Dr. h.c. Hans Pretzsch
	2. Prof. Dr. Anja Rammig
	3. Prof. Dr. Paul-Henry Cournède, *CentraleSupélec*
	4. Prof. Dr. Youcef Mammeri, *Université de Picardie*

Die Dissertation wurde am 26. Oktober 2015 bei der Technischen Universität München eingereicht und durch das Wissenschaftszentrum für Ernährung, Landnutzung und Umwelt am 7. Juni 2016 angenommen.

The kingdom of God is as if a man should scatter seed on the ground. He sleeps and rises night and day, and the seed sprouts and grows; he knows not how.

Mark 4:26-27

CONTENTS

ABSTRACT / ZUSAMMENFASSUNG

Functional-structural plant growth models (FSPMs) have emerged as the synthesis of mechanistic process-based models, and geometry-focussed architectural models. In terms of spatial scale, these models can essentially be divided into small-scale models featuring a topological architecture – often facing data-demanding parametrisations, parameter sensitivity, as well as computational heaviness, which imposes problematic limits to the age and size of in dividuals than can be simulated – and large-scale models based on a description of crown shape in terms of rigid structures such as empirical crown envelopes – commonly struggling to allow for spatial variability and plasticity in crown structure and shape in response to local biotic or abiotic growth conditions.

In response to these limitations, and motivated not least by the success-story of spatial density approaches in theoretical populations ecology, the spatial distribution of foliage in plants in this thesis is characterised in terms of spatial leaf density, which allows for a completely local description that is a priori unrestricted in terms of plasticity, while being robust and computationally efficient. The thesis presents dynamic growth models specifically developed for crops and trees, exploring different mathematical frameworks in continous and discrete time, while critically discussing their conceptual suitability and exploring analytical simplifications and solutions to accelerate simulations.

The law of Beer-Lambert on the passing of light though an absorbing medium allows to infer the local light conditions based on which local biomass production can be computed via a radiation use efficiency. A key unifying mechanism of the different models is the local expansion of leaf density in the direction of the light gradient, which coincides with the direction most promising with regard to future biomass productivity. This aspect falls into the line of teleonomic and optimization-oriented plant growth models, and allows to set aside the otherwise complex modelling of branching processes. The principle induces an expansive horizontal and upward-directed motion of foliage. Moreover, it mechanistically accounts for a slow-down of the horizontal expansion as soon as a neighbouring competitor's crown is reached, since the appropriate region is already shaded, implying a corresponding adaptation of the light gradient. This automatically results in narrower crowns in scenarios of increased competition, ultimately decreasing biomass production and future growth due to lesser amount of intercepted light. In an extension, the impact of water availability is incorporated into the previously light-only dependency

of biomass production by means of a novel hydraulic model describing the mechanistic balancing of leaf water potential and transpiration in the context of stomatal control. The allocation of produced biomass to other plant compartments such as roots and above-ground wood, e.g. by means of the pipe model theory, is readily coupled to leaf density dynamics.

Simulation results are compared against a variety of empirical observations, ranging from long-term forest inventory data to laser-recorded spatial data, covering multiple abiotic environmental conditions and growth resources as well as stand densities and thus degrees of competition. The models generate a series of complex emergent properties including the realistic prediction of biometric growth parameters, the spontaneous adaptability and plasticity of crown morphologies in different competitive scenarios, the empirically documented insensitivity of height to stand density, the accurate deceleration of height growth, as well as popular allometric relationships – altogether demonstrating the potential of leaf density based approaches for efficient and robust plant growth modelling.

Funktionell-strukturelle Pflanzenmodelle vereinen die Wachstumsmechanismen prozeßbasierter Modelle mit der Geometrie architektonischer Modelle. Solche Modelle laßen sich im Wesentlichen unterteilen in kleinmaßstäbliche Modelle mit topologischer Architektur – die häufig datenintensive Parameterisierungen, Parametersensitivität sowie hohe Rechenintensität mit sich ziehen – und großmaßstäbliche Modelle, die auf einer Beschreibung der Kronenform mittels rigider Strukturen wie etwa empirischen Kronenhüllen basieren – und der räumlichen Variabilität und Plastizität der Kronenstruktur und -form gegenüber lokaler biotischer oder abiotischer Faktoren bisweilen nur schwer Rechnung tragen können.

Vor diesem Hintergrund, und nicht zuletzt motiviert durch den Erfolg räumlicher Dichtemodelle in dertheoretischen Ökologie, wird die räumliche Verteilung des Pflanzenblattwerks in dieser Arbeit mittels der räumlichen Blätterdichte charakterisiert, die eine vollständig lokale Beschreibung ohne a priori Plastizitätseinschränkungen ermöglicht und zugleich robust und recheneffizient ist. Die Dissertation stellt dynamische Wachstumsmodelle für Feldfrüchte und Bäume vor, untersucht verschiedene mathematische Ansätze in stetiger und diskreter Zeit, diskutiert kritisch deren konzeptuelle Eigung und erkundet analytische Vereinfachungen und Lösungen um Simulationen zu beschleunigen.

Das Lambert-Beer'sche Gesetz über den Durchgang von Licht durch ein absorbierendes Medium erlaubt die Bestimmung lokaler Lichtbedingungen innerhalb der Krone, auf Basis derer die lokale Biomaßenproduktion berechnet wird. Ein zentraler Mechanismus der ver-

schiedenen vorgestellten Modelle ist die lokale Ausbreitung der Blätterdichte in Richtung des Lichtgradienten, welcher mit der hinsichtlich zukünftiger Biomaßenproduktivität aussichtsreichsten Richtung zusammenfällt. Diese Komponente orientiert sich an teleonomischen und optimalen Pflanzenwachstumsmodellen, und ermöglicht die ansonsten komplexe Modellierung von Verzweigungsprozeßen außer Betracht zu laßen. Der Ansatz induziert eine horizontale sowie aufwärtsgerichtete Ausbreitungsbewegung des Blattwerks. Darüber hinaus bedingt er mechanistisch eine Verlangsamung der horizontalen Ausbreitung sobald die Krone eines benachbarten Konkurrenten erreicht wird, da der entsprechende Bereich bereits beschattet ist und sich der lokale Lichtgradient entsprechend ändert. Dies führt automatisch zu schmaleren Kronen im Falle erhöhten Wettbewerbs, und damit schlußendlich zu verringerter Biomaßenproduktion und zuzünftigem Wachstum aufgrund verringerter Lichtabsorption. In einem zusätzlichen Schritt wird der Einfluß von Wasserverfügbarkeit der bisher betrachteten Lichtabhängigkeit der Biomaßenproduktion mittels eines neu entwickelten hydraulischen Modells, das im Kontext stomataler Kontrolle das mechanistische Gleichgewicht von Wasserpotential und Transpiration bestimmt, hinzugefügt. Die Allokation produzierter Biomaße zu weiteren Pflanzenkompartimenten wie Wurzeln und oberirdischem Holz, etwa mittels der "Pipe Model Theory" kann ohne Weiteres in die Blätterdichtedynamik eingebettet werden.

Die Modellsimulationen werden mit einer Reihe empirischer Beobachtungen verglichen, die von langfristigen Forstinventurdaten bis hin zu lasererfassten räumlichen Daten reichen, und vielfältige abiotische Umweltbedingungen und Wachstumsfaktoren sowie Bestandesdichten und folglich Wettbewerbsgrade abdecken. Die Modelle generieren zahlreiche komplexe emergente Eigenschaften, zu denen die realistische Vorhersage biometrischer Wachstumsparameter, die spontane Anpassungsfähigkeit und Plastizität der Kronenmorphologien in verschiedenen Wettbewerbsszenarien, die empirisch beschriebene Unempfindlichkeit der Baumhöhe gegenüber der Bestandesdichte, die korrekte Verlangsamung des Höhenwachstums sowie die Übereinstimmung mit allometrischen Gesetze gehören – und so insgesamt das Potential blätterdichtebasierter Modelle zur effizienten und robusten Pflanzenwachstumsmodellierung verdeutlichen.

NOTATION

Mathematical notation

$\mathbb{R}_+$ non-negative real numbers $\{x \in \mathbb{R} : x \geq 0\}$

S^2_+ upper half of the unit sphere $\{x \in \mathbb{R}^2 \times \mathbb{R}_+ : \|x\| = 1\}$

∇_x Nabla operator $\left(\frac{\partial}{\partial x_1}, \frac{\partial}{\partial x_2}\right)$ or $\left(\frac{\partial}{\partial x_1}, \frac{\partial}{\partial x_2}, \frac{\partial}{\partial x_3}\right)$ (depending on whether $x \in \mathbb{R}^2$ or $x \in \mathbb{R}^3$)

$\|x\|$ Euclidean norm $\sqrt{x_1^2 + x_2^2}$ or $\sqrt{x_1^2 + x_2^2 + x_3^2}$ (depending on whether $x \in \mathbb{R}^2$ or $x \in \mathbb{R}^3$)

$\delta_a(x)$ Dirac delta distribution centred in a

Model variables and parameters

$\clubsuit(x)$ spatial density of leaf area in $x \in \mathbb{R}^3$ [$m^2\,m^{-3}$] (static or at time $t \in \mathbb{R}_+$ or in year $n \in \mathbb{N}_0$, depending on context)

$\spadesuit(x)$ spatial density of horizontal leaf area in $x \in \mathbb{R}^2$ [$m^2\,m^{-2}$] (static or at time $t \in \mathbb{R}_+$, depending on context)

$\|x\|_Y$ distance from roots to foliage in $x \in \mathbb{R}^3$ along the branch network [m]

SLA specific leaf area [$m^2\,g^{-1}$]

SWV specific wood volume [$m^3\,g^{-1}$]

PAR photosynthetically active radiation [J $time^{-1}$] (at time $t \in \mathbb{R}_+$ or over year $n \in \mathbb{N}$, depending on context)

RUE radiation use efficiency [$g\,J^{-1}$]

P pipe model theory parameter [m^{-1}]

PREFACE

Half a billion years after their first appearance, land plants have penetrated into almost every spot of the continents, permeating and enabling past and present terrestrial biological diversity of inestimable value. Their ecosystem services to humans include oxygen, food, remedies, material, energy as well as social and aesthetic aspects. Inseparably tied to their abiotic environment, plants reduce erosion and mass movements, remove aerosols, affect the water cycle and regulate local up to global atmospheric dynamics. In a global carbon cycle that is increasingly affected by anthropogenic activity, their role as sinks, by assimilating atmospheric carbon through photosynthesis, and as sources through respiration, decomposition or burning, is well recognized (IPCC, 2000). The unprecedentedness of anticipated or suspected climatic change, such as higher temperature and photosynthetically active radiation as well as decreased precipitation (IPCC, 2007), and their uncertain impact on and interaction with the global vegetation stress the need for models allowing reliable predictions today, in order to ensure the own sustainability as well as continued efficient provision of ecosystem services of the plant kingdom.

Quantitative plant models, both for such practical use and decision support, but likewise for the less application-oriented purpose of advancing botanical knowledge for its own sake, are written in the language of mathematics. Mathematical formalism allows to bridge the gap from an initial biological hypothesis to its validation or falsification in comparison to real data – a continual interaction that ultimately culminates in scientific progress (Thornley and Johnson, 2000). Plant modelling has largely benefited from the development of sophisticated mathematical concepts and methods that allowed the concise, efficient and elegant formulation of biological processes or phenomena as well as their implementation for computational processing.

This thesis aims at contributing to the field of mathematical plant modelling by introducing and applying new methodology. This includes the novel characterisation of the spatial distribution of leaves in terms of spatial densities. The success story of density-based models in theoretical population ecology encourages to apply the fundamental idea to the description of foliage in an attempt to overcome challenges currently faced by prevailing concepts. Indeed, the realistic yet efficient representation of plant architecture is an important open question reaching from the scale of a single large tree to that of global vegetation models. We believe that density approaches can give new impetus in this matter. Models in this thesis are largely based on the concept of teleonomy, i.e. a supposed goal-directedness of growth processes, and

its application to spatial dynamics. Teleonomic modelling has proven realistic and efficient across many scales, from organ to ecosystem level. Yet, applications in conjunction with spatial dynamics are still scarce, a gap this thesis attempts to contribute to fill. In combination, these two approaches are used to model the spatial dynamics of crown development in crops and trees, with a particular focus on the local plastic response to light resources as well as competition for these, which poses a current major challenge for functional-structural plant models.

Considering spatial foliage density in plant growth models implies the inevitable sacrifice of topological structure, i.e. information on the network of branches, which limits the number of physiological functions, especially small-scale transport processes that can be accounted for mechanistically. This as well as the density scale in general suggest the framework to be used in models focussing rather on the macroscopic (but nonetheless local) tendencies of crown dynamics, and make simplifications appropriate to this objective. Throughout this thesis, these serve the purpose of keeping the number of model parameters small without forfeiting the key dynamical mechanisms. We thus aim at identifying a concise, simple and effective as possible set of mechanisms required to realistically capture complex spatial effects of plant growth over time.

THESIS OUTLINE

In part I of this thesis, we develop and contextualise the conceptual and methodological bases later used in the models presented in part I. Chapter 1 revisits types of plant growth models with a special focus on functional-structural models, in which physiological functioning is coupled with a spatial structure, and discusses their contribution as well as current challenges. Current ways to characterize the distribution of foliage in spatially explicit models are subsequently critically reviewed, seamlessly followed on by the introduction and discussion of spatial density-based characterizations of foliage in chapter 2. Based on this, chapter 3 presents a series of general principles and modelling techniques used throughout the subsequent modelling part II.

In chapter 4, we present a two-dimensional time-continuous continuity equation model for the foliation and growth dynamics of crops. A rigorous mathematical analysis of the model equations allows a significantly simpler expression of the solution as well as faster simulations. The model is tested against empirical data from sugar beet. As a transition from this two-dimensional , continuous-time setting to the later, extensively studied three-dimensional, discrete-time approach for trees, chapter 5 explores the suitability of a continuity equation framework for the modelling of tree crown dynamics in three dimensions over several growth cycles. We discuss conceptual difficulties

of this approach as well as two propositions to partially circumvent them. A focal point of this thesis in the form of a time-discrete model, describing the evolution of leaf density from one year to the next, is presented in chapter 6. Simulation results are compared against various types of empirical observations for European beech, reaching from long-term forest inventory data to Lidar-recorded spatial data. The model generates a series of remarkable emergent properties, and motivates hypotheses on the morphological crown dynamics of beech. In addition to the previous light-only dependence of local biomass production, the impact of soil water availability is incorporated into the latter growth model by means of a novel hydraulic model describing the mechanistic balancing of leaf water potential and transpiration, followed by a comparison of simulation results to an extensive long-term empirical data set. Chapter 7 supplements the previous tree models in that it presents a method to assign a realistic possible branch system to a given leaf distribution. Chapter 8 concludes and discusses future perspectives.

Part I.

Preliminaries

1

PRINCIPLES OF SPATIAL PLANT MODELLING

In the first section 1.1 of this introductory chapter, we revisit different categories of present-day approaches in plant modelling, in particular classified into empirical, process-based, architectural and functional-structural models, with an additional reference to teleonomic models. This is followed by a critical review of current ways of representing plant architecture in these models in section 1.2, motivating the introduction and application of spatial density-based characterisations of foliage in the subsequent chapter 2.

1.1 TYPES OF PLANT GROWTH MODELS

1.1.1 *Empirical models*

Empirical models describe plant behaviour directly by fitting a particular type of equation or system thereof to an empirically acquired data set. They do not account for physical laws, biological information such as physiological processes involved in growth and morphogenesis, or knowledge of the structure of the system (Thornley and Johnson, 2000). Empirical models summarize real data; predictions are made by means of interpolation or regression. Without the need for either mechanistic or teleonomic hypotheses (cf. section 1.1.5), empirical relationships are relatively simple to establish and can make robust and reliable predictions as long as anticipated growth conditions are within the scope of preceding observations. They reach their boundaries when the latter condition is no longer satisfied, i.e. when being confronted to stand structures, species distributions or site conditions beyond the range on which they were calibrated (Lacointe, 2000). This shortcoming is of particular concern in light of climatic change, and has contributed to the development of process-based models, which attempt to capture plant dynamics mechanistically.

1.1.2 *Process-based models*

Classical process-based models (see Landsberg, 1986, for an overview of the basic properties) characterize plants in terms of compartments such as foliage, shoots and roots, and express these and related variables in terms of total quantities such as weight, surface area per unit

soil surface or nitrogen content (Vos et al., 2007). The set of organs of a particular type is simplified to an average organ that represents functional traits without individual, let alone spatial differentiation. The leaf area index (cf. section 2.3.2) is the classical variable used to characterize foliage and compute light interception in process-based models, mostly using Beer-Lambert's law and appropriate extinction coefficients (e.g. Baldocchi et al., 2000; Lai et al., 2000). Global values for photosynthesis, respiration and resource allocation, possibly coupled to nutrient and water cycles, determine a plant's carbon balance and growth (Sievänen et al., 2000).

The idea of unveiling causal relationships both within a plant and with its environment predestines process-based models for the prediction of unprecedented environmental conditions (Bossel, 1996), for instance with regard to altered water and nutrient availability, temperature, polluants, herbivores or human intervention (Le Roux et al., 2001).

The leaf area index does not capture canopy structure and heterogeneity which however strongly affects light interception and thus photosynthesis (Vos et al., 2010). Likewise, the distribution of carbon between productive and non-productive tissues (Givnish, 1988; Nikinmaa, 1992; Le Roux et al., 2001) and gas-exchange properties of foliage (Landsberg and Gower, 1997) depend highly on the spatial structure of the tree (Sievänen et al., 2000). Modelling inner-plant water and nutrient transport processes (Perttunen et al., 1996) as well as plant-environment interactions such as radiation transfer and local light interception (Sarlikioti et al., 2011), requires a realistic 3D characterisation of the plant's structure. The relationship is bilateral since the plant's structural development depends on the local physiological processes (Sievänen et al., 2000).

Additional problems in which explicit information about the spatial structure of a plant is important, include competition phenomena within and between species, tree-herbivory interactions, the optimisation of spatial structure in production systems (e.g. through pruning), the exploration of hypotheses involving a strong interaction of structure and physiology as well as the visualisation of growth processes, e.g. for teaching purposes (Sievänen et al., 2000; Vos et al., 2007).

1.1.3 *Architectural models*

Parallel to and for a long time independent from process-based models, the development of architectural models, also named morphological, structural or geometric growth models, took place. Originally, these aimed merely at the dynamic description of plant structure in terms of positions, orientations and shapes of plant organs. Plants are described as closed cybernetic systems with an autonomous development, and interactions with their environment are not taken into

account (Vos et al., 2007). The work of Honda (1971) and follow-up models represent this approach. Most notable is the work of Lindenmayer (1968a,b) that gave rise to the long-lasting formalism of L-systems (Prusinkiewicz and Lindenmayer, 1990), a parallel rewriting system and formal grammar that exploits the modularity of plants, i.e. their composition of repetitive units (de Reffye et al., 1988; Room et al., 1994).

1.1.4 *Functional-structural models*

Kurth (1994) addressed the hitherto scarce integration of physiological processes into the dynamics of architectural models, or inversely, the extension of process-based models by their architectural counterparts. Implementing this combination, Sorrensen-Cothern et al. (1993), Perttunen et al. (1996), Kurth (1996) and de Reffye et al. (1997) were among the first to inaugurate the era of functional-structural models (Sievänen et al., 2000; Godin and Sinoquet, 2005; Vos et al., 2007; Hanan and Prusinkiewicz, 2008; Sievanen et al., 2014). This approach is exemplified by the extension of the originally purely architectural L-systems by physiological components, resulting in context sensitive, parametric or open L-systems, in which rewriting rules are affected by the local environments of plant modules (Prusinkiewicz and Lindenmayer, 1990; Mech and Prusinkiewicz, 1996; Kurth and Sloboda, 1997) or the interactions between the latter (e.g. Mathieu et al., 2008, 2009). Functional-structural models thus focus on the inseparable feedback between structure and function (Vos et al., 2010): Structure affects function in that for instance it defines local light conditions that affect photosynthesis, while structural developments, such as bud breaking and shoot proliferation, are themselves simultaneously controlled by function.

The definition of functional-structural models is often based on the notion of elementary units or modules, which constitute plants in terms of a collective and interconnected network (Sievänen et al., 2000; Barthélémy and Caraglio, 2007; Sievanen et al., 2014). This unit is commonly a metamer, i.e. a single internode possibly bearing axillary buds or leaves at its tip. This characterisation of the plant contains a geometrical and a topological component: The former identifies the locations of plant parts in 3D space, which is particularly useful to model interactions with the environment, while the latter addresses the physical connections between these plant parts, which is used to model the inner-plant transport processes (Le Roux et al., 2001; Godin and Sinoquet, 2005).

In spite of these arguments in favour of an explicit 3D geometrical-topological structure, it is not without reason that empirical and process-based models are still the standard tool for plant modelling

at the community level and beyond (Le Roux et al., 2001). Firstly, the parametrisation of functional-structural models can be very data demanding (Sievänen et al., 2000; Letort et al., 2008). The spatial roughness of process-based models is accompanied by an aggregation and averaging of several parameters which in functional-structural models are by construction non-constant (e.g. Dauzat, 1993). A high sensitivity of its parameters challenges a model's robustness and makes it susceptible to serious error propagation. Secondly, the level of detail and potentially large number of elementary units of most functional-structural plant models can be challenging in terms of the computational performance of simulations. Indeed, this has led some tree growth models to artificially limit the number of potential modules (e.g. 5000 in the model by Sterck and Schieving (2007) and 10000 in the LIGNUM model (Sievänen et al., 2000)), which imposes problematic limits to the age and size of individuals than can be simulated. In particular, Sievänen et al. (2000) ascribed computational heaviness to a potential pairwise comparison of individual modules, e.g. in a source-sink allocation model as well as to problems of scale, e.g. computing leaf-specific hourly photosynthesis throughout years. Cescatti (1997) adds the high computational demand due to the complex simulation of radiative transfer to this list. The method of structural factorisation developed by Cournède et al. (2006) reduces computational time significantly by utilising the repetitiveness of patterns generated by L-systems. However, specifically designed for models with merely a topological and without a geometrical structure, applying it to the general spatial case with locally varying environmental conditions such as light incidence is not straightforward.

Sievänen et al. (2000) concluded a fundamental impossibility of simulating deliberately large trees using topological functional-structural models – which curiously stands in direct contradiction to the very requirement for the elementary unit in these models, namely being "small enough to allow its micro environment to be treated as spatially homogeneous, but [...] large enough to ensure that the number of units does not become prohibitively large when simulating big trees" (Sievänen et al., 2000) (a definition that, moreover, cell biologists might not unduly challenge as being arbitrary).

The increase in computational power over the past one and a half decades has not been able to fundamentally change this situation. For instance, pairwise comparison of n modules requires $\mathcal{O}(n^2)$ operations, illustrating that the computational demand of simulations of old trees with a number of metamers exceeding the above-mentioned limits by about two orders of magnitude is out of proportion to the increase in computational power ever since. It is thus not surprising that present-day topological tree growth models still focus on the simulation of young individuals, rarely exceeding the sapling stage (Sievänen et al., 2008; Hemmerling et al., 2008; Lu et al., 2011; Wang

et al., 2012; Lintunen et al., 2012; Nikinmaa et al., 2014; Gao et al., 2014).

1.1.5 *Teleonomic models*

Thornley and Johnson (2000) considered the concept of hierarchies of organisation levels in plants, given, for example, by biosphere > ecosystem > stand > plant > organ > tissue > cell. In this terminology, empirical models, which do not address lower level causal mechanisms nor interpret a fitted relationship in the framework of higher-level purpose, describe the behaviour of one hierarchical level merely in terms of attributes of that particular level. In contrast, mechanistic models, i.e. process-based and functional-structural models in the previous terminology, try to explain processes at a given hierarchical level by understanding the behaviour of lower levels: A system is reductionistically broken down into its components, studied and reintegrated to explain responses at the higher level. Lastly, teleonomic models attempt to understand behaviour at lower levels by considering constraints or requirements at a higher level. In an evolutionary context, the latter may refer to the maximisation of growth rate. Dewar (2010) provided a discussion of similar and alternative objectives. Such an apparent goal or purpose (cf. Monod, 1972) then determines the behaviour at the lower levels that is needed to attain it. As an example from phyllotaxis, the successive leaves along a plant stem often draw the golden angle. Instead of attempting to reproduce the complex biophysical and biochemical mechanisms at the microscale, teleonomic models assuming the maximisation of light interception (Leigh, 1972) or, alternatively, the optimal packing density (Ridley, 1982) as higher goals, which lower level mechanisms supposedly work towards, have been proposed, and managed indeed to explain the observed pattern.

A priori, teleonomic approaches can be used at any level of detail, in spatially explicit just as well as in compartmental models. Fisher (1992) and Farnsworth and Niklas (1995) revisited architectural models in the context of optimizing light interception, while Mäkelä et al. (2002) provided a review of functional teleonomic and optimisation models at the plant level. Canell and Dewar (1994) and Le Roux et al. (2001) addressed teleonomy in the context of carbon allocation models. Strigul et al. (2008) and Dewar et al. (2008) made teleonomic assumptions for structure and function, respectively, at the landscape scale and beyond. Miscellaneous recent approaches in the field were summarised by McMurtrie and Dewar (2013).

1.2 REPRESENTATION OF FOLIAGE IN SPATIAL PLANT MODELS

As integral as controversial to plant modelling is the choice of the appropriate level of model detail and complexity, and the decision as to which processes are necessary to consider explicitly and which can be simplified in consideration of realism, clarity, robustness, computational efficiency and even theoretical analysability. Not surprisingly, scientific debate on the legitimacy of assumptions and simplifications is a constant companion in the field of plant modelling (e.g. Thornley and Johnson, 2000; Bugmann, 2001; Sievanen et al., 2014, and references therein). In this section we review different ways to characterize the shape and structure of plant crowns as well as the spatial distribution of foliage in order of detail and complexity. We follow the categorisation of representation of plant architecture in terms of global, spatial, geometric and topological information suggested by Godin (2000) and complete it with model examples.

1.2.1 *Global representations*

A global representation refers to the crown being described only in terms of an enveloping surface. These reach from simple forms such as (truncated) spheres, ellipses, cylinders, cones and paraboloids to more complex asymmetric and composite surface parametrisations (see references in Sinoquet and Andrieu, 1993; Cescatti, 1997; Godin and Sinoquet, 2005). Leaf distribution is commonly assumed homogeneous within a crown envelope (but see section 2.1.1).

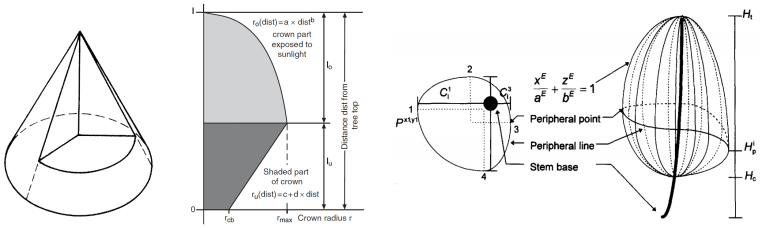

(a) (b) (c)

Figure 1.: Examples of global geometric representations. (a) A simple cone, adapted from Mawson et al. (1976), (b) Axisymmetric crown composed of a truncated paraboloid and an upside down conical frustum, from Pretzsch (2009). (c) complex asymmetric surface parametrisation, from Cescatti (1997).

In principle, these representations can be incorporated into functional-structural models. For instance, the dynamics of the variables that define crown shape in figure 1b (crown height, radius etc.) are coupled to other, empirically described dynamic growth variables, which in

turn depend on the present structure of the tree and its competitors (see Pretzsch et al., 2006).

1.2.2 *Spatial representations*

Godin (2000) referred to a spatial representation when plant architecture is expressed as an assembly of regular cells or voxels in 3D space, containing plant components and information on biological attributes such as leaf density. Beyond the original definition by Godin (2000) with a focus on cubic voxels, it appears reasonable to extend the notion of cells to a more general set of geometric bodies, such as the disks, disk segments and annuli considered in the WHORL model (Sorrensen-Cothern et al., 1993), figure 2a, the BALANCE model (Grote and Pretzsch, 2002; Rötzer et al., 2010), figure 2b, and, similarly, the two-dimensional model by Sonntag (1996) based on a quadratic tessellation of space, which immediately translates into a 3D model after rotation around the vertical axis, figure 2c. All of the above models contain functional-structural properties in that, for instance, light incidence in a cell depends on leaf density in surrounding cells, while, in turn, cell-specific photosynthesis affects local leaf density.

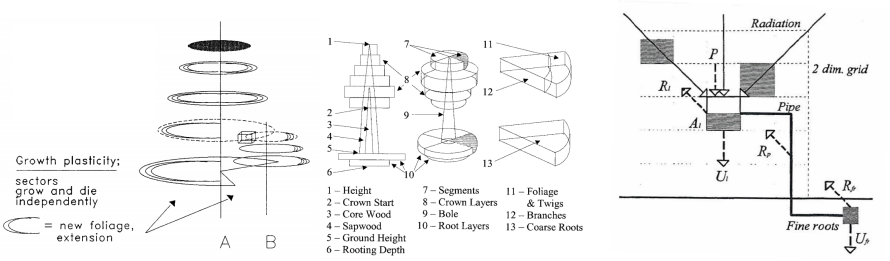

(a) (b) (c)

Figure 2.: Examples of spatial representations. (a) and (b) Crown structure is characterized by vertically stacked disks, composed of segments, adapted from Sorrensen-Cothern et al. (1993) and Grote and Pretzsch (2002), respecitively. (c) Space (2D, implying radial symmetry) is divided into quadratic cells containing leaf area, from Sonntag (1996).

1.2.3 *Geometric representation*

Geometric representations differ from spatial representations in that they explicitly describe the spatial distribution of plant organs, i.e. no longer based on an imposed cell-structurisation of space or the plant, however not yet taking into account the connections between them. Godin (2000) mentioned the spatial distribution of leaves or roots as examples. Indeed the latter has been considered in density-based

root growth models for over a decade (Reddy and Pachepsky, 2001; Dupuy et al., 2005, 2010), figure 3. It is all the more surprising that, to our knowledge, the former has not been considered in any plant growth model prior to this work. We return to the spatial leaf density and related variables in the chapter 2, before using it for modelling purposes.

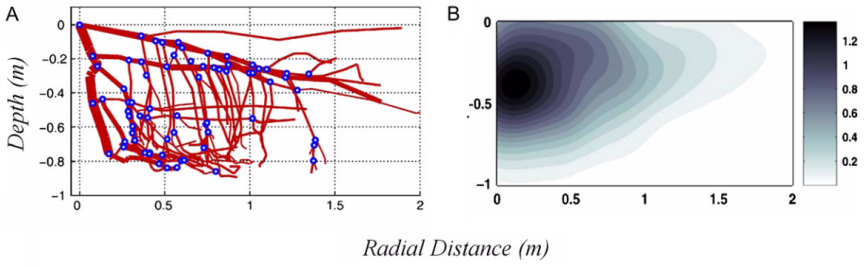

Figure 3.: From geometrical-topological root structure to spatial root density, adapted from Dupuy et al. (2010).

1.2.4 *Topological representation*

Finally, topological representations account for the interconnected network of plant organs. Explicit and mechanistic modelling of any inner-plant substance transport processes requires a topological framework. Branching processes are central to such growth models, and it is thus not surprising that there lies the main application area for L-systems. Apart from few exceptions like the Greenlab model (Yan et al., 2004; Cournède et al., 2006) topological models include a geometrical structure, since otherwise one of the main criticisms towards non-structural process-based models, namely the lack of an accurate description of local light incidence, would equally apply.

The generic shape of foliage is all but uniform in topological models. The scale ranges from detailed polygon meshes (Allen et al., 2005) to simplified geometries such as ellipsoids (Sterck et al., 2005), rhombi (Rauscher et al., 1990), figure 4a – the former include leaf orientations in terms of azimuth and inclination – or spheres (Takenaka, 1994), figure 4b. Sometimes foliage is merely described as a cylinder mantle surrounding wood segments (Kellomäki and Strandman, 1995; Perttunen et al., 1998), figure 4c.

Although exceptions confirm the rule (there are topological models without geometrical structure), the above categories of representation can essentially be ordered according to their level of detail:

$$\text{global} \subset \text{spatial} \subset \text{geometrical} \subset \text{topological representation}$$

Smoothing the distribution of organs in a topological representation and ignoring organ connections yields a geometric representation.

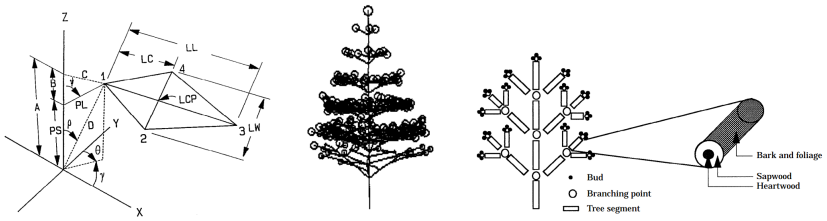

(a) (b) (c)

Figure 4.: Examples of topological representations. Foliage represented as (a) rhombi, from Rauscher et al. (1990), (b) spheres, adapted from Takenaka (1994), and (c) mantles around wood segments, adapted from (Perttunen et al., 1998).

Discretising a geometric density according to a particular predefined cell structure results in a spatial representation, which, after merging individual cells into one geometric body, becomes a global representation.

1.2.5 *Conclusion*

Global models as presented in section 1.2.1 are only to a limited extend suitable to allow for crown plasticity. Their often homogeneous interior does not account for the influential spatial distribution of leaves (Cescatti, 1997). More importantly though, their empirically predefined shape parametrisations, no matter how complex, represent too tight a corset that cannot allow for the actual variability in crown structure and shape in response to local biotic or abiotic growth conditions, including the local availability of growth resources and competition with surrounding individuals.

Models based on spatial representations discussed in section 1.2.2 face the same issue if the underlying cell-structure or other shape constraints restrict variability and plasticity. In the BALANCE model (Grote and Pretzsch, 2002; Rötzer et al., 2010) for instance, the radii of the vertically arranged disks interpolate an empirical equation that predefines and constrains crown shape in an identical manner.

Section 1.1.4 already pointed out major challenges faced by growth models based on topological representations presented in section 1.2.4, most notably with regard to the simulation of old and large individuals where the number of organs exceeds computational feasibility. In addition to that, most topological models have difficulties allowing for arbitrary spatial plasticity as well: Whereas shoot longitudinal growth is indeed often modelled more or less mechanistically, the branching angle and phyllotaxy are mostly predefined (Takenaka, 1994; Perttunen et al., 1998; Balandier et al., 2000). Yet all of these variables have a strong impact on tree form as early demonstrated by

Honda (1971). Fixing crucial architectural parameters such as these a priori puts barriers to plasticity problems these models are able to address.

2

LEAF AREA DENSITIES

Section 1.2 of the previous chapter already pointed to challenges of global, spatial and topological representations of crown morphology and foliage in the sense of Godin (2000) in certain modelling contexts. In response to this methodological gap, we investigate the capacity of a geometrical representation, specifically in terms of the three- and two-dimensional concepts of leaf area density and horizontal leaf area density, respectively. This chapter defines, motivates and contextualises these notions, while bearing in mind empirical methods and records.

2.1 LEAF AREA DENSITY

The most important role in the spatial characterisation of tree crowns throughout this thesis is played by the leaf area density $\clubsuit(x) \geq 0$ [$m^2\,m^{-3}$], where $x = (x_1, x_2, x_3) \in \mathbb{R}^2 \times \mathbb{R}_+$ identifies a position in 3D space, $\mathbb{R}^2 \times \{0\}$ representing the local horizon. Following the definition of the related classical leaf area index (see section 2.3.2), $\clubsuit(x, t)$ is defined as the spatial density of one-sided green leaf area in x at time t (see also Sinoquet and Andrieu, 1993). A particularly important property of the leaf area density is its continuous dependence on the space variable x.

For a given bounded phase space, computing leaf area density is basically independent of the number of leaves, which predestines it for old and large trees. As opposed to global, spatial and even certain topological models in the sense of Godin (2000), leaf area density is not restrictive in terms of shape or in any other way, which suggests it in particular for the modelling of plasticity and spatial variability.

A key argument in favour of the use of leaf area density is the supposedly needless over-complication of a topologically characterized crown structure on a more macroscopic scale. Consider the two photographs in figure 5 showing the the Bavaria Buche, a famous European beech tree in southern Germany, estimated to have been between 500 and 800 years old, measuring 22 meters in height and more than 30 meters in crown diameter by the time it was destroyed by lightning in autumn 2013 (Kratzer, 2013). The number of metamers within its very complex topological branch system (figure 5a) is beyond present modelability (cf. section 1.1.4). And yet this does not seem to matter

(a) (b)

Figure 5.: Bavaria Buche in 1988 before and after foliation. With kind permission by Christoph Reischl.

with regard to the apparent regularity of the distribution of foliage we observe in figure 5b. Or else, the tree achieves this very regularity by adapting its topology accordingly. Indeed, individuals of the same species and the same age growing in similar environmental conditions can show very similar foliage distributions although exhibiting very different branch system topologies. This is particularly true for old and large trees which are beyond the feasibility of present topological functional-structural models. The apparent higher hierarchical goal of attaining a certain leaf distribution seems to govern processes on the lower topological level. In this thesis, we thus closely follow an idea formulated by Thornley and Johnson (2000) in conjunction with the definition of teleonomic models: "It is of course assumed that the diversity of the possible mechanisms at the lower levels is able to satisfy these [higher level] requirements". Hence, we focus on supposed higher level drivers for the dynamics of the spatial distribution of foliage, under the tacit assumption that a plastic tree will find a topological way, i.e. in terms of bifurcations at the right time and the right place, to enable a given distribution. This allows to simulate crown dynamics, in particular those of old trees, in an unrestrictedly plastic, yet minimally complicated model framework.

It should not be overlooked that characterizing foliage in terms of spatial leaf area density is not merely an attempt to make simulations of crown dynamics more efficient and robust compared to topological models. The concept has considerable value in itself and is able to address questions that models based on global, spatial or topological representations will have difficulty responding to, e.g. exploring the isolated impact of unrestrained phototropism on morphological crown dynamics discussed in detail in section 3.3.

2.1.1 *Empirical measurements and use in models*

We have found only a single example of an empirical measurement that comes close to determining leaf area density. Fleck (2001) established total leaf area of large branches and divided this quantity by the volume of a branch-enveloping polyhedron. This branch-specific leaf area density distinguishes itself from leaf area density as defined here in that it is not local in the narrow sense, not defined in the space between branches and thus in particular not spatially continuous.

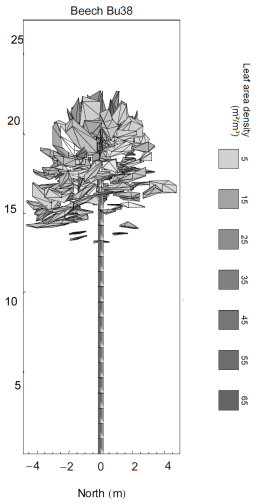

Figure 6.: Empirical branch-specific leaf density of a beech tree, adapted from Fleck (2001).

Some tree models based on a global representation do not assume a homogeneous distribution of leaves in the crown envelope (Wang et al., 1990; Wang and Jarvis, 1990; Baldwin et al., 1997; Porté et al., 2000). Instead, local leaf area density is empirically described in terms of the product of two functions, often based on Beta or Weibull distributions, taking height and distance from the trunk as arguments, respectively. The assumptions of independence of the horizontal and vertical distributions of leaf area density as well as the axial symmetry of the density, in order to simplify the acquisition procedure, are debatable.

To our knowledge, no functional-structural tree growth model describing the dynamics of leaf area density as defined here exists to date. The theoretical 2D approach by Sonntag (1996) (cf. figure 2a), essentially a cellular automaton model, however, is worth mentioning in this context. In a non-topological way similar to the one pursued throughout this thesis, space is divided into cells that contain a cell-specific amount of leaf area density which affects and is affected by spatial tree growth dynamics. Yet, some of the model assumptions do not apply in a reasonable way if the size of a cell would tend to zero, which demonstrates the incompatibility with the present spatially continuous leaf area density concept.

2.2 HORIZONTAL LEAF AREA DENSITY

In the case when the vertical structure of a plant or plant community is secondary to the horizontal occupation of space, the horizontal leaf area density, $\spadesuit(x)$ [$m^2\,m^{-2}$] for $x = (x_1, x_2) \in \mathbb{R}^2$ can be a suitable variable to describe foliage distribution in a less complex and computationally demanding way than the 3D leaf area density. It is formally defined as the vertical integral over the latter variable,

$$\spadesuit(x_1, x_2) = \int_0^\infty \clubsuit(x_1, x_2, x_3)\, dx_3.$$

It contains information about the total quantity of foliage above a given ground position, but not on its vertical distribution. The horizontal leaf area density is particularly suited for modelling spatial dynamics if the following assumptions are satisfied:

- Radiation can reasonably be simplified to be vertical only
- Inter-individuals crown overlap is either negligible or sufficiently even
- Intra-individual processes are only little affected by height

In particular Beer-Lambert's law (see section 3.1) plays a significant role with regard to the first two assumptions.

A few empirical parametrisations of $\spadesuit$ exist, mostly for crops, and can be found in the works of Fukai and Loomis (1976), Myneni et al. (1986), Cohen and Fuchs (1987), Wang et al. (1990) and Sinoquet et al. (1991). Common acquisition techniques include the stratified clipping method and the silhouette method (see Sinoquet and Andrieu, 1993, for details).

2.3 RELATED VARIABLES

In 1981, Ross asserted that "Experimental data on the horizontal variability and two-or three-dimensional distribution of phytomass and phytoarea are very scarce" – a fact that is as true today as it was three and a half decades ago. This is all the more surprising given that two very related variables, the vertical leaf area distribution and especially the leaf area index have experienced considerable popularity. We return to specific shortcomings of these variables in contrast to $\clubsuit$ and $\spadesuit$ in the context of the computation of light interception in section 3.1.

2.3.1 *Vertical area leaf density*

The horizontal leaf area density $\spadesuit$ was defined as the vertical integral over the leaf area density $\clubsuit$. Taking the normalized horizontal integral

instead, yields the vertical leaf area density $\mathrm{LAD_v}$ [$\mathrm{m^2\,m^{-3}}$] in height x_3 as

$$\mathrm{LAD_v}(x_3) = \frac{1}{\mathrm{CPA}} \cdot \int_{\mathbb{R}^2} \clubsuit(x_1, x_2, x_3)\, dx_1\, dx_2, \tag{1}$$

where CPA denotes the crown projection area, i.e. the area of the projection of the support of $\clubsuit$ onto the x_1x_2-plane.

Vertical leaf area density is often used to quantify the vertical variation in light transmittance within the canopy (Vose et al., 1995). Although the horizontal homogeneity of the $\mathrm{LAD_v}$ variable is not without controversy (Wang and Jarvis, 1990; Stenberg et al., 1994; Cescatti, 1997), its range of applications covers canopy gas exchange models (see Meir et al., 2000, and references therein) as well as models for forest structure and productivity, water use and atmospheric deposition to the forest canopy (see Vose and Swank, 1990, and references therein).

Meir et al. (2000) revisited methods for determining $\mathrm{LAD_v}$, which include destructive sampling (Kato et al., 1978; Hollinger, 1989; McWilliam et al., 1993) and the optical point-quadrat method (MacArthur and Horn, 1969; Aber, 1979). All in all, measuring and estimating $\mathrm{LAD_v}$ remains difficult and tedious. Empirical parametrisations of $x_3 \mapsto \mathrm{LAD_v}(x_3)$, often based on Beta or Weibull functions, have been presented by Allen (1974), Waring (1983), Wang et al. (1990), Mori et al. (1991), Maguire and Bennett (1996), Cescatti (1997), Jerez et al. (2005), Weiskittel et al. (2009) and Nelson et al. (2014).

Due to the lack of horizontal information, vertical leaf area density is only of limited value for problems of spatial competition (but Kikuzawa and Umeki (1996) used it to study vertical competition in a multi-layer forest) and the horizontal occupation of space. Moreover, it requires a priori knowledge on an additional parameter, the crown projection area CPA – without which, different degrees of horizontal crown expansion, e.g. in the case of columnar versus spreading trees, would no longer be comparable.

2.3.2 *Leaf area index*

Watson (1947) defined the leaf area index LAI [$\mathrm{m^2\,m^{-2}}$] as the total one-sided area of leaf tissue per unit ground surface area. In terms of the formerly defined variables, it computes as

$$\begin{aligned}
\mathrm{LAI} &= \int_0^\infty \mathrm{LAD_v}(x_3)\, dx_3 \\
&= \frac{1}{\mathrm{CPA}} \cdot \int_{\mathbb{R}^2} \spadesuit(x_1, x_2)\, dx_1\, dx_2 \\
&= \frac{1}{\mathrm{CPA}} \cdot \int_{\mathbb{R}^3} \clubsuit(x_1, x_2, x_3)\, dx_1\, dx_2\, dx_3
\end{aligned}$$

The simplicity of this non-spatial variable has not derogated its extensive use in, among others, productivity models, and soil-vegetation-atmosphere transfer models (see Meir et al., 2000, and references therein) as well as models of light interception and productivity, deposition of atmospheric chemicals, evapotranspiration, and site water balance (see Vose et al., 1995, and references therein). The popularity and wide-spread applications of the LAI are reflected in the large number of reviews of estimation methods, including those by Kvet and Marshall (1971), Ross (1981), Chason et al. (1991), Smith et al. (1991), Fassnacht et al. (1994), Dufrêne and Bréda (1995), Küssner and Mosandl (2000) and Bréda (2003).

(At times, the non-spatial variable LAD $= \frac{1}{H} \cdot$ LAI where H denotes tree or canopy height is also called leaf area density and is obviously not to be confused with the local leaf area density $\clubsuit = \clubsuit(x)$.)

In the following, for the sake of brevity and better readability, we write (horizontal) leaf density in place of (horizontal) leaf area density.

2.4 SPATIAL DENSITY IN DYNAMIC POPULATION MODELS

Modern theoretical ecology could not be imagined without spatial density-based models. By arguing that a large enough biological population can reasonably be described in terms of a spatially continuous density distribution, modellers take a step back from the individual members of the population and consider the bigger picture. Whereas movement, reproduction and death patterns of a singular individual can be extremely complicated to describe, let alone predict, these effects may average out at the scale of the population. The most prominent example of this is the relatedness of the random walk and Brownian motion to the diffusion process modelled by the fundamental solution of the heat equation on the individual and collective scale, respectively. Indeed, the smoothness of the spatial density with respect to both space and in many applications also time suggests describing its spatio-temporal dynamics in terms of continuity equations. For a spatial density $u = (x, t)$ where $t \in \mathbb{R}_+$ denotes time, the basic form of such a model reads

$$\frac{\partial}{\partial t} u = f - \nabla_x \cdot J, \tag{2}$$

where the reaction term f accounts for local birth and death rates, e.g. in a logistic way, and J is a flux that transports individuals through space under conservation of total mass. In many applications J is given by an advection-diffusion flux, i.e. $J = -D\nabla_x u + v \cdot u$ for a velocity field v and a diffusivity $D > 0$, which reduces to the extensively studied classical reaction-diffusion equation when $v \equiv 0$. Coupled systems of such equations allow to include interactions between several populations. We refer to the standard works by Okubo

and Levin (2002) and Cantrell (2013) on reaction-(advection-)diffusion in ecological modelling and to the review by Pierre (2010) on results on the existence of global solutions of reaction-diffusion systems. In plant modelling, El Hamidi et al. (2008) provided an example of this approach on the ecosystem scale by considering the spatial density of plant individuals and using it to describe competition.

The suitability of spatial density in the ecological context increases with an increasing number of members of a population. The large number of leaves – or, in a manner of speaking, members of a (strongly interconnected) leaf population – especially in old trees, locally accounting for units of leaf area, offers strong support for the spatial density approach.

The model presented in chapter 4, describing the continuous expansion of the foliage of crops over the course of one season, is indeed based on (2). In chapter 5, we explore how the evolution of leaf density of trees over several growth cycles can be expressed in the framework of continuity equations.

3

GENERAL MODEL FEATURES

Having introduced leaf density and horizontal leaf density as the basic modules of the plant growth models presented in the subsequent chapters 4, 5 and 6 of this thesis, here, we present several basic characteristics that are shared by the different models.

3.1 BEER-LAMBERT'S LAW

Foliage characterized in terms of leaf density has the properties of a continuous light-absorbing medium, through which travelling radiation decreases in intensity according to Beer-Lambert's law (see for example Ingle Jr and Crouch (1988) for the straightforward mechanistic derivation). For a photosynthetically active radiation $\text{PAR}(v)$ reaching a tree with given leaf density ♣ from direction $v \in S^2_+$, the radiation in a point $x \in \mathbb{R}^3$ is thus given by

$$\text{PAR}(v) \cdot \exp\left(- \int_{x+\mathbb{R}_+ \cdot v} v \cdot N(\xi) \cdot T(\xi) \cdot \clubsuit(\xi)\, d\xi \right), \tag{3}$$

where $N(x) \in S^2_+$ and $T(x) \in [0,1]$ denote the average normal to the leaf surface and leaf transmittance in x, respectively. Accordingly, the total radiation in x reads

$$\int_{S^2_+} \text{PAR}(v) \cdot \exp\left(- \int_{x+\mathbb{R}_+ \cdot v} v \cdot N(\xi) \cdot T(\xi) \cdot \clubsuit(\xi)\, d\xi \right) dv.$$

For the simplified case of merely vertical light incidence, $v = (0,0,1)$, $\text{PAR}(v) = \text{PAR}$, and constant leaf angles and transmittance throughout the crown, (3) reduces to

$$\text{PAR} \cdot \exp\left(-\lambda \cdot \int_{x_3}^{\infty} \cdot \clubsuit(x_1, x_2, \xi_3)\, d\xi_3 \right), \tag{4}$$

with the extinction coefficient

$$\lambda = N_3 \cdot T \in [0,1]\,. \tag{5}$$

(4) points to a key motivation of the variable ♠, since the radiation reaching the ground point $(x_1, x_2, 0)$ can be expressed as

$$\text{PAR} \cdot \exp(-\lambda \cdot \spadesuit(x_1, x_2)). \tag{6}$$

Hence, if we make do with the above simplifications and are merely interested in the globally intercepted radiation, considering ♠ provides the same amount of information as the much more complex ♣.

Leaf transmittance is normally merely species-specific and does not vary within the crown, i.e. $T(x) = T$. The variable $N(x)$, accounting for leaf inclination, can principally be chosen according to species-specific leaf angle distribution functions (see Ross, 1981, Sinoquet and Andrieu, 1993, and in particular the comparative review by Wang et al., 2007). Due to the tediousness of the measurements involved in determining leaf inclinations in trees (Sarlikioti et al., 2011), the simple approach of assuming constant leaf inclinations is still very common (Sinoquet and Andrieu, 1993, e.g. in the models by Higashide, 2009 and Najla et al., 2009). It is also inevitable in conjunction with horizontal leaf density ♠. We make the same simplification, $N(x) = N$, in the models based on leaf density.

Beer-Lambert's law has experienced popularity in numerous spatial (Sorrensen-Cothern et al., 1993; Sonntag, 1996; Grote and Pretzsch, 2002) and topological (Takenaka, 1994; Kellomäki and Strandman, 1995; Rauscher et al., 1990; Balandier et al., 2000) models. Historically, Nilson (1971) first motivated the application of Beer-Lambert's law to light transmittance on the scale of an LAI-characterised stand, triggering extensive follow-up use in process-based models. The associated theoretical assumptions, notably the uniformity of the distribution of leaves in the canopy, have been subject to criticism (Sinoquet et al., 2005, and references therein). The LAI-based application of Beer-Lambert's law should thus be understood rather as an empirical remedy, and be distinguished from the more mechanistic application in conjunction with leaf density ♣.

As in the case of LAI, information on the vertical leaf density $\mathrm{LAD_v}$ (cf. (1)) is also not sufficient to deduce light interception in a reliable mechanistic way. As a counterexample, consider for some radius r, height h and constant $\overline{♣}$, the two leaf densities

$$♣_1(x) = \begin{cases} \overline{♣} & \text{if } \|(x_1, x_2)\| \leq r,\ 0 \leq x_3 \leq h \\ 0 & \text{else} \end{cases}$$

$$♣_2(x) = \begin{cases} \overline{♣} & \text{if } \|(x_1, x_2)\| \leq r,\ h - \epsilon \leq x_3 \leq h \\ \pi r^2 \cdot \overline{♣} \cdot \delta_{(0,0)}(x_1, x_2) & \text{if } 0 \leq x_3 < h - \epsilon \\ 0 & \text{else} \end{cases}$$

In the first case, leaf density fills a cylinder uniformly, in the second case it is essentially concentrated on the vertical axis. Both have the same vertical leaf density

$$\mathrm{LAD_v}(x_3) = \overline{♣} \quad \text{for } 0 \leq x_3 \leq h$$

as well as crown projection area πr^2 for all $0 < \epsilon \leq h$. However, the total amounts of intercepted vertical light by $\clubsuit_1$ and $\clubsuit_2$ equal $\pi r^2 \cdot (1 - \exp(-h \cdot \overline{\clubsuit}))$ and $\pi r^2 \cdot (1 - \exp(-\epsilon \cdot \overline{\clubsuit})) \xrightarrow[\epsilon \to 0]{} 0$, respectively, which can differ arbitrarily.

In summary, we argue that both $\clubsuit$ and even $\spadesuit$ can provide mechanistic and thus more reliable information on intercepted radiation compared to LAI and LAD_v.

3.2 RADIATION USE EFFICIENCY

Models throughout this thesis assume a linear response of dry matter production to light incidence in accordance with the concept of radiation use efficiency introduced by Monteith (1972, 1977). The existence of this relationship is particularly curious in view of the strongly non-linear response of leaf photosynthesis to light incidence. Medlyn (1998) provided an extensive discussion on the physiological basis of the linearity.

Monteith's conversion efficiency has been used in many other growth models both at the scale of the whole tree (e.g. West, 1993; Bartelink et al., 1997) and, as done in this thesis, at the local shoot level (Sorrensen-Cothern et al., 1993; Takenaka, 1994; Kellomäki and Strandman, 1995).

Curiously, radiation use efficiency RUE not only reduces model parameters and simplifies computations, it is also a necessity for the very use of horizontal leaf density $\spadesuit$. Again assuming vertical radiation and constant leaf angles and transmittance, the light-dependent production of dry matter in $x \in \mathbb{R}^3$ for a given leaf density $\clubsuit$ and photosynthetically active radiation PAR reads

$$\mathrm{RUE} \cdot \mathrm{PAR} \cdot \lambda \cdot \clubsuit(x) \cdot \exp\left(-\lambda \cdot \int_{x_3}^{\infty} \clubsuit(x_1, x_2, \xi_3)\, d\xi_3\right), \tag{7}$$

and the total net production above the ground point $(x_1, x_2, 0)$ equals

$$\begin{aligned} \int_0^{\infty} \mathrm{RUE} \cdot \mathrm{PAR} \cdot \lambda \cdot \clubsuit(x) \cdot \exp\left(-\lambda \cdot \int_{x_3}^{\infty} \clubsuit(x_1, x_2, \xi_3)\, d\xi_3\right) dx_3 \\ = \mathrm{RUE} \cdot \mathrm{PAR} \cdot \left(1 - \exp\left(-\lambda \cdot \spadesuit(x_1, x_2)\right)\right). \end{aligned} \tag{8}$$

In fact, if the relationship between net production and light incidence were anything but linear, the integral in the first line of (8) could not be reduced to an expression in terms of $\spadesuit$. The existence of RUE thus enables the reasonable use of $\spadesuit$.

3.3 PLASTICITY, PHOTOTROPISM AND TELEONOMY

In most contexts, crown plasticity refers to a tree's ability to locally adapt its above-ground form in order to capture light as much and

efficiently as possible. This comprises not only phototropism on the shoot level, i.e. the directional growth towards light (see the extensive reviews by Iino, 1990; Whippo, 2006; Hohm and Fankhauser, 2013, for physiological and ecological details), but also light-dependent branch growth rates (Strigul et al., 2008) as well as the physiological degradation of shaded branches (Stoll and Schmid, 1998). Strigul et al. (2008) mentioned plasticity patterns in conifers, broad-leaf trees, tropical and temperate forests, and address reasons for differences in their respective magnitudes in terms of different histories and ecological strategies (see also Kleunen and Fischer, 2005).

In a landscape-scale model, based on a global representation of tree crown shape, plasticity in regard to light and competition for it has culminated in the perfect plasticity approximation (Strigul et al., 2008), where the assumption of trees growing almost unrestrictedly toward the most open space simplifies stand structure in computations. Sorrensen-Cothern et al. (1993) modelled plasticity based on a spatial architectural representation. Phototropic plasticity is also incorporated in various ways in several topological tree growth models, e.g. when the longitudinal growth or the production of new shoots is related to the local light climate (e.g. Takenaka, 1994; Ballaré, 1994; Kellomäki and Strandman, 1995; Sterck et al., 2005; Qu and Wang, 2011).

Several of the above mentioned approaches implicitly feature teleonomic characteristics: The interception of light is considered in conjunction with biomass production, and thus plasticity for the sake of light interception can be seen as serving the higher purpose of growth maximisation. Models in this thesis are strongly based on this last rationale. Indeed, since net biomass production is proportional to local leaf density and local light interception, the direction of the local light gradient (cf. (4)),

$$\nabla_x \,\mathrm{PAR} \cdot \exp\left(-\lambda \cdot \int_{x_3}^{\infty} \clubsuit(x_1, x_2, \xi_3)\, d\xi_3\right) \in \mathbb{R}^3, \tag{9}$$

(analogous for the case of non-vertical radiation, according to (3)) coincides in fact with the direction of the greatest increase net biomass productivity, i.e. net biomass production (7) divided by the local leaf density $\clubsuit(x)$. The local expansion towards the light – or equivalently, in a manner of speaking, the direction most favourable in terms of anticipated future local biomass productivity – i.e. in the direction of the light gradient (9) and its analogue for horizontal leaf density,

$$\nabla_x \,\mathrm{PAR} \cdot \exp\left(-\lambda \cdot \spadesuit(x_1, x_2)\right) \in \mathbb{R}^2, \tag{10}$$

play a central role in the spatial model dynamics in this thesis.

3.4 COMPETITION FOR LIGHT

Competition for light in plant communities is considered to dominate competition for all other resources (Sorrensen-Cothern et al., 1993), and it plays a fundamental role in this thesis. In the case of a population of m plants with leaf densities $\clubsuit_1, \ldots, \clubsuit_m$, potentially shading each other, the generalisation of (4) for the light incidence in a point $x \in \mathbb{R}^3$ is given by

$$\text{PAR} \cdot \exp\left(- \int_{x_3}^{\infty} \sum_{i=1}^{m} \lambda_i \cdot \clubsuit_i(x_1, x_2, \xi_3)\, d\xi_3 \right). \tag{11}$$

The case of non-vertical radiation (cf. (3)) is analogous. Similarly, the generalisation of (6) and analogue of (11) for the case of n horizontal leaf densities $\spadesuit_1, \ldots, \spadesuit_m$ reads

$$\text{PAR} \cdot \exp\left(- \sum_{i=1}^{m} \lambda_i \cdot \spadesuit_i(x_1, x_2) \right). \tag{12}$$

Now, if the local expansion of a plant follows the spatial gradient of (11) or (12), its horizontal expansion will come to a rest when meeting another crown, since this region is already shaded by the competitor, hence the x_1x_2-entries of the light gradient vanish. In teleonomic terms, at this point, an additional horizontal expansion is no longer beneficial in terms of the maximisation of biomass production. Here, we follow Sorrensen-Cothern et al. (1993) in the assumption that the local response to shading does not depend on whether it is caused by external or self-shading.

This particular model mechanism of spontaneous self-organisation and adaptation to the current competitive environment brings about a realistic reduced horizontal expansion of a simulated crown under competition compared to that of a solitary individual. However, a lesser occupation of horizontal space than in the case of the spatially isolated crown implies a higher degree of self-shading for the individual, and thus a lesser biomass production in the middle and long term.

The empirical data used for model validation in this thesis thus focusses on density experiments in crops and trees. The data sets themselves demonstrate the strong dependence of the magnitude of growth and size variables on field or stand density. In other models, this dependence is often taken into account in terms of density-specific parameters or empirical competition indices (reviewed thoroughly by Burkhart and Tomé, 2012), to which the challenges described in section 1.1.1 apply. In contrast, in our models, parameters are merely species-specific, and competition effects are entirely accounted for by the above described mechanisms.

3.4.1 *Perodic boundary conditions*

In the applied models in chapters 4 and 6, we compare model simulations to data from even-aged monospecies stands which are either planted in a regular pattern from the start, in the case of crops, or, in the case of mature tree stands, which developed a spatially even distribution over a long period of competition (Cooper, 1961; Ford, 1975; Kenkel, 1988). We take advantage of the regular horizontal spacing in these cases by simulating merely an average plant growing on a two-dimensional unit cell, whose centre represents the position of the seed and later stem base. Surrounding competitors are taken into account by simulating the occurrence of foliage, as well as local light conditions in particular, beyond the cell as the periodic continuation of those within (cf. Rapaport, 2004). A competitor's foliage perceived by the simulated plant growing towards the cell border is thus given by its own at the opposite side of the cell. This allows for the symmetry of growth among regularly spaced plants of a homogeneous community, in which each member grows and shades its environment in similar measure. This approach is justified if the number of individuals at the border of the stand is small compared to the number of individuals in the regularly spaced interior, which is the case for our data sets.

The size and shape of the unit cell is either defined, if known, by the plant positions. In the regularly planted field simulated in chapter 4, in which seed positions lie on a regular two-dimensional grid, a plant's cell is given by the rectangular tile of the Voronoi tessellation with the plants' sowing positions as generating point set. If merely the stand density SD [m^{-2}], i.e. number of individuals per unit stand area, is known, as in chapter 6, the area of the cell is given by $\frac{1}{SD}$, and its shape can be defined as a disk. Over the course of a field experiment, stand density gradually decreases as the result of occasional harvest or natural death of single individuals, thus reducing the pressure of spatial competition on the remaining members of the populations. In simulations, this is accounted for by dynamically increasing the size of the simulated average plant's cell, i.e. expanding its boundary, out from the cell centre corresponding to the appropriate stand density at the respective point in time.

3.5 BIOMASS ALLOCATION

Lacointe (2000) and Le Roux et al. (2001) classified models for the allocation of produced biomass in trees, distinguishing between approaches based on empirical coefficients and allometric relationships, teleonomy (often denoted functional balance in this context), transport-resistance models, and sink interactions. Here, we briefly address the first two of these categories as these are applied in models in this thesis, and refer to the above mentioned reviews as well as the more

recent one by Franklin et al. (2012) for a broader overview of the alternative approaches, further details and examples.

In a first step, the partitioning of biomass between different plant compartments or organs can be assessed empirically. Brouwer (1962) observed that for constant environmental conditions, allocation coefficients of shoots and roots are roughly constant. In other cases, specific plant ontogeny can lead to coefficients that vary over time (cf. Le Roux et al., 2001). We apply such a time-depended empirical approach in the crop model presented in section 4.

The empirical findings of Brouwer (1962) can also be interpreted from a teleonomic point of view. If the rate of uptake of a particular resource is assumed proportional to the mass of the organ type it is assimilated or acquired by, and if the internal physiological processes of the plant require a certain fixed ratio of the different resources, then, in order to maximize functioning, the allocation coefficients quantifying the partitioning of produced biomass to the different compartments and thus determining mass increments will tend to constants. These might change, for instance, because changing environmental conditions lead to the violation of the first assumption. Historically, Davidson (1969) first described this idea mathematically, giving rise to a large number of follow-up approaches in the modelling of shoot-root-allocation ratios (see Thornley and Parsons, 2014, and references therein).

3.5.1 *The pipe model theory*

A similar rationale underlies the pipe model theory (Shinozaki et al., 1964) for trees. Observations of a species-specific constant ratio between the conductive cross-sectional area of a branch and the leaf mass attached to it and its daughter branches gave rise to the conceptual image of a sapwood pipe leading from the roots up to a leaf, in charge of its hydraulic as well as mechanical support. In particular, a pipe's mass is assessed proportional to the product of the leaf mass at its tip and the root-to-leaf distance along the branch system. Branches and ultimately the trunk are the result of joining pipes. This functional explanation follows Leonardo da Vinci's observation of the preservation of cross-sectional areas at branching points in the early sixteenth century (Richter, 1970).

The theory goes on to attribute the transformation of conductive sapwood into heartwood to the abscission of leaves causing a functional shutdown of the appropriate pipes. This also explains the tapering of the below-crown part of the trunk despite the absence of first order branching points: This part contains pipes that once connected to branches that were shed at some point in time, cf. figure 7.

Besides extensive empirical findings in support of the theory, it is has also been subject to controversy, as the ratio of sapwood area

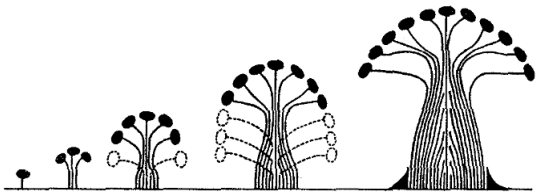

Figure 7.: Original caption: "Diagrammatic representation of the pipe model of tree form, showing the successive accumulation of disused pipes in the trunk associated with the progress of tree growth", from Shinozaki et al. (1964).

to leaf mass or leaf area has been observed to vary with tree height and age, site quality, stand vigour and density, water availability and average vapour pressure deficit in some cases (West, 1993; Mencuccini and Grace, 1995; White et al., 1998; Mokany et al., 2003, and references therein). However, to date, these variations as well as hypotheses on their origins and suggestions for improvements are not uniform enough to point to an obvious general direction as to how to adjust the original theory (Beyer, R., Lehnebach, R., Letort, V., Heuret, P., unpublished manuscript).

In this thesis, we follow in the tradition of numerous approaches that applied the original pipe model theory in conjunction with the allocation of biomass in trees, including but not limited to the works by Mäkelä (1986), Prentice et al. (1993), Hauhs et al. (1995), Perttunen et al. (1996), Williams et al. (1996), Allen et al. (2005), Kubo and Kohyama (2005), Cournède et al. (2006), Sterck and Schieving (2007) and Mathieu et al. (2009).

It should be noted that the application of the pipe model theory in these models, just as in ours, is essentially identical to the use of the Preßler law, which postulates a proportionality of leaf mass to the area of the annulus that is the last tree ring (Preßler, 1865). Under the assumption of a constant specific wood volume, the appropriate proportionality constant plays the same role as the pipe parameter of Shinozaki et al. (P in the equations below). On a quantitative level, the two propositions thus amount to the same, differing merely in their more conceptually and empirically oriented perspectives, respectively.

In the tree models presented in this thesis, the allocation of a given, locally available biomass quantity $B(x)$ in a point x comprises its partitioning into $p \cdot B(x)$ units of new leaf mass in x (inducing an increase in $\clubsuit(x)$), and $(1-p) \cdot B(x)$ units of sapwood mass for the pipe that is mechanically and hydraulically supporting the new foliage, $p \in [0,1]$ denoting a partitioning factor yet to be determined.

Denoting the length of the pipe leading from the roots to x along the branch network by $\|x\|_Y$ (see below), the pipe model theory requires the equation

$$\underbrace{(1-p)\cdot B(x)}_{\substack{\text{mass available}\\ \text{for the pipe}}} = \underbrace{P\cdot \overbrace{p\cdot B(x)}^{\substack{\text{leaf}\\ \text{mass}}}\cdot \overbrace{\|x\|_Y}^{\substack{\text{pipe}\\ \text{length}}}}_{\substack{\text{mass required}\\ \text{for the pipe}}} \tag{13}$$

for a given, species-specific pipe model proportionality factor $P > 0$ [m^{-1}] to hold. Solving (13) yields the partitioning factor

$$p = p(x) = \frac{1}{1 + P\cdot\|x\|_Y}. \tag{14}$$

In the context of leaf density, the pipe model theory allows to deduce the total sapwood mass of a tree with given ♣ as

$$\int_{\mathbb{R}^3} P\cdot \underbrace{\frac{1}{SLA}\cdot \clubsuit(x)}_{\text{leaf mass density}} \cdot \|x\|_Y \, dx, \tag{15}$$

where SLA [$m^2\, g^{-1}$] denotes specific leaf area, supposed constant. Moreover, the area of the sapwood part of a cross-section of the trunk at its base (not accounting for bulking) equals

$$\int_{\mathbb{R}^3} P\cdot \frac{1}{SLA}\cdot \clubsuit(x)\cdot SWV\, dx,$$

where SWV [$m^3\, g^{-1}$] denotes specific wood volume, also assumed constant.

The spatially continuous and in particular non-topological nature of the leaf density concept implies that a sensible function $\|\cdot\|_Y$ that maps a leaf position $x \in \mathbb{R}^3$ to its distance to the roots is not obvious. Here, we use the following heuristic approximation length of the root-to-leaf path to x:

$$\begin{aligned} \|x\|_Y &= x_3 - \frac{\|(x_1,x_2)\|}{\tan(\varphi)} + 2\cdot\frac{\|(x_1,x_2)\|}{\sin(\varphi)} \\ &= x_3 + (2-\cos(\varphi))\cdot\frac{\|(x_1,x_2)\|}{\sin(\varphi)} \end{aligned} \tag{16}$$

The idealised pathway thus consists of three segments: A trunk-associated segment leading from the origin up to height $x_3 - \frac{\|(x_1,x_2)\|}{\tan(\varphi)}$, where a branch-associated segment of length $\frac{\|(x_1,x_2)\|}{\sin(\varphi)}$, leading straight to x, bifurcates at the given angle $\varphi \in \left[\frac{\pi}{2}, \pi\right[$, which represents the average angle that the trunk confines with first order branches. Following Sonntag (1996), root length is assumed to be equal to branch length, thus the factor 2 in the second summand in the first line of (16).

All models presented in this thesis proved to be highly insensitive to the particular choice of $\|x\|_Y$ in (16). Specifically, varying the average branching angle φ had virtually no impact on simulation results. This is not surprising given that the upper ground part of $\|x\|_Y$ basically ranges between $\|x\|$ and $x_3 + \|(x_1, x_2)\|$, and these values differ only very little for typical leaf positions x during the entire growth process (in particular, crown radius is commonly one magnitude smaller than tree height). The insensitivity extends to the assumption regarding root length. For instance, alternatively following Valentine (1985) by assuming of a proportionality between pipe length below and above ground, i.e. root- and stembase-to-leaf length, respectively, and assessing $\|x\|_Y = (1 + C) \cdot \left(x_3 + (1 - \cos(\varphi)) \cdot \frac{\|(x_1,x_2)\|}{\sin(\varphi)}\right)$ for reasonable $C \in]0, 1[$, had again no measurable impact.

Part II.

Models

4

CONTINUOUS-TIME MODELLING OF CROP GROWTH

We start off the applications of the spatial density-based characterisation of foliage to plant growth modelling with a two-dimensional model for crops, based on horizontal leaf density $\spadesuit = \spadesuit(x,t)$, where $x \in \mathbb{R}^2$ for the remainder of this chapter. The relatively small height of crops as opposed to trees motivates the use of this simpler variable, before, in the subsequent, tree-oriented chapters, we will be primarily concerned with the 3D leaf density $\clubsuit$.

We model growth over the course of one year, and describe the continuous expansion and increase of foliage during that time with an equation of the form (2), more specifically

$$\frac{\partial}{\partial t}\spadesuit(x,t) = a(x,t) - s(x,t) - \nabla_x \cdot J(x,t). \tag{17}$$

The reaction term $a - s$ comprises the allocation of produced biomass to foliage as well as leaf senescence. In the model, these two terms are obtained by first computing global allocation and senescence at the whole-plant scale, $a_\spadesuit = a_\spadesuit(t)$ and $s_\spadesuit = s_\spadesuit(t)$, and then applying a weight function to obtain the local terms $a(x,t)$ and $s(x,t)$. The flux term J essentially describes a motion towards the light in the spirit of section 3.3.

Section 4.1 presents model hypotheses and equations for the individual plant as well as a population. In Section 4.2, we demonstrate how the model can be related to the porous medium equation, before using this transformation to obtain certain theoretical results as well as to speed up the computations. In section 4.3, the model is tested against experimental data from three sugar beet populations varying in density.

The complete model was previously presented by Beyer et al. (2015a).

4.1 MODEL DESCRIPTION

In this section we present the biological concepts which form the basis for our model. The equations are specifically derived for the case of sugar beet, which has two kinds of organ compartments, foliage

and roots. In principle, they generalize to other plants by considering further types of compartments (e.g. stem and fruit in the case of sunflower or maize).

The time domain for the validity of the model is limited to the classical cropping season of the sugar beet, from sowing to harvest. Botanically, sugar beet is a biannual plant featuring a very different development in the second year.

According to the considerations on Beer-Lambert's law and radiation use efficiency in sections 3.1 and 3.2, respectively, the net biomass production [$\mathrm{g\,s^{-1}}$] of a horizontal leaf density ♠ at time t reads

$$b(t) = \mathrm{RUE} \cdot \mathrm{PAR}(t) \cdot \int_{\mathbb{R}^2} 1 - \exp(-\lambda \cdot ♠(x,t))\, dx \tag{18}$$

for a photosynthetically active radiation $\mathrm{PAR}(t)$ [$\mathrm{J\,m^{-2}\,s^{-1}}$] reaching the plant from above at time t, a radiation use efficiency RUE [$\mathrm{g\,TJ^{-1}}$] and an extinction coefficient λ.

The global allocation and sensequence functional terms specified in the following are inspired by the LNAS model presented by Cournède et al. (2013) and Chen and Cournède (2014). For the specific case of sugar beet, the totally produced biomass (18) is divided between the plant's two organ compartments foliage and root system. Total allocation to foliage and roots [$\mathrm{g\,s^{-1}}$], respectively, at time t are

$$\begin{aligned} a_{♠}(t) &= \gamma(t) \cdot b(t) \\ a_{\surd}(t) &= (1 - \gamma(t)) \cdot b(t) \end{aligned} \tag{19}$$

for a time-dependent ratio $\gamma(t) \in [0,1]$ governing the partitioning. Following Guerif and Duke (1998), we use the following empirical function to describe it:

$$\gamma(t) = \gamma_0 + (\gamma_f - \gamma_0) \cdot F_a(\tau(t)), \tag{20}$$

where F_a denotes the cumulative distribution function of a log-normal law with an underlying normal law of mean μ_a and standard deviation σ_a. Its argument $\tau(t) = \int_0^t T(u)\, du$ [°C days] denotes thermal time, where $T(t)$ (in °C) is the temperature at time t. The values γ_0 and γ_f denote the initial and eventual foliage-to-root biomass distribution ratio, respectively.

The quotient of cumulative senescent leaf mass and cumulative green leaf mass is 0 at $t = 0$, and monotonically tends to 1 as t becomes large. This motivates to describe the course of the global leaf senescence, $s_{♠}(t)$ [$\mathrm{g\,s^{-1}}$] over time by means of a time-delayed version of a cumulative distribution function F_s of a log-normal law with an underlying normal law of mean μ_s and standard deviation σ_s, i.e.

$$\frac{\int_0^t s_{♠}(u)\, du}{a_{♠}(0) + \int_0^t a_{♠}(u)\, du} = \widehat{F}_s(t), \tag{21}$$

where $a_{\spadesuit}(0) = \gamma_0 \cdot b(0)$, $b(0) = b_0$ is the mass of the seed at time $t = 0$, and

$$\widehat{F}_s(t) = \begin{cases} F_s\big(\tau(t) - \tau_s\big) & \text{if } \tau(t) \geq \tau_s \\ 0 & \text{else} \end{cases},$$

$\tau_s > 0$ denotes the thermal time at which senescence starts. Hence

$$s_{\spadesuit}(t) = \frac{d}{dt}\Big(\widehat{F}_s(t) \cdot A_{\spadesuit}(t)\Big), \tag{22}$$

where $A_{\spadesuit}(t) = a_{\spadesuit}(0) + \int_0^t a_{\spadesuit}(u)\, du$ denotes the cumulative production of foliage until time t. For later use we also define the cumulative leaf senescence $S_{\spadesuit}(t) = \int_0^t s_{\spadesuit}(u)\, du$.

The increase and decrease of foliage hitherto computed at the whole-plant scale are now transferred to the local level in terms of functions a and s satisfying

$$\int_{\mathbb{R}^2} a(x,t)\, dx = a_{\spadesuit}(t) \cdot \text{SLA} \quad \text{and} \quad \int_{\mathbb{R}^2} s(x,t)\, dx = s_{\spadesuit}(t) \cdot \text{SLA},$$

SLA denoting specific leaf area [$m^2\, g^{-1}$], which is assumed to be constant over the growth process. We make the simple approach of the local allocation to foliage being proportional to the existing local foliage quantity:

$$\begin{aligned} a(x,t) &= \frac{\spadesuit(x,t)}{\int_{\mathbb{R}^2} \spadesuit(x,t)\, dx} \cdot a_{\spadesuit}(t) \cdot \text{SLA} \\ s(x,t) &= \frac{\spadesuit(x,t)}{\int_{\mathbb{R}^2} \spadesuit(x,t)\, dx} \cdot s_{\spadesuit}(t) \cdot \text{SLA} \end{aligned} \tag{23}$$

This completes the reaction term of (17).

We now specify the propagation term $J = J(x,t)$ of (17), using a slightly different form than (10):

$$J(x,t) = -k \cdot a(x,t) \cdot \nabla_x \spadesuit(x,t) \tag{24}$$

with a mobility constant $k > 0$. The flux magnitude thus corresponds to the local allocation of foliage. The gradient we use here, $\nabla_x \spadesuit(x,t)$, pointing in the direction of the greatest rate of decrease in horizontal leaf density – inducing a motion away from high and towards low $\spadesuit$, corresponding to shaded and lit regions, respectively – points in the same direction as the local light gradient,

$$\nabla_x \exp(-\lambda \cdot \clubsuit(x,t)) = -\lambda \cdot \exp(-\lambda \cdot \clubsuit(x,t)) \cdot \nabla_x \clubsuit(x,t)$$

We thus merely omit the exponential diffusion coefficient affecting the local flux magnitude, while preserving the direction of the phototropic flux (cf. 3.3). This choice will later allow a rigorous mathematical treatment of (17).

The description of a population P of plants in a field requires a few modifications in order to take inter-individual competition for light into account. An indexed equivalent of (17) reads

$$\frac{\partial}{\partial t}\spadesuit^{(p)} = a^{(p)} - s^{(p)} - \nabla_x J^{(p)} \qquad \text{for every plant } p \in P.$$

In this setting, the portion of light reaching a ground point x now equals $\exp\big(-\lambda \cdot \sum_{p\in P} \spadesuit^{(p)}(x,t)\big)$, as detailed in section 3.4. The generalisation of the biomass production (18) for plant $p \in P$ reads

$$b^{(p)}(t) = \text{RUE} \cdot \text{PAR}(t) \cdot \int_{\mathbb{R}^2} \frac{\spadesuit^{(p)}(x,t)}{\sum_{\pi\in P} \spadesuit^{(\pi)}(x,t)} \cdot \left(1 - \exp\left(-\lambda \cdot \sum_{\pi\in P} \spadesuit^{(\pi)}(x,t)\right)\right) dx.$$

The weight coefficient $\frac{\spadesuit^{(p)}(x,t)}{\sum_{\pi\in P} \spadesuit^{(\pi)}(x,t)}$ assigns intercepted light to the different individuals, and is the natural choice in absence of information on the vertical distribution of the foliage of the members of P. Nevertheless, strictly speaking, it makes the tacit presupposition that the relative vertical profiles are similar, which had been one of the conditions for the reasonable use of $\spadesuit$ in section 2.2.

Based on $b^{(p)}(t)$, total allocation and senescence, as well as the local reaction terms, $a^{(p)}$ and $s^{(p)}$, are computed for each plant just as before. In particular, the functions p, F_a and $\widehat{F}_s$ in (20) and (22) are the same for each individual. Lastly, the generalisation of the flux term (24) for plant p reads

$$J^{(p)}(x,t) = -k \cdot a^{(p)}(x,y,t) \cdot \nabla_x \left(\sum_{\pi\in P} \spadesuit^{(\pi)}(x,t)\right).$$

4.2 REDUCTION TO THE POROUS MEDIUM EQUATION

The obtained system of equations, containing the relatively heavy to numerically compute continuity equation (17), can be significantly simplified in the case of a single plant, i.e. one which is not (yet) exposed to competition. This is achieved by transforming it into the well-studied porous medium equation, for which an explicit solution is known for specific initial conditions.

Proposition 1. Consider a single, spatially isolated plant with horizontal leaf density $\spadesuit = \spadesuit(x,t)$. Let $\spadesuit$ be subject to parabolic initial conditions and no further boundary conditions. Then $t \mapsto A_\spadesuit(t)$ can be expressed in terms of a first-order ordinary differential equation.

Proof. We will derive the desired equation constructively: Entering the equality

$$\text{SLA} \cdot \int_{\mathbb{R}^2} \spadesuit(x,t)\, dx = A_\spadesuit(t) - S_\spadesuit(t)\,. \tag{25}$$

into the definitions of $a_\spadesuit$, $s_\spadesuit$ and J, (17) becomes

$$\frac{\partial}{\partial t}\spadesuit = \nabla_x \cdot \left(\frac{k \cdot a_\spadesuit}{A_\spadesuit - S_\spadesuit} \cdot \spadesuit \cdot \nabla_x \spadesuit \right) + \spadesuit \cdot \frac{a_\spadesuit - s_\spadesuit}{A_\spadesuit - S_\spadesuit},$$

where we dropped the arguments x, t for short. Let $v(x,t) = \frac{\spadesuit(x,t)}{A_\spadesuit(t) - S_\spadesuit(t)}$, then

$$\frac{\partial}{\partial t} v = k \cdot a_\spadesuit \cdot \nabla_x \cdot (v \cdot \nabla_x v)\,.$$

Let $H(t) = \frac{k}{2} \cdot A_\spadesuit(t) + H_0$, with H_0 depending on the chosen initial conditions (see below), and define the new variable $\nu = H(t)$ and the function $w = w(x, \nu)$ such that $v(x,t) = w(x, H(t))$. This yields the porous medium equation

$$\frac{\partial}{\partial \nu} w = \nabla_x \cdot (2w \cdot \nabla_x w)\ . \tag{26}$$

For parabolic initial conditions and no further boundary conditions, an explicit solution of (26) over the whole $\mathbb{R}^2$ is in fact known as the Zel'dovich-Kompaneets-Barenblatt solution (Vazquez, 2007). It reads

$$w(x,\nu) = \max\left(0, \frac{C}{\sqrt{\nu}} - \frac{\|x\|^2}{16\nu}\right) \tag{27}$$

for $\nu > 0$, where the constant C is chosen to be in accordance with the given initial conditions: We have

$$\int_{\mathbb{R}^2} w(x,\nu)\, dx = 8\pi C^2,$$

independently of ν. Applying this to the definition of w yields for $t = 0$

$$A_\spadesuit(0) \cdot 8\pi C^2 = \int_{\mathbb{R}^2} \spadesuit(x,0)\, dx,$$

and the latter term equals $\frac{A_\spadesuit(0)}{\mathrm{SLA}}$. Hence $C = \frac{1}{\sqrt{8\pi \cdot \mathrm{SLA}}}$. The value of the constant H_0 follows after fixing the radius of the initial support of $\spadesuit$ at $t = 0$, which we do by choosing $\spadesuit(\cdot, 0)$ as a Dirac delta function.

By definition of w we have

$$\spadesuit(x,t) = \left(A_\spadesuit(t) - S_\spadesuit(t)\right) \cdot w\left(x, \frac{k}{2} \cdot A_\spadesuit(t) + H_0\right). \tag{28}$$

Recalling $S_\spadesuit(t) = \widehat{F}_S(t) \cdot A_\spadesuit(t)$ and $\frac{d}{dt} A_\spadesuit(t) = a_\spadesuit(t)$, (18) reads

$$\frac{d}{dt} A_\spadesuit(t) = \gamma(t) \cdot \mathrm{RUE} \cdot \mathrm{PAR}(t) \cdot \int_{\mathbb{R}^2} 1 - \exp\left(-\lambda \cdot A_\spadesuit(t) \cdot (1 - \widehat{F}_S(t)) \cdot w\left(x, \frac{k}{2} \cdot A_\spadesuit(t) + H_0\right)\right) dx. \tag{29}$$

Entering (27) into (29) yields after a change of variables

$$\frac{d}{dt}A_{\spadesuit}(t) = \frac{A(t)}{2}\cdot \int_0^{R(H(t))} \left(1 - \exp\left(\frac{B(t)\cdot A_{\spadesuit}(t)}{\sqrt{H(t)}}\cdot\left(C - \frac{r^2}{16\cdot\sqrt{H(t)}}\right)\right)\right)\cdot r\,dr,$$

where $R(t) = \sqrt{16\cdot C\cdot\sqrt{t}}$, $C_1(t) = 8\pi\cdot \text{RUE}\cdot \text{PAR}(t)\cdot\gamma(t)$ and $C_2(t) = -\lambda\cdot(1-\widehat{G}_s(t))$ for short. The upper integration limit $R(t)$ is the radius of the disk-shaped support of the appropriate w, beyond which w and therefore the entire integrand vanish. Finally, we have

$$\frac{d}{dt}A_{\spadesuit} = CC_1\sqrt{2k\cdot A_{\spadesuit} + 4H_0} + \frac{kC_1\cdot A_{\spadesuit} + 2H_0C_1}{C_2\cdot A_{\spadesuit}}\cdot\left(1 - \exp\left(\frac{2CC_2\cdot A_{\spadesuit}}{\sqrt{2k\cdot A_{\spadesuit}+4H_0}}\right)\right), \quad (30)$$

as desired.

□

Corollary 1. Under the same assumptions as in proposition 1, the dynamics of ♠ are known up to an explicitly known ordinary differential equation as well.

Proof. A solution of (30) provides ♠ via (28) minding (27). □

Remark 1. Since $a_{\surd}(t) = \frac{1-\gamma(t)}{\gamma(t)}\cdot\frac{d}{dt}A_{\spadesuit}(t)$, cf. (19), root allocation is also known up to an ordinary differential equation. Alternatively, the ordinary integral equation

$$a_{\surd}(t) = \frac{1-\gamma(t)}{\gamma(t)}\cdot f\left(\int_0^t \frac{p(u)}{1-p(u)}\cdot a_{\surd}(t)\,du\right)$$

holds, where f is as in $\frac{d}{dt}A_{\spadesuit}(t) = f\big(A_{\spadesuit}(t)\big)$ in (30).

Remark 2. A key theoretical property of solution (27) (as also for solutions of a more general porous medium equation) is that it has a compact support for all fixed times (Vazquez, 2007). This is conserved under the carried out transformations and thus holds for ♠ as well. Not least, this feature, known as finite speed of propagation, is a desirable one from a biological point of view.

It also implies the existence of a so-called free boundary, dynamically separating regions with foliage, $\spadesuit > 0$, from those without, $\spadesuit = 0$. In our case this boundary can for each $t \geq 0$ be straightforwardly determined as the circle centred in the sowing position with radius $\sqrt{16\cdot C\cdot\sqrt{H(t)}}$, while the speed of propagation is the derivative with respect to t of this expression.

4.3 SIMULATIONS

For an isolated plant with no further boundary constraints, we can resort to (30) for the entire length of a simulation. Figure 8 illustrates the behaviour of ♠ as well as total root and leaf allocation, $A_{\surd}(t)$ and $A_{\spadesuit}(t)$, respectively, over time.

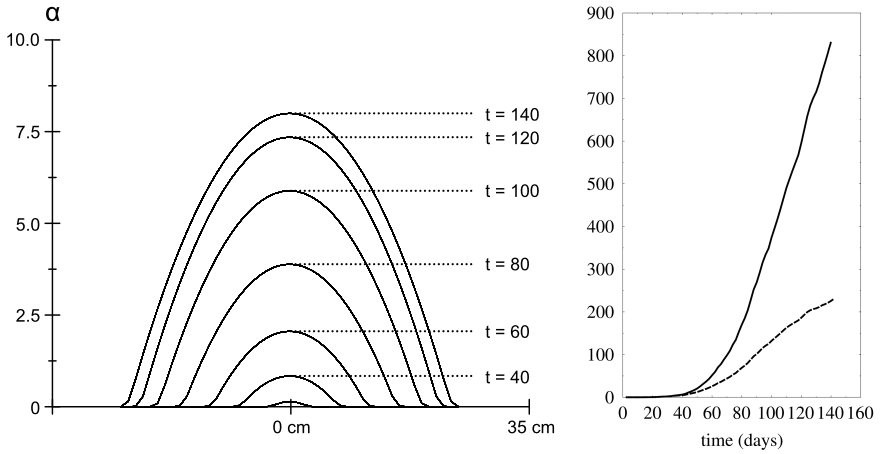

(a) (b)

Figure 8.: Simulation of an isolated plant. Model parameters are the ones used in section 4.3.1.1. (a) Vertical cross-section of the axially symmetric graph of ♠(x, t) for various times t [days]. We notably observe the properties theoretically derived before. (b) Total root $A_{\surd}(t)$ (solid line) and leaf mass $A_{\spadesuit}(t)$ (dashed line) production [g].

4.3.1 *Spatially homogeneous field*

A regularly spaced field such as the one considered in section 4.3.1.1 below is simulated according to the procedure detailed in section 3.4.1: We simulate a single, average plant on a rectangular cell, with length and width corresponding to half of the vertical and horizontal distance of the sowing positions, respectively, while accounting for its competitors, growing and shading symmetrically, through periodic cell boundary conditions.

In this context and against the background of numerical computation, the benefit of the transformation carried out in section 4.2 becomes apparent: Starting from sowing at $t = 0$, we can compute the growth dynamics of a plant in a homogeneous field by resorting to the ordinary differential equation (30) instead of the partial differential equation (17), up to the moment when the plant's foliage first reaches

the Voronoi cell boundary, corresponding to canopy closure.

From that moment onward, (17) is used to compute growth. However, in our simulations we observe that in the further course of time, the space between neighbouring plants is progressively filled with foliage and that, in fact, the quantity

$$\max_{x\in\Sigma} ♠(x,t) - \min_{x\in\Sigma} ♠(x,t)\ ,$$

where $\Sigma \subset \mathbb{R}^2$ denotes the plant's Voronoi cell, tends to zero as t becomes large. Accepting the respective computational error, this suggests to pass on to the case of a spatially uniform $♠ = ♠(t)$ once the above difference falls below a suitably small value.

In this case, having $\nabla_x ♠ = 0$, (17) reduces to

$$\frac{d}{dt}♠(t) = \frac{a_♠(t) - s_♠(t)}{|\Sigma|} \cdot \text{SLA}. \tag{31}$$

where $|\Sigma|$ denotes the area of Σ. Integration yields

$$\begin{aligned} ♠(t) &= \frac{A_♠(t) - S_♠(t)}{|\Sigma|} \cdot \text{SLA} \\ &= \frac{\left(1 - \widehat{F}_s(t)\right) \cdot A_♠(t)}{|\Sigma|} \cdot \text{SLA}. \end{aligned}$$

Entering this into (18), minding (19), results in the ordinary differential equation

$$\frac{d}{dt}A_♠(t) = \text{RUE}(t) \cdot \text{PAR}(t) \cdot \gamma(t) \cdot |\Sigma| \cdot \left(1 - \exp\left(-\lambda \cdot \frac{\left(1 - \widehat{F}_s(t)\right) \cdot A_♠(t)}{|\Sigma|} \cdot \text{SLA}\right)\right). \tag{32}$$

This particular case corresponds to the approach by Cournède et al. (2008), where however $|\Sigma|$ is additionally a function of time.

Hence the only time interval in which the direct use of (17) is actually inevitable begins at the moment of canopy closure and ends when the plant's Voronoi cell is covered with foliage in a quasi-uniform manner. For both the time periods before and after that, it is merely an ordinary differential equation which is to be numerically dealt with.

As an aside, we note that an explicit solution of (32) is readily found for $t < \tau_s$, i.e. in case of a very dense field for which ♠ is quasi-uniform from some time $\bar{t}$ onward before senescence first takes effect. In this case, entering the right hand side of (32) into (31) minding $\widehat{F}_s = s_♠ = 0$ yields

$$\frac{d}{dt}♠(t) = \text{RUE} \cdot \text{PAR}(t) \cdot \gamma(t) \cdot |\Sigma| \cdot (1 - \exp(-\lambda \cdot ♠(t)))$$

Substituting

$$v(t) = \exp(\lambda \cdot \spadesuit(t))$$

yields

$$\frac{d}{dt}v(t) = \lambda \cdot \text{RUE} \cdot \text{PAR}(t) \cdot \gamma(t) \cdot |\Sigma| \cdot (v(t) - 1)$$

which has the solution

$$v(t) = (\exp(\lambda \cdot \spadesuit(t_0)) - 1) \cdot \exp\left(\int_0^t \lambda \cdot \text{RUE} \cdot \text{PAR}(t) \cdot \gamma(t) \cdot |\Sigma|\, dt\right) + 1$$

for $t \in [\bar{t}, \tau_s]$.

4.3.1.1 *Comparison to data*

Field experiments were conducted in 2008 in the Beauce plain near Pithiviers, France, N48°10′ 12″, E2°15′7″ by the French Technical Industrial Sugarbeet Institute (I.T.B., Paris). A single commercial cultivar (Radar) was sown on April 11 with a distance of 50 cm in between rows and two different distances between seed-plots, 18 cm and 12 cm. After plant emergence (corresponding to the date when 80% of the final population was reached), which occurred on April 28, the most uniform sections of a large sugar beet field were selected for the trials. Two weeks later, one plant out of two was removed in a subset of the lower density section, yielding a configuration with 36 cm between two plants of a row. The three populations thus correspond to 5.4, 10.9 and 16.4 plants m^{-2}. Irrigation and fertilisation were conducted for all densities to ensure unstressed conditions. Lemaire et al. (2009) provided further details. Daily mean values of air temperature [°C] and solar radiation [J m^{-2}] were obtained from French meteorological advisory services (Météo France) 5 km away from the experimental site.

The seed mass b_0, the specific leaf area SLA and the thermal time until senescence τ_s could be deduced from direct measurement, and were found to be 0.003 g, 0.013 $\text{m}^2\,\text{g}^{-1}$ and 400 C° days, respectively. Following Andrieu et al. (1997) and Hodáňová (1972), the extinction coefficient λ was set to 0.7. Parameters γ_0, γ_f, μ_a, σ_a, μ_s, σ_s (cf. (18), (20), (22) respectively) correspond to those identified by Cournède et al. (2013).

The two remaining parameters, the radiation use efficiency RUE and the diffusion coefficient k, were estimated by model inversion, using the experimental data of the three configuration densities. Table 1 summarizes.

RUE	k	γ_0	γ_f	μ_a	σ_a	μ_s	σ_s	λ	b_0	SLA	τ_s
4.3	**30**	0.9	0.2	5.7	1.05	8.0	0.37	0.7	0.003	0.013	400

Table 1.: Values of model parameters, newly estimated ones indicated in bold.

Figure 9 illustrates the results of simulations of the three different density scenarios, using the estimated parameters. The graphs accord well with the given data for $A_{\vee}$ and $A_{\spadesuit}$, which vary considerably in magnitude among the three densities. The fact that the model adapts well to these different conditions, despite a common set of parameters for all scenarios, corresponds precisely to the phenomenon described in section 3.4.

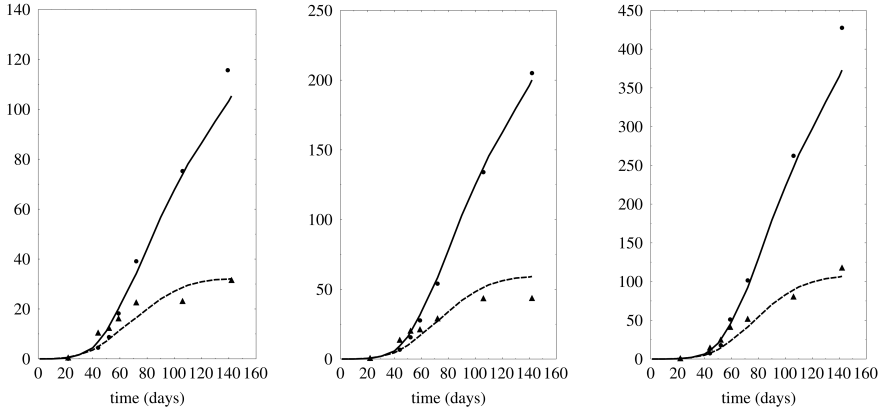

(a) 16.4 plants m^{-2} (b) 10.9 plants m^{-2} (c) 5.4 plants m^{-2}

Figure 9.: Comparison of simulations using the parameters listed in table 1 to experimental data on $A_{\vee}(t)$ (solid line, bullets) and $A_{\spadesuit}(t)$ (dashed line, triangles) [g], per plant, for three different field densities.

Model variables corresponding to different densities are obviously identical up to the moment when one plant's foliage first meets that of a neighbour (canopy closure). This is an advantage of the present model over comparable ones where some parameters and thus the growth dynamics depend on the field density throughout the entire simulation, e.g. the Greenlab model for sugar beet (Lemaire et al., 2009) or maize (Ma et al., 2008).

Inversely, the data available to us allows to deduce from the points in time, when the production curves corresponding to different densities first begin to significantly deviate from one another, the moments when in the lower density cases neighbouring plants enter competition. Our simulations show that the parametrized model, in terms of the speed of spatial propagation of ♠ (cf. remark 2), is indeed well in accordance with these times, specified by Lemaire et al. (2009).

4.3.2 *Heterogeneous field*

An irregularly planted, heterogeneous field has to be approached in the way presented at the of section 4.1, taking each plant individually

into account. The possibility of speeding up the simulation for early times remains unaffected by this: For as long as the foliage of a particular plant $p \in P$ does not meet that of any other plant, i.e. for those $t \in \mathbb{R}_+$ for which

$$\spadesuit^{(p)}(x,t) > 0 \;\Rightarrow\; \spadesuit^{(\pi)}(x,t) = 0 \quad \text{for all } \pi \in P \setminus \{p\}$$

holds for all $x \in \mathbb{R}^2$, the growth of plant p can be computed via (30).

Moreover, we note the experimental observation that, under periodic boundary conditions, the field as a whole tends to a spatially uniform cumulative leaf area index:

$$\max_{x\in\mathbb{R}^2} \sum_{\pi\in P} \spadesuit^{(\pi)}(x,t) - \min_{x\in\mathbb{R}^2} \sum_{\pi\in P} \spadesuit^{(\pi)}(x,t) \xrightarrow[t\to\infty]{} 0\,.$$

Thus, if the centre of attention lies merely on the overall production of the field rather than the evolution of its individuals, as before, one may pass on to a uniform cumulative $\spadesuit$ and the appropriate ordinary differential equation once the computational error can be said to be sufficiently small - and hence, in a manner of speaking, treat the entire field as a single plant with a uniform horizontal leaf density.

As an illustration of the model's performance in a heterogeneous case we take on an exercise carried out by Cournède et al. (2008): Three field scenarios, depicted in figure 10, corresponding to different success rates of germination, are considered. This is motivated by the interest in identifying effects of compensation of the lower density fields compared to the high density one.

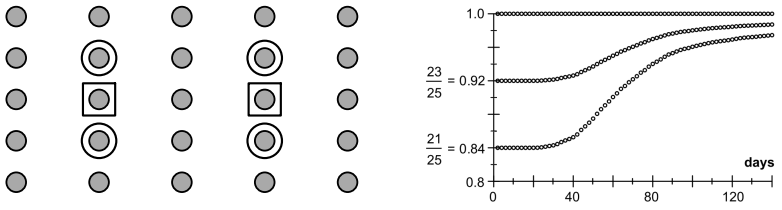

(a) (b)

Figure 10.: (a) Three field scenarios of (i) all indicated 25 plants, (ii) the 23 not marked with a square and (iii) the 21 not marked with a circle, respectively. The distances between neighbouring sowing locations are 50 cm horizontally and 18 cm vertically. (b) Cumulative biomass production $\int_0^t b(u)\,du$ over time t of scenarios (ii) and (iii) divided by that of (i). The initial ratios of $\frac{23}{25}$ and $\frac{21}{25}$ caused by the missing plants, gradually increase, indicating a compensation effect due to less intense competition.

Running the three simulations (using the system parameters obtained in section 4.3.1.1) and plotting the ratio of the total biomass

production of each of the heterogeneous fields with 23 and 21 plants, respectively, to the total biomass production of the homogeneous field with 25 plants, points indeed to a compensation effect: The initial production deficit due to the missing, ungerminated plants, is partly compensated for by the growth of the others, which are subject to less inter-individual competition than in the homogeneous case. These results are also in good accordance with those observed by Cournède et al. (2008).

4.4 DISCUSSION

In summary, our time-continuous model based on horizontal leaf density successfully captures density-dependent growth dynamics of sugar beet. With merely species-specific model parameters, the model mechanism of spatial expansion in the direction of the greatest decrease of horizontal leaf density brings about a spontaneous adaptation with respect to competitors. By simplifying the mobility coefficient of the actual spatial gradient of light incidence, we were able to describe the dynamics of ♠ in terms of a partial differential equation that could be related to the porous medium equation, thus allowing to express its solution in terms of an ordinary differential equation for the case of a single plant. The model framework is generic enough to allow not only other organ compartments beyond foliage and roots considered here, but also additional physiological processes and constraints, which have been kept to a minimum in this approach, to be incorporated.

Depending on the intended purpose of the model, the use of horizontal leaf density ♠ is not inevitably limited to plants that are small in height. We illustrate this by means of the following modelling perspective: Over a wide range of conditions, the insensitivity of tree height to stand density has been observed (Lanner, 1985). Moreover, in the long term, mono-species even-aged stands generally tend towards a regular horizontal distribution of individuals (Cooper, 1961; Ford, 1975; Kenkel, 1988). These observations suggest an alignment of the vertical leaf area profiles across the individuals, which strongly motivates the use of horizontal leaf density ♠ to model canopy dynamics in such scenarios in place of the more complex and computationally heavy 3D leaf density ♣. Introducing empirical functions for height-related processes where necessary could make up for the lack of vertical information in ♠. A particularly interesting phenomenon to model in this context are gap dynamics, more specifically the closure of a light gap resulting from a fallen branch or tree by the surrounding crowns. Figure 11 shows the vertical projection of a terrestrial laser scan taken in a pure, even-aged beech stand. The gap induced by the removal of a tree is visibly closed as the surrounding crowns locally

extent their crowns along the light gradient pointing towards the interior of the gap. In the case of an approximate vertical homogeneity across individual crowns, this process is essentially a horizontal one, suggesting the use of ♠ for an efficient modelling approach.

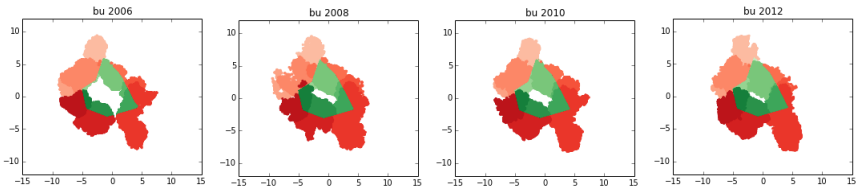

Figure 11.: Vertical projections of eight Lidar-recorded 69±4 year-old beech tree crowns reconquering a gap over a duration of six years near Freising, Germany. The vertices of the green polygon mark the stem bases. With kind permission from Dominik Bayer.

5

CONTINUOUS-TIME MODELLING OF TREE GROWTH

The formation and continuous expansion of leaves during organogenesis lends itself to a description in terms of the general continuity equation (2), and has been illustrated in the previous chapter. In this and the following chapters, we turn our focus to the dynamics of tree crowns, for which the three-dimensional leaf density ♣ is a more appropriate variable than the previously considered horizontal leaf density ♠, which lacks information in the now more important vertical direction. In particular, the interplay of foliage and wood, which we approach by means of the pipe model theory (section 3.5.1), calls for new modelling techniques.

Modelling leaf density dynamics of trees at a large time scale, i.e. the evolution of $t \mapsto \clubsuit(\cdot, t)$ over several years, instead of the short time scale period of foliation, proves to be conceptually more challenging, although at first glance, it might appear amenable to (2) as well: Emblematically speaking, a tree's leaf density gradually moves upward and horizontally outward over the years, while simultaneously increasing in total quantity.

Upon closer look, however, the compatibility of leaf density dynamics and (2) becomes arguable from a mechanistic point of view. Whereas the reaction term f could still reasonably be related to the formation of new foliage during bud break, the flux term J lacks a biophysical basis. Leaves do not move in the sense of biological populations; instead, the abstract expansive motion of leaf area in the course of the tree's growth is the consequence of old leaves falling and new ones forming in different positions. What is more, the process is accompanied by a corresponding formation of sapwood. This last mechanism is also the reason why the formation of new leaves cannot be considered as merely a local process: Whether in terms of the pipe model theory or a different rule, the allocation of biomass locally produced by a leaf occurs at the global scale, manifesting itself from the tip of a branch all the way down to the roots. Now, if we aim to describe the motion of leaf density in a time-continuous way, we can certainly not account for the above mechanism by incorporating the formation of new sapwood pipes for a continuously moving leaf density at each infinitesimal time step: The toal sapwood mass corre-

sponding to some leaf density ♣ is a positive quantity (namely (15)), and cannot be covered by the infinitsimal amount of biomass produced by ♣ in an infinitesimal time step. Quite apart from that, forming an entire set of pipes, corresponding to the appropriate leaf density, at each infinitesimal would imply an infinite amount of sapwood after any given positive time interval.

These considerations lead to the sobering revelation that while an equation of the type (2) may principally have the potential to capture leaf density dynamics, it is a priori unable to do so by reflecting the actual underlying mechanisms. Nevertheless, continuity equations have proven to allow concise and efficient descriptions of natural phenomena, motivating the aims of this chapter, which are to explore, within the above-described constraints, remaining possibilities of describing the evolution of leaf density for trees on a large time scale in this particular framework. In this way, the chapter forms a transition from the previous one, based on a similar technical setting in 2D, to the consecutive ones, likewise focussing on trees in three dimensions, yet in a more biologically appropriate discrete-time approach. As opposed to those, this more theoretical excursus puts a stronger emphasis on conceptual modelling as well as qualitative dynamics rather than quantitative evaluation. Our aims are thus to explore how a continuity equation approach can be accommodated to tree crown dynamics, to identify the potential of the former for the description of the latter and to better understand their interplay.

Throughout the following, we define two principles as basic requirements for any reasonable approach, namely

- a consistent mass budget in the way that all of the biomass produced by a given leaf density is indeed allocated (cf. section 3.5)
- the balance between leaf area quantity and location on the one hand, and corresponding sapwood pipe mass on the other hand, formulated in the pipe model theory (section 3.5.1), being maintained at all times

Against the background of the a priori constraints of a continuity equation approach described above, this chapter presents two model approaches that allow for the above two guidelines in two conceptually different ways. In section 5.1, we describe crown dynamics from a top down perspective, that puts aside local processes, by accommodating biomass production and allocation as well as the pipe model theory at the global tree scale. In contrast, as well as in response to certain shortcomings of the latter, section 5.2 presents a fully local approach, in which locally produced biomass is also allocated locally. Since, as follows from the above considerations, this is not possible via describing the actual mechanisms, we devise a hypothetical process

different from the real one, but which exhibits very similar features to those of actual organogenesis while being expressible in terms of (2). Section 5.3 concludes with a comparative discussion.

Without comparison to empirical data, we restrict ourselves to a qualitative analysis of the spatial model dynamics in this chapter. For the sake of convenience, we assume vertical and supposedly constant light incidence.

5.1 A GLOBAL APPROACH

5.1.1 *Model description*

In this first approach, the conceptual inconsistency of a flux term J, describing the gradual motion of leaf density from a top-down perspective, and a biologically motivated reaction term f is avoided by considering the relative leaf density subject to a mass-conserving transport equation, i.e. (2) with $f \equiv 0$, based on which absolute leaf density is deduced by filling the relative leaf density by means of information on whole-tree-level mass.

This model was previously presented by Beyer et al. (2014).

We consider the relative leaf density

$$\widehat{\clubsuit}(x,t) = \frac{\clubsuit(x,t)}{\int_{\mathbb{R}^3} \clubsuit(\xi,t)\, d\xi}$$

from which, at any time t, absolute leaf density $\clubsuit(\cdot,t)$ is inferred via

$$\clubsuit(x,t) = c(t) \cdot \widehat{\clubsuit}(x,t) \tag{33}$$

for an appropriate total leaf area quantity $c(t) > 0$. Throughout the simulation, $\widehat{\clubsuit}$ is subject to the transport equation

$$\frac{\partial}{\partial t}\widehat{\clubsuit}(x,t) = -\nabla_x \cdot J(x,t) \tag{34}$$

for a flux term $J \in \mathbb{R}^3$. This formulation implies $\int_{\mathbb{R}^3} \widehat{\clubsuit}(x,t)\, dx = 1$ for all times t, as desired. Similar as in chapter 4 we choose

$$J(x,t) = k \cdot \clubsuit(x,t) \cdot \nabla_x L(x,t), \tag{35}$$

(cf. section 3.3) where

$$L(x,t) = \text{PAR} \cdot \exp\left(-\lambda \cdot \int_{x_3}^{\infty} \clubsuit(x_1, x_2, \xi_3, t)\, d\xi_3\right)$$

denotes the light incidence in the point $x \in \mathbb{R}^3$ at time t (based on the absolute leaf density) for an instantaneous photosynthetically active radiation PAR reaching the tree, as described in detail in section 3.1 (cf. (4)).

In order to determine $c(t)$, we compute the total instantaneous biomass production at time t at the tree level, which reads

$$B(t) = \int_{\mathbb{R}^3} \text{RUE} \cdot \lambda \cdot \clubsuit(x,t) \cdot L(x,t)\, dx,$$

as detailed in section 3.2 (cf. (7)), RUE denoting radiation use efficiency. Assuming that produced biomass is instantly allocated, and additionally, becomes senescent after a certain time span τ_s no matter to which compartment it was allocated (e.g. the pipe model theory (section 3.5.1) implies that a leaf and its sapwood pipe becomes senescent at the same time), the living biomass at time t is given by

$$M(t) = \int_0^t B(u) - B(u - \tau_s)\, du. \tag{36}$$

This mass $M(t)$ consists of foliage and sapwood mass, and thus, following the pipe model theory, the equation

$$M(t) = \underbrace{\int_{\mathbb{R}^3} \frac{1}{\text{SLA}} \cdot c(t) \cdot \widehat{\clubsuit}(x,t)\, dx}_{\text{total leaf mass}} + \underbrace{\int_{\mathbb{R}^3} \frac{1}{\text{SLA}} \cdot c(t) \cdot \widehat{\clubsuit}(x,t) \cdot P \cdot \|x\|_Y\, dx}_{\text{total sapwood mass, cf. (15)}} \tag{37}$$

is required to hold, from which we obtain

$$c(t) = \frac{M(t)}{\int_{\mathbb{R}^3} \frac{1}{\text{SLA}} \cdot \widehat{\clubsuit}(x,t) \cdot (1 + P \cdot \|x\|_Y)\, dx}.$$

The model is completed by an initial condition, which we take to be Dirac in the origin, $\clubsuit(x,0) = \delta_0(x)$.

In summary, at any point in time, leaf density $\clubsuit$ is obtained by rescaling $\widehat{\clubsuit}$ minding the total living mass, (36), and the pipe model theory, (37). This approach can be related to a simple centralistic, common pool biomass distribution scheme (cf. Marcelis, 1994; Kurth and Sloboda, 1997). Simultaneously, $\clubsuit$ determines the dynamics of $\widehat{\clubsuit}$ in (34).

5.1.2 *Simulations*

Measureable model parameters used in the following simulations correspond to those referenced in table 2, the remaining ones were set to $k = 6$, $\text{PAR} \cdot \text{RUE} = 0.05$, $P = 0.1$ and $\tau_s = 1$, different values yield very similar qualitative dynamics. Figure 12 shows the evolution of leaf density $t \mapsto \clubsuit(\cdot, t)$ for a spatially isolated tree with no surrounding competitors. The light gradient induces a half-spherical-like vertical and horizontal expansion, resulting in an overall broad crown shape. Although leaf density in the centre of the crown envelope is significant, we observe the predominant presence of foliage at the upper crown hull.

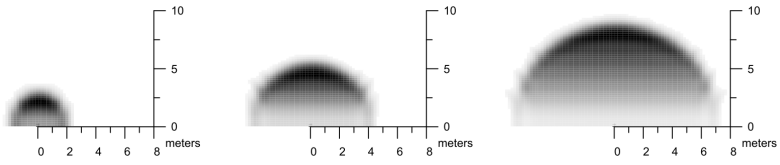

(a) (b) (c)

Figure 12.: Qualitative leaf density dynamics of a spatially isolated simulated tree (vertical cross section) at (a) 20, (b) 70 and (c) 150 years. Black colouring represent the maximal leaf density at the respective time, gray areas have linearly less leaf density. Note the high degree of self-similarity across time.

Figure 13 illustrates the model behaviour in a competition scenario. As described in detail in section 3.4.1, competitors of the same age around the simulated tree are accounted for by means of periodic boundary conditions across the boundary of a cell in which the tree grows and whose surface area is the inverse of the exogenously given stand density at the appropriate moment in time. Here we used the time-dependent stand density shown in figure 15, sub-plot 3.

As described in detail in section 3.4, competition with surrounding individuals results in the limitation of the horizontal expansion of the simulated tree due to the light gradient vanishing at the boundary of the cell in which it grows, given that leaf density and consequently local light conditions on the other side of the boundary are simulated equal to those within. Apart from that, the pattern remains similar to the isolated case in figure 12, namely in terms of the curved shape and increased concentration of foliage at the top of the tree, but also the persistence of leaves in the interior part.

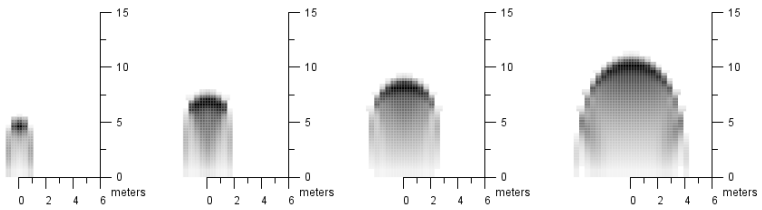

(a) (b) (c) (d)

Figure 13.: Qualitative leaf density dynamics of a simulated tree in competition with neighbours at (a) 25, (b) 60, (c) 90 and (d) 140 years. Time-dependent stand density, defining the boundary region (cf. section 3.4.1 for details), corresponds to the one shown in figure 15, sub-plot 3 (cf. also section 6.2.1).

The overall crown shape generated by the model can be related to a broad crown morphology, and the higher concentration of leaf density at the hull, particularly at the top, reflects many species' crown structure. Nevertheless, the considerable density in the crown interior in both the isolated and the competition scenario remains arguable. It is in particular the result of the global rescaling (33), where available biomass is distributed even to regions where, realistically, significant quantities of leaves are no longer formed. This demonstrates the need for local control over modelled foliage dynamics and motivates the subsequent section based on a different methodological approach.

5.2 A LOCAL APPROACH

The key drawback of the previous approach is a simplistic redistribution of available biomass following a global-scale determination of it. In this section, we present a contrasting alternative that strongly focusses on the locality of biomass production and allocation. The continuity equation (2) lends itself to the general objective of a local process description, however, as reasoned in the introduction to this chapter, this equation type is not compatible with the actual biophysical mechanisms. This, in turn, leaves only one possibility from a modelling point of view, which is to describe a different, hypothetical process, inspired by actual organogenesis and generating dynamics very similar to the real ones, but which has the property of being expressible in terms of (2). In this section we describe a possible such approach.

In the introduction to this chapter we noted the impossibility of coupling the continuous motion of leaf density with the simultaneous formation of a complete set of corresponding new sapwood pipes at every infinitesimal time step. This motivates the basic approach of this section's model to extent existing pipes while the leaves that they support are moving. In the following section, we motivate and formalize this approach in detail. For the sake of clarity, we initially ignore the processes of biomass allocation to foliage and the senescence of old leaves – as well as the senescence of sapwood associated therewith in the framework of the pipe model theory –, and incorporate these afterwards, thus defining the complete model.

5.2.1 *Model description*

MASS-CONSERVING MOVEMENT OF LEAF DENSITY Under the temporary premise of a conservation of total leaf area following from the non-consideration of leaf formation as well as abscission, we start off with the equation

$$\frac{\partial}{\partial t}\clubsuit(x,t) = -\nabla_x \cdot \left(k^*(x,t) \cdot J(x,t)\right) \tag{38}$$

for the motion of leaf density along the vector field

$$J(x,t) = \clubsuit(x,t) \cdot \nabla_x L(x,t), \tag{39}$$

similar to (35), and with a local magnitude coefficient $k^*(x,t) \geq 0$ that we derive in the following, subject to the two basic principles itemized at the end of the introduction to this chapter. Note that total leaf area is indeed conserved in (38), reflecting the specific above defined scenario.

Since we do not account for the senescence of foliage in this section, we also set aside the senescence of sapwood, in view the tight link between these two components in the pipe model theory. This setting requires the sapwood pipes corresponding to a leaf density at a time $t + dt$ to be built on those at time t, which support the leaf density at this point in time. Consequently, in order to provide the continued support of a moving leaf density, the existing pipes need to be extended appropriately. Extending the sapwood pipe supporting foliage in x at time t according to the infinitesimal movement of that foliage at time t as formulated in (38), requires

$$k^*(x,t) \cdot \nabla_{J(x,t)} \|x\|_Y \cdot P \cdot \frac{1}{\text{SWV}} \tag{40}$$

units of biomass, $\nabla_{J(x,t)} \|x\|_Y$ denoting the directional derivative of the pipe length function (16) with respect to J.

This local demand for biomass is covered with the instantaneous local biomass production in x at time t, i.e. (cf. (7), section 3.2)

$$b(x,t) = \text{RUE} \cdot \text{PAR} \cdot \lambda \cdot \clubsuit(x,t) \cdot \exp\left(-\int_{x_3}^{\infty} \lambda \cdot \clubsuit(x_1, x_2, \xi_3, n)\, d\xi_3 \right). \tag{41}$$

Equalling the locally available $b(x,t)$ with the (k^*-dependent) locally demanded biomass in (40), yields

$$k^*(x,t) = \frac{b(x,t) \cdot \text{SWV}}{\nabla_{J(x,t)} \|x\|_Y \cdot P} \tag{42}$$

for the magnitude of the local leaf density motion in (38). The figure on the right illustrates the basic mechanism. Every moving leaf remains attached to its constantly extending sapwood pipe, thus allowing for the pipe model theory at all times. The approach is also consistent in terms of mass balance, since all of the produced biomass is indeed allocated (implicitly, to the sapwood pipe extensions).

Emblematically speaking, moving leaves leave a trail of sapwood along their trajectory defined by J. The resulting local demand for sapwood mass is precisely met by the local biomass production. A different perspective on the mechanism is to interpret the mass-conserving motion of a leaf

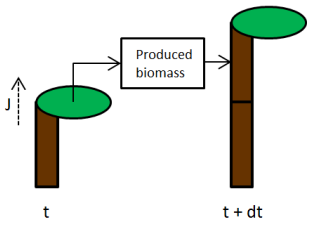

density (in an appropriate direction) as the result of the local allocation of locally produced biomass to the longitudinal growth of shoots that push along the leaves they support.

Under the given premises of this section, only the particular choice of $k^*(x,t)$ in (42) for the mobility coefficient in (38) ensures a consistent mass budget, while simultaneously preserving the pipe model balance: For higher values, leaves move too fast in order for the appropriate necessary pipe extensions to be constructed by means of what is available in terms of instantaneously produced biomass. For lower values, on the other hand, leaves move so slow that there is a surplus of available biomass that is not used for the extension of the pipes. In the next paragraph, we use this last feature in the context of allocation to foliage, while additionally accounting for leaf abscission.

Note that

$$\nabla_{J(x,t)}\|x\|_{\mathrm{Y}} = \|J(x,t)\| \cdot \underbrace{\nabla_{\frac{J(x,t)}{\|J(x,t)\|}}\|x\|_{\mathrm{Y}}}_{\approx 1}$$

since J generally points away from the origin, and $\|x\|_{\mathrm{Y}}$ is approximately of the same order of magnitude as $\|x\|$ for typical x in this scenario (i.e. $\|(x_1,x_2)\| \ll x_3$; on the x_3-axis we have equality). Thus, the denominator of $k^*(x,t)$ contains a factor approximately equal to $\|J(x,t)\|$, which implies that the magnitude of the total flux $k \cdot J$ does not depend much on the actual local length of J. In the given setting, this is not surprising when recalling that the degree of extension of supporting sapwood pipes is primarily governed by the local biomass production.

FOLIAGE FORMATION AND ABSCISSION The basic idea to incorporate the formation of new foliage based on locally produced biomass is to choose the mobility coefficient $k(x,t)$ for the motion of leaf density smaller than $k^*(x,t)$ in (42), and to use the remainder, i.e.

$$\underbrace{b(x,t)}_{\substack{\text{locally}\\ \text{available}\\ \text{biomass}}} - \underbrace{k(x,t)\cdot\nabla_{J(x,t)}\|x\|_{\mathrm{Y}}\cdot P\cdot\frac{1}{\mathrm{SWV}}}_{\substack{\text{biomass locally}\\ \text{required for } \clubsuit\text{-motion}}}$$

for the creation of new foliage in x at time t. The latter, of course, requires the simultaneous formation of new root-to-leaf sapwood pipes in order to continue accommodating the pipe model theory. Altogether, assigning the above quantity to the formation of new foliage and the appropriate sapwood pipes results in an increase of leaf density in x by

$$\mathrm{SLA}\cdot p(x)\cdot\left(b(x,t) - k(x,t)\cdot\nabla_{J(x,t)}\|x\|_{\mathrm{Y}}\cdot P\cdot\frac{1}{\mathrm{SWV}}\right) \tag{43}$$

where $p(x) = \frac{1}{1+P\cdot\|x\|_{\mathrm{Y}}}$ as in (14), detailed in section 3.5.1.

Lastly, we incorporate the senescence and abscission of old leaves. This is not a straightforward step, as in our current setting, we are unable to differentiate between old foliage that has existed and been subject to a motion for a longer time than leaves that have only just been formed, and it would not seem reasonable to treat them equally. We thus introduce an age-dependency of the leaf density variable,

$$\clubsuit(x,t) = \clubsuit(x,t,a) \quad \text{with } a \in [0,A],$$

with $\int_0^A \clubsuit(x,t,a)\,da$ numbering the total leaf density in x at time t. Leaves that are newly created, as described above, are assigned age 0. They subsequently age, while being subject to the described motion. At the final age of A, they fall off, thereby decreasing the total leaf density in the respective point. In this setting, sapwood pipes corresponding to dropped leaves persist, and, in biological terms, become non-conductive and turn into heartwood, in accordance with the pipe model theory.

For the sake of convenience, we assume that neither biomass production nor leaf transport depend on leaf age, i.e. $\clubsuit(x,t)$ in the flux (39) and the biomass production (41) is simply replaced by $\int_0^A \clubsuit(x,t,a)\,da$. With this in mind, our full model reads

$$\frac{\partial}{\partial t}\clubsuit(x,t,a) = -\nabla_x \cdot (k(x,t)\cdot J(x,t)) - \frac{\partial}{\partial a}\clubsuit(x,t,a) \tag{44a}$$

$$\clubsuit(x,t,0) = \text{SLA}\cdot p(x)\cdot\left(b(x,t) - k(x,t)\cdot\nabla_{J(x,t)}\|x\|_Y\cdot P\cdot\frac{1}{\text{SWV}}\right) \tag{44b}$$

$$\clubsuit(x,t,A) = 0 \tag{44c}$$

$$\clubsuit(x,0,a) = \begin{cases}\clubsuit_0(x) & \text{if } a = 0\\ 0 & \text{else}\end{cases} \tag{44d}$$

(44a) describes the (age-independent) spatial motion of leaf density, similar to the preliminary (38), as well as the ageing process. The two boundary conditions (44b) and (44c) account for the formation of new ($a = 0$) foliage (cf. (43)) and the abscission of old ($a = A$) leaves, respectively. Again we use $\clubsuit_0(x) = \delta_0(x)$ for the initial condition (44d).

SPECIFYING THE MOBILITY COEFFICIENT For $k \equiv k^*$, (44b) reduces to $\clubsuit(x,t,0) = 0$ for all x and all $t > 0$, resulting in the complete disappearance of foliage after A time steps. On the other hand, for $k \equiv 0$, (44a) and (44b) reduce to

$$\frac{\partial}{\partial t}\clubsuit(x,t,a) = -\frac{\partial}{\partial a}\clubsuit(x,t,a)$$
$$\clubsuit(x,t,0) = \text{SLA}\cdot p(x)\cdot b(x,t)$$

respectively, without any spatial expansion of leaf density whatsoever. A sensible $k(x,t)$ thus lies between 0 and $k^*(x,t)$. In the following, we propose a possible value.

For arbitrary but fixed $k(x,t)$ denote by

$$\begin{aligned} T_k(x,t) &= k(x,t) \cdot \nabla_{J(x,t)} \|x\|_Y \cdot P \cdot \frac{1}{\text{SWV}} \\ \text{and} \quad F_k(x,t) &= p(x) \cdot (b(x,t) - T_k(x,t)) \end{aligned} \tag{45}$$

the biomasses that are locally used for the extension of existing shoots and for the formation of new leaf area, respectively, cf. (43). $T_k(x,t)$ can also be interpreted as the cumulative longitudinal growth of unit shoots supporting a given number of units of leaf density in x, and $F_k(x,t)$ as the cumulative formation of new leaves in x. The quotient of these two quantities, i.e. the ratio of leaf formations to shoot longitudinal growth in x may be related to the phyllochrone, the interval between leaf appearances along a shoot. The simplifying assumption of a constant phyllochrone (cf. Davidson et al., 2015) thus motivates the approach

$$F_k(x,t) = c \cdot T_k(x,t)$$

for a global constant $c > 0$. Inserting this into (45) yields

$$k_c(x,t) = \frac{p(x) \cdot b(x,t) \cdot \text{SWV}}{(p(x)+c) \cdot \nabla_{J(x,t)} \|x\|_Y \cdot P} \tag{46}$$

Indeed $k_c(x,t) \in]0, k^*(x,t)[$ as desired since $k_c(x,t) = \frac{p(x)}{p(x)+c} \cdot k^*(x,t)$. $c = 0$ and $c = \infty$ correspond to the two degenerate cases described above, illustrating that in practice the parameter $\frac{1}{c}$ plays the role of a mobility constant: the larger $\frac{1}{c}$, the faster the transport of leaf area.

5.2.2 *Simulations*

Measureable model parameters used in the simulations correspond again to those referenced in table 2, the remaining ones were exemplarily set to $c = 1$, $\text{PAR} \cdot \text{RUE} = 4$, $P = 0.43$ and $A = 1$. For the above choice of k in our model (44a–d), figure 14 shows the evolution of leaf density in a competition scenario. The pattern is rather different from the one in figures 12 and 13. We no longer observe the arguable occurrence of foliage within the crown, and instead merely at the hull. This is due to foliage systematically moving away from the place of its formation before eventually disappearing due to abscission, thus gradually evacuating lower level regions. This last process is increasingly delayed with increasing leaf life span A, inducing a more gradual decrease of leaf density towards the interior of the crown and downwards (not shown). The generated crown shape is conic rather than round, and, as such, characteristic of many conifer trees.

5.3 DISCUSSION

As a transition from the continuous-time, two-dimensional crop model of chapter 4 to the applied 3D tree model with a discrete, one year

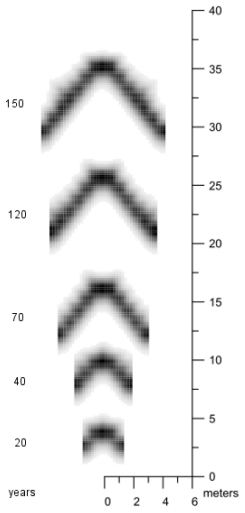

Figure 14.: Qualitative leaf density dynamics of a simulated tree in competition (technical details as in figure 13). An isolated tree differs essentially only in that the cone-like crown extends rectilinear all the way down to the ground.

time step presented in the subsequent chapter 6, we explored the compatibility of a continuity equation approach with the spatio-temporal growth of trees – an idea that, although seemingly suggesting itself, proved controversial upon closer inspection, notably due to the particular nature of leaf organogenesis and its relation to wood formation. Within these constraints, we presented two conceptually different approaches in order to study to what extent these limits can be bent or overcome. Despite the difficulties of the general framework, we managed to incorporate key desirable features in both models, namely a consistent mass balance and the continual satisfaction of the pipe model theory.

Our first, top-down model presented in section 5.1 generated an interesting crown shape, some desirable properties of which we encounter again in the discrete-time model presented in the next chapter. Yet the global allocation scheme led to arguable effects that demonstrated the need for a more local approach, which we subsequently developed in section 5.2. In the first two parts of section 5.2.1 in particular, we endeavoured to show how the developed model mechanisms, even though at times contrasting real organogenesis, follow straight from an initial set of objectives and constraints that had been kept as general as possible. Within this framework, we proceeded in a more specific direction, when specifying the mobility coefficient and thus the partitioning of available biomass between the formation of new leaves and the biomass-demanding transport of foliage. Indeed, featuring a concentration of leaf density at the crown hull, the key deficit of the model presented in 5.1 no longer appeared in this approach. Future work, based on the general framework laid out here, could explore choices for the mobility coefficient k beyond the one in (46).

In view of certain biologically controversial technical aspects, we have omitted a more extensive parameterisation and evaluation of the approaches in this chapter in favour of a more extensive study

and data-based analysis of the tree growth model presented in the following chapter. As a time-discrete approach, it will not face the conceptual challenges highlighted throughout this chapter, thus allowing for a more biologically sound framework.

6

DISCRETE-TIME MODELLING OF TREE GROWTH

In this chapter we present a growth model in discrete time for rhythmically growing trees (in the sense of Hallé et al., 1978, and Barthélémy and Caraglio, 2007), where leaf density is computed from one year to the next. By $\clubsuit(x, n)$ we denote the supposedly constant leaf density in x during the vegetational period (between foliation and leaf senescence) of year $n \in \mathbb{N}_0$. Instead of the previously considered continuous evolution $t \mapsto \clubsuit(\cdot, t)$, the leaf density $\clubsuit(\cdot, n+1)$ of year $n+1$ is now inferred from the previous year's leaf density $\clubsuit(\cdot, n)$.

This model was presented by Beyer et al. (2015b).

6.1 MODEL DESCRIPTION

In a first step, we consider the case of vertical radiation, and address the impact of different light models in section 6.4. Denoting the cumulative photosynthetically active radiation that reaches the tree with a given leaf density $\clubsuit$ from above in year n by $\mathrm{PAR}(n)$, the cumulative radiation reaching the point $x \in \mathbb{R}^3$ in year n reads, similar as before,

$$L(x, n) = \mathrm{PAR}(n) \cdot \exp\left(-\int_{x_3}^{\infty} \lambda(x, n) \cdot \clubsuit(x_1, x_2, \xi_3, n)\, d\xi_3\right), \quad (47)$$

and the cumulative biomass production in x in year n is given by

$$B(x, n) = \mathrm{RUE} \cdot L(x, n) \cdot \lambda(x, n) \cdot \clubsuit(x, n), \quad (48)$$

as described in detail in sections 3.1 and 3.2, respectively.

To infer the leaf density $\clubsuit(\cdot, n+1)$, the scalar field $B(\cdot, n)$ is now translated along the local light gradient field $\nabla_x L(\cdot, n)$, according to the principles of unconstrained phototropic plasticity as well as dynamic maximization of light interception and biomass production (cf. section 3.3). Specifically, the locally produced quantity $B(x, n)$ is moved from x to the position

$$x + k \cdot \nabla_x L(x, n),$$

where it is subsequently allocated, $k > 0$ denoting a mobility constant. The locality of this mechanism explicitly reflects the concept of branch

autonomy, the empirically established observation that branches are largely functionally independent, i.e. carbon uptake and export of a specific branch along the way to the roots is independent of the rest of the tree (Sprugel et al., 1991). The concept is closely related to the modularity in plants, i.e. the idea of plant components acting and responding as independent units (Sprugel et al., 1991; Sorrensen-Cothern et al., 1993, and references therein).

Hence, inversely, for a given point $x \in \mathbb{R}^3$, the total biomass assigned to it for allocation equals

$$\mathcal{B}(x,n) = \sum_{\substack{\xi\in\mathbb{R}^3:\\ x=\xi+k\cdot\nabla_x L(\xi,n)}} B(\xi,n). \tag{49}$$

Similar as in section 5.2, the allocation of $\mathcal{B}(x,n)$ in x comprises its partitioning between new foliage in x and supporting sapwood according to the pipe model theory. As described in detail in section 3.5.1,

$$\mathfrak{B}(x,n) = \text{SLA} \cdot p(x) \cdot \mathcal{B}(x,n)$$

numbers the increment of leaf density in x for year $n+1$ as the result of the production in year n, with

$$p(x) = \frac{1}{1 + P \cdot \|x\|_Y},$$

as in (14), in accordance with the pipe model theory, and SLA denoting specific leaf area. Simultaneously, the mass $\mathcal{B}(x,n) \cdot (1 - p(x))$ forms the appropriate sapwood pipe.

Assuming the senescence and abscission of leaves to be a matter of time only, i.e. foliage that was created $n_{\text{sen}} > 0$ years ago falls, the leaf density of year $n+1$ in x is given by

$$\clubsuit(x,n+1) = \clubsuit(x,n) + \mathfrak{B}(x,n) - \mathfrak{B}(x,n-n_{\text{sen}}). \tag{50}$$

For the particular case of deciduous trees where $n_{\text{sen}} = 1$, this simplifies to

$$\clubsuit(x,n+1) = \mathfrak{B}(x,n).$$

This discrete dynamical system is completed by an initial condition, which we describe to be Dirac in the origin $x = (0,0,0)$, i.e. $\clubsuit(x,0) = \clubsuit_0(x) = \delta(x)$ and where $\int_{\mathbb{R}^3} \clubsuit_0(x)\,dx$ equals the surface area of the cotyledon.

Along the creation of foliage, new sapwood pipes are formed as described above. Pipes corresponding to dropped foliage persist, yet gradually become non-conductive and, over time, turn into heartwood (Shinozaki et al., 1964; Valentine, 1988; Sterck and Schieving, 2007). Thus, taking into account all pipes that have ever been formed, yields

$$\sum_{k=0}^{n} \int_{\mathbb{R}^3} \mathcal{B}(x,k) \cdot p(x) \cdot P \cdot \text{SWV}\,dx$$

for the cross-sectional area at the trunk base, $C(n)$, in year n, SWV denoting specific wood volume. As in the pipe model theory, swelling effects are not accounted for. The diameter is computed as $2\sqrt{C(n)/\pi}$.

As an extra, it corresponds to our approximation of $\|x\|_Y$ defined in (16) that the foliage supported by a first order branch bifurcating from the trunk at height $h \geq 0$ is assumed to lie on the cone surface

$$\partial K(h) = \left\{ x \in \mathbb{R}^3 : \|(x_1, x_2)\| \cdot \cos(\theta) = (x_3 - h) \cdot \sin(\theta) \right\},$$

which implies that the trunk's cross-sectional area at height h in year n equals

$$\sum_{k=0}^{n} \int_{\bigcup_{\eta \geq h} \partial K(\eta)} \mathfrak{B}(x,k) \cdot p(x) \cdot P \cdot \text{SWV}\, dx,$$

which in fact yields the complete geometry of the trunk.

The model extends straightforwardly in order to account for competition for light among m individuals with leaf densities $\clubsuit_1(\cdot, n), \ldots, \clubsuit_m(\cdot, n)$ in year n as detailed in section 3.4. For this case, the light reaching the foliage of tree $i \in \{1, \ldots, m\}$ in x changes from (47) to

$$L_i(x,n) = \text{PAR}(n) \cdot \frac{\lambda_i(x,n) \cdot \clubsuit_i(x,n)}{\sum_{j=1}^{m} \lambda_j(x,n) \cdot \clubsuit_j(x,n)} \cdot \exp\left(-\int_{x_3}^{\infty} \sum_{j=1}^{m} \lambda_j(x,n) \cdot \clubsuit_j(x,n)\, dx_3 \right),$$

where the fraction $\frac{\lambda_i(x,n) \cdot \clubsuit_i(x,n)}{\sum_{j=1}^{m} \lambda_j(x,n) \cdot \clubsuit_j(x,n)}$ is the part of the radiation incidence in x that is attributed to tree i. In particular, it reduces to 1 if tree crowns do not occupy common space.

Accordingly, (48), (49) and (50) change to

$$\begin{aligned} B_i(x,n) &= \text{RUE} \cdot L_i(x,n) \cdot \lambda_i(x,n) \cdot \clubsuit_i(x,n) \\ \mathcal{B}_i(x,n) &= \sum_{\substack{\xi \in \mathbb{R}^3: \\ x = \xi + k \cdot \nabla_x L_i(\xi,n)}} B_i(\xi, n) \\ \clubsuit_i(x, n+1) &= \clubsuit_i(x,n) + \text{SLA} \cdot p(x) \cdot \left(\mathcal{B}_i(x,n) - \mathcal{B}_i(x, n - n_{\text{sen}}) \right) \end{aligned}$$

respectively, for each individual $i \in \{1, \ldots, m\}$ of the population.

6.2 SIMULATIONS

DATA SET DESCRIPTION European beech (*Fagus sylvatica* L.) is the most important deciduous tree species in the natural forests of Central Europe (Ellenberg, 1996). Its overwhelming inner crown variability and crown plasticity, particularly in response to light, compared to other native trees species (Pretzsch, 2014) suggest it for an application

of our model. Originally established in 1871 at the age of 48 years, the long-term experimental plot Fabrikschleichach 15 of European beech is among the oldest of the world. It is located in the sub-montane zone 470 m above sea level (10°34′16″E, 49°55′07″N) in the ecological region "Fränkischer Keuper und Albvorland, Wuchsbezirk Steigerwald". The mean annual temperature is 7.5 °C with a precipitation of 820 mm. During the vegetation period of 150 days (days $\geq$ 10 °C), the temperature averages 14.5 °C accompanied by 420 mm of precipitation. The survey area represents very good growth conditions for beech (Franz et al., 1995).

Different thinning treatments have been applied on three sub-plots of the site, resulting in different stand densities shown in figure 15.: While merely dead trees have been removed in sub-plot 1, sub-plot 2 has been moderately and sub-plot 3 heavily thinned (see Verein der deutschen Forstlichen Versuchsanstalten, 1902; Gutmann, 1926, for details).

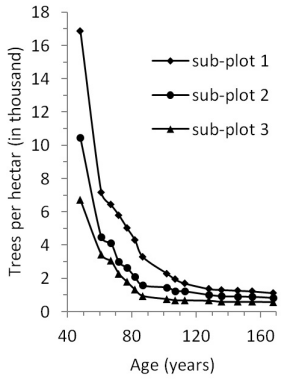

Figure 15.: Stand densities over time. Redrawn from Pretzsch et al. (1994).

6.2.1 *Comparison to long-term data*

As the model does not cover tree mortality and harvesting, the number of trees per unit area over time is an input variable (figure 15). As detailed in section 3.4, in place of the entire stands, we simulated a single average tree for each stand, while accounting for competition by means of dynamic periodic boundary conditions along a cell, in which the tree grows and whose surface area corresponds to the density of the stand at the appropriate time (cf. section 3.4.1).

Table 2 summarizes the model parameters, three of which were estimated by model inversion based on the data of sub-plot 1 and 3 shown in figures 16a,c. As in Letort et al. (2008), PAR, assumed constant, and RUE are merged.

Figures 16 and 17 show the results of simulations against the empirical height, diameter at breast height and, only for one moment in time, mean crown radii data, from the three different sub-plots, respectively. Note that the data of sub-plot 2 and the one in figure 17 were not

Parameter	Value	Reference
SWV [$m^3\ g^{-1}$]	0.0013	Bouriaud et al. (2004)
SLA [$m^2\ g^{-1}$]	0.0232	Bouriaud et al. (2003)
$N(x,n)$ [1]	$(0,0,1)$	Monsi and Saeki (2005)
Λ [1]	1.0	Wang et al. (2004)
φ [°]	138.5	Bayer et al. (2013)
$\int \clubsuit_0$ [m^2]	$6.01 \cdot$ SLA	Coll et al. (2004)
RUE $\cdot$ PAR [$g\ m^{-2}\ y^{-1}$]	14.72	
k [1]	0.0013	
P [m^{-1}]	0.43	

Table 2.: Model parameters. Unreferenced parameters were estimated (see text).

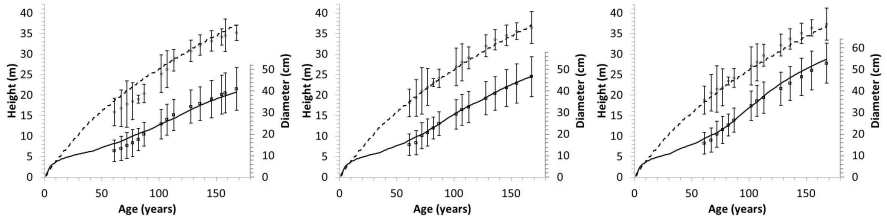

(a) sub-plot 1 (b) sub-plot 2 (c) sub-plot 3

Figure 16.: Comparison of simulated to empirical stand average and standard deviation data of tree height (dashed line, circles, left axis) and diameter at breast height (solid line, circles, right axis) over time and three sub-plots differing in stand density.

used for the calibration and can thus be used for the validation of the model's predictive capacity.

Figure 18a shows the cross-section of the crown corresponding to the simulations of sub-plot 1 in the course of time. The shape is indeed similar to that of a typical beech crown in such growth conditions (figure 18b).

As a contrast, figure 19a shows the simulated crown of an at all times spatially isolated tree. The artificial absence of any vegetal competition in the simulation can only partially account for the unrestrained horizontal expansion that is not realistic during the early growth shown in the figure. We come back to this aspect of the model in detail and discuss possible implications as to other growth determinants at early stages in section 6.3. Irrespective of this, we note that in terms of shape, the simulated tree bears indeed some resemblance to a mature singular beech tree (figure 19b).

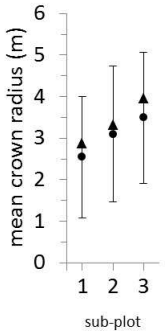

Figure 17.: Simulated (triangle) and empirical mean crown radii (bullet) with standard deviations at 180 years.

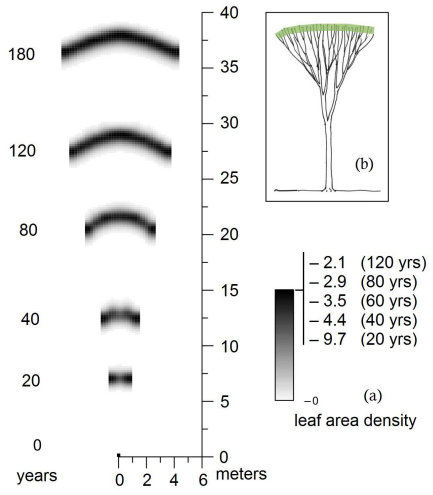

Figure 18.: (a) Vertical cross-section of a simulated crown over time. (b) Schematic representation of the crown structure of adult beech in even-aged pure stands, adapted from Pretzsch (2014).

6.2.2 *Comparison to laser scanned crowns*

Terrestrial laser scanning (TLS) can provide a large amount of information on tree geometry beyond the traditional measures of tree height, crown height and crown radii in terms of forest and individual tree parameters (Van Leeuwen and Nieuwenhuis, 2010; Pretzsch, 2011) and even the inner structure of tree crowns (Bayer et al., 2013). In this section we test empirical laser scans against the spatial output of our model, which, to our knowledge, is an unprecedented validation method in the area of individual tree growth models.

Scans were acquired for sub-plot 3 of the experimental site in March 2012 using the Riegl LMS-Z420i laser scanning system. Its infrared laser beams do typically not penetrate tree compartments, hence a dense canopy can significantly distort a scan image. This motivated to scan trees in leafless conditions and to compare the model's leaf area density to a spatial twig density as described below. For the same reason we used a the last-pulse (or last-target) distance mea-

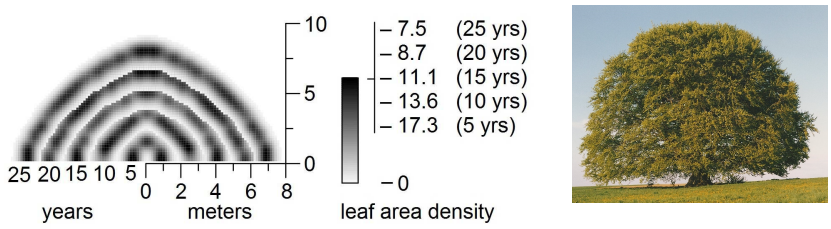

(a) (b)

Figure 19.: (a) Vertical cross-section of a simulated singular tree over 20 years. Note the self-similarity of the shapes, which extends to older crowns in equal measure (not shown). (b) Bavaria Buche (cf. section 2.1).

surement mode in which the last echo of the laser impulse is used for distance recording, allowing the laser beam to penetrate the tree crown further than using the regular, first-pulse mode. In order to cover the trees thoroughly and minimize additional distortion, we took a total of 10 upright and tilted scans from five regularly distributed positions within the stand, and merged those into one image. Bayer et al. (2013) elaborated further on general technical and procedural details, and also addressed the impracticality of applying automatic skeletonisation algorithms to scans at the forest stand scale.

Figure 20.: Tree laser scan point cloud and isolated twig structures.

Individual trees and subsequently their respective twigs were manually isolated from the final scan image (figure 20). To avoid unnecessary tediousness, we focused on twigs in the upper part of the crown where leaf density is actually significant (cf. also figure 18b). Altogether we obtained a total of 10 samples.

We presume that 3D twig density and leaf area density essentially differ only by a multiplicative constant. Equivalently, relative twig density and relative leaf area density, both normed such that their integrals equal 1, should roughly coincide. For the same grid used in the numerical model computations, the former is obtained from a given laser scan point cloud by first assigning to each voxel the number of laser points it contains. Dividing this absolute frequency by the total number of points and the voxel volume yields a (step-

function) density with integral 1 for each sample. Denote these by $\widehat{\mathfrak{a}}_i(x)$, $x \in \mathbb{R}^3$, $i = 1, \ldots, m$, with $m = 10$. Now, let

$$x \mapsto \overline{\mathfrak{a}}(x) = \frac{1}{m} \cdot \sum_{i=1}^{m} \mathfrak{a}_i(x) \qquad \text{and} \qquad \sigma_{\mathfrak{a}} = \sqrt{\frac{1}{m} \cdot \sum_{i=1}^{m} \|\overline{\mathfrak{a}} - \mathfrak{a}_i\|^2}$$

denote their mean and standard deviation, respectively, where $\|\cdot\|$ is an L^p-norm (i.e. $\|f\| = \left(\int_{\mathbb{R}^3} |f(x)|^p \, dx\right)^{\frac{1}{p}}$). Figure 21 gives a visual comparison of $\overline{\mathfrak{a}}(x)$ and the relative simulated density $\frac{\clubsuit(x)}{\int_{\mathbb{R}^3} \clubsuit(\xi)\, d\xi}$ of the appropriate time.

The positive density in lower regions may on the one hand be attributed to the relatively small size of ten samples that we were able to obtain: Whereas single unusually low branches resulting from randomness have presumably little relevance in the case of a large sample set, they may act distortively otherwise. On the other hand, it may also challenge the idealized foliage distribution of figure 18b to some extent. In any case, we observe an increased concentration of the empirical density in the upper regions that are in fact close to the simulated one (figure 21b).

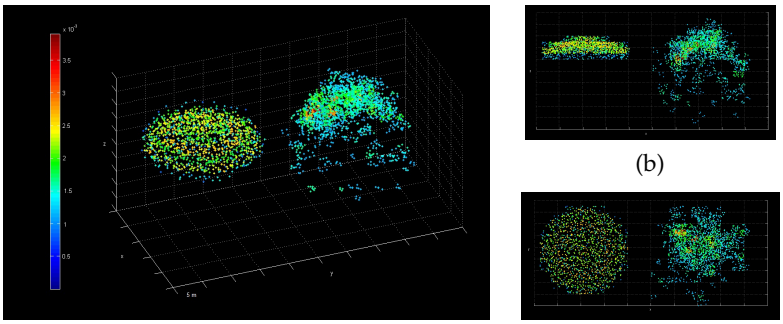

(a) (b) (c)

Figure 21.: (a) Oblique, (b) side and (c) top view of mean empirical (right) and simulated (left) relative twig- and leaf area density, $\overline{\mathfrak{a}}$ and $\frac{\clubsuit}{\int \clubsuit}$, respectively. The figures also illustrate the agreement of real and simulated height (figure 16c, top right) and crown radius (figure 17 right). See text for quantitative comparison.

We can quantitatively compare the empirical densities to the simulated one by computing their distance $d_{\clubsuit,\mathfrak{a}} = \left\| \frac{\clubsuit}{\int \clubsuit} - \overline{\mathfrak{a}}_i \right\|$ and comparing it to the sample standard deviation $\sigma_{\mathfrak{a}}$. Indeed, $\frac{\clubsuit}{\int \clubsuit}$ appears to be well contained in the $\sigma_{\mathfrak{a}}$-ball about $\overline{\mathfrak{a}}$ for all L^p norms: In particular, we obtained $d_{\clubsuit,\mathfrak{a}} = 0.0138 < 0.0182 = \sigma_{\mathfrak{a}}$ in the L^2 norm and $d_{\clubsuit,\mathfrak{a}} = 0.0035 < 0.0254 = \sigma_{\mathfrak{a}}$ in the L^∞ norm, respectively. Thus, the simulated crown is within the standard range of crown shapes at the given age and growth conditions, as desired.

6.2.3 *Comparison to allometric rules*

Allometric scaling laws establish relations between different growth dimensions of an organism. For two such quantities x and y, an allometric equation is of the form $x \propto y^{\beta}$. Allometrically relating characteristic dimensions of trees has proven expedient and although in general the investigated allometric exponents β do vary, depending on specific conditions (Pretzsch and Dieler, 2012), that corridor is in fact rather narrow (Pretzsch, 2010). The 3/4-power law has received particular attention, which, in its broadest formulation states that an organism's metabolic rate Q scales to its body mass W as $Q \propto M^{\frac{3}{4}}$. The relationship has been observed in many particular cases across several length scales (see references in West et al., 1999a). Pretzsch (2006) found empirical evidence from long-term experimental plots, including the one presented in section 6.2, that is supportive of the 3/4-power scaling.

West et al. (1997) initiated a series of models associated to the term of metabolic scaling theory, aiming to explain the relationship in an as general as possible theoretical framework. In the plant specific follow-up model by West et al. (1999a), the law is derived from the optimization of different hydrodynamic and energetic properties of a space-filling, fractal-like network of root-to-petiole tubes. Whereas individual tube radii are assumed constant throughout the tree in the original model, this assumption is relaxed in follow-up work (West et al., 1999a), in which conductive pipes, loosely embedded into non-conducting heartwood, are allowed to vary in diameter along their path.

This often called metabolic scaling theory has been heavily contested both conceptually and empirically. We refer to Petit and Anfodillo (2009) for an extensive list of references challenging logical and mathematical assertions, as well as a critical discussion of arguable anatomical and physiological assumptions and conclusions of the theory.

This criticism of the 'WBE models', and at the same time the indisputable occurrence of the 3/4-rule in the flora, have motivated to put the development of plant models that can reproduce the rule in a more realistic, yet simple as possible framework on the agenda of the functional-structural plant modelling community – a project, which to date, has not culminated in success (Michael Renton, personal communication). We check our parameterized model for whether the 3/4-rule appears as an emergent property.

The model provides the total mass of the tree and its total net biomass production ($\sim$ metabolic rate) in year n as

$$W(n) = \underbrace{\sum_{i=0}^{n_{\text{sen}}-1} \int_{\mathbb{R}^3} \frac{\clubsuit(x, n-i)}{\text{SLA}}\, dx}_{\text{total leaf mass}} + \underbrace{\sum_{i=0}^{n} \int_{\mathbb{R}^3} \frac{\clubsuit(x, i)}{\text{SLA}} \cdot P \cdot \|x\|_{\text{Y}}\, dx}_{\text{total wood mass}}$$

and

$$Q(n) = \int_{\mathbb{R}^3} B(x,n)\,dx$$

respectively. Figure 22 shows $\log(Q(n))$ against $\log(W(n))$ in the same three simulation contexts as before. The close linear regressions based on the last 173 (of total 180) simulated years yield allometric exponents 0.765, 0.762, 0.773 for the three sub-plot conditions, respectively. Including the first 7 years as well yields slightly deviant exponents 0.787, 0.785, 0.794 respectively. We address the arguable applicability of the model in very early growth stages in section 6.3. Altogether, our model simulations are in very good agreement with the desired value of 0.75, even across different stand density scenarios.

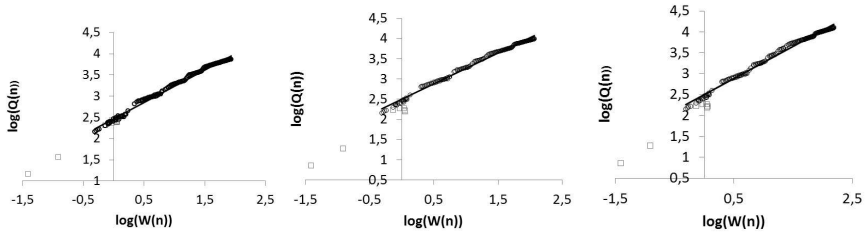

sub-plot 1 sub-plot 2 sub-plot 3

Figure 22.: $\log(Q(n))$ against $\log(W(n))$ for $n = 1,\ldots,7$ (grey squares) and $n = 8,\ldots,180$ (circles), the latter with linear regression lines with slopes 0.765, 0.762, 0.773, respectively. In all cases $R^2 > 0.95$. These lines are undistinguishable from suitable ones with slope 0.75.

6.3 DISCUSSION

Our discrete-time model based on leaf density ♣ and the local expansion thereof along the local light gradient $\nabla_x L$ accurately reproduced (figure 16a,c) and predicted (figures 16b, 17, 18, 21, and 22) the growth of European beech in even-aged pure stand conditions. The spontaneous self-organization of simulated tree crowns depending on the competitive situations present in the different sub-plots demonstrated the model's adaptability.

6.3.1 *Emergent properties*

Section 3.4 already discussed the model property of a reduced horizontal expansion and consequently decreased biomass production and thus trunk diameter growth (figure 16) in the case of higher competition, despite a common set of model process parameters.

The property of the experimental data set that tree height appears to vary only little between the different densities (figure 16) has been

observed for a reasonable range of stand densities (Lanner, 1985). It is also an emergent phenomenon of the model.

The same holds for the decreasing slope of the tree height curve. With increasing height, increasingly longer soil-to-leaf pathways require more biomass for the formation of the appropriate sapwood pipes according to the pipe model theory – biomass that is not available for foliage. This leads to relatively lower local leaf densities which in turn result in a smaller light gradient and thus a decelerated height growth, in terms of our model. In a theoretical analysis, Mäkelä (1986) had already linked the pipe model theory to the slowdown of height growth.

One of the most striking features of the model is the emergence of the $^3/_4$-rule, especially across different competitive conditions. We believe our model to be based on less controversial assumptions than the WBE model while at the same time not being less concise. Although we have not yet been able to derive this property rigorously, we believe that our approach represents a major step in the quest for functional-structural plant models to generate the rule.

6.3.2 *Conclusions*

Under the given additional model assumptions, the crown shapes in (figure 18a) and off (figure 19a) competition – as a matter of fact qualitatively practically independent of the parameter values – could be regarded as the morphology of a tree whose spatial expansion is solely determined by positive phototropism. This may give a qualitative impression of the extent to which a species' growth follows this principle or, inversely, for which other determinants and architectural constraints are more influential. In particular, it suggests the crown form of European beech to be strongly determined by the imperative of local growth towards light. Indeed, compared to most other Central European tree species, European beech is known for its high crown plasticity and efficient space occupation, expressed for instance in terms of a highly variable crown size vs. stem size allometry (Pretzsch, 2014) and its ability to quickly close light gaps caused by natural or human disturbances (Dieler and Pretzsch, 2013).

Our model would predict the shape of an at all times perfectly isolated beech tree to be similar to figure 19a even in early growth stages – which is not the case. Instead, at early ages, vertical growth dominates horizontal expansion (Krahl-Urban, 1962; Roloff, 2001), pointing out a limitation of the model and indicating that in this phase other growth strategies prevail. The vertical escape from herbivores and even more importantly, other competitors such as grasses and shrubs which are not considered in our model, suggests itself as an explanation (King, 1990; Peters, 1997). Curiously, we observed the same increased allocation of biomass more towards vertical than

horizontal growth in our competition simulations (figure 18a). This could suggest that this very behaviour is genetically imprinted to such an extent, that, in juvenile stages, it applies whether the tree grows in isolation or not, before eventually, in later stages (seen in figure 19), the plasticity in terms of almost unconstrained local phototropism prevails (King, 1990). It could explain the peculiarity of beech to start with rather slim crowns followed by a wider and wider extension as the evolutionary outcome of coping with the selective pressure. We hypothesize that beech as a late-successional species which has to establish and grow in the deep shade invests into height growth on the expense of lateral expansion in the early stage. This enables surviving in or even growing out of the understory phase. This strategy of coping with crowding changes completely in favour of lateral extension as soon as beech arrives in the overstory. At this point, its efficient space occupation by lateral extension outcompetes neighbors (Pretzsch, 2006, 2010).

Lastly, the applicability of the model in young stages may be arguable in light of the factual strong impact of topology during very early growth. Spatial foliage distribution at this point could be considered too irregular for leaf area density to be reasonably applied.

3D Laser scan data has an invaluable potential in the field of structure-based plant modelling as it can assess tree geometry in unprecedented detail. Here, we have attempted a first step in the direction of Lidar-based individual tree growth model validation. While currently still facing technical and methodological challenges, this field is bound to gain popularity in the coming decades as the development of fast, mobile and ultra-high-definition laser scanners along with the appropriate data treatment algorithms advances.

6.4 IMPACT OF THE LIGHT MODEL

So far, we have simplified light incidence as being vertical only, i.e.

$$\mathrm{PAR}(v) = \mathbb{1}_{\{v=(0,0,1)\}}(v) \cdot \mathrm{PAR}$$

for $v \in S^2_+$. While this is not an uncommon assumption in functional-structural (e.g. Sorrensen-Cothern et al., 1993) or process-based models (e.g. Norby et al., 2001), reality is more complex. In this section we investigate the effects of choosing a different light model in the previously presented tree growth model by means of replacing vertical light incidence by common altitude- and azimuth-dependent models for diffuse and direct radiation, respectively. Throughout this section, we consider the northern hemisphere and let $\mathbb{R}^2 \times \{0\}$ denote the local horizon.

A standard approach to assess diffuse radiation is the still radially symmetric but elevation-dependent standard overcast sky model proposed by Moon and Spencer (1942) (see also Ross, 1981). For a given

vertical light incidence PAR, radiation from direction $v \in S^2_+$ is given by

$$\text{PAR}(v) = \text{PAR} \cdot \frac{1 + 2 \cdot \sin(\theta)}{3}, \quad \text{where } \theta = \arctan\left(\frac{v_3}{\|(v_1, v_2)\|}\right) \tag{51}$$

denotes the elevation angle, i.e. the angle that v draws with the local horizon. Some topological tree growth models make exclusive use of this light model, i.e. without additional direct radiation, tacitly assuming the latter to be relatively negligible in comparison to diffuse light (Takenaka, 1994; Perttunen et al., 1996).

As for direct radiation, for the sake of illustration, and similar to Hollinger (1989) and Mariscal et al. (2004), we consider the simplified case of an equinox, where the course of the sun is locally perceived by an observer as a half-circle rotated by $\alpha \in [0°, 90°]$, the elevation angle of the sun at twelve o'clock in local solar time, about the vector $(0, -1, 0)$ pointing west, i.e. the set

$$E = \left(\begin{pmatrix} \cos(t) \\ \cos(\alpha) \cdot \sin(t) \\ -\sin(\alpha) \cdot \sin(t) \end{pmatrix} : t \in [\pi, 2\pi] \right) \subset S^2_+$$

Similar to Brisson et al. (2004), for $v \in K$, we approximate radiation intensity by a cosine function of the hour angle $h = h(v) = \arccos(v \cdot (0, -\cos(\alpha), \sin(\alpha))) \in [-90°, 90°]$, which is $0°$ at solar noon, yielding

$$\text{PAR}(v) = \mathbb{1}_{v \in K}(v) \cdot \text{PAR} \cdot \frac{1 + \cos(2 \cdot h(v))}{2} \tag{52}$$

for the radiation from $v \in S^2_+$. In the graphical results below, we used $\alpha = 45°$ for the elevation angle; results were very similar for other plausible values.

Figure 23 compares the spatial output of simulations run based on merely vertical radiation, diffuse radiation in terms of the standard overcast sky model as well as direct radiation as described above, respectively, where the total amount of incoming radiation is the same for all three cases. Not surprisingly, a higher portion of vertical as opposed to oblique light induces a more pronounced height growth. Apart from this vertical translation of the leaf density profiles, we observe a very slightly more upward-curved shape in the case of the standard overcast sky model compared to the one with vertical radiation, as well as a slight inclination of leaf density towards the south for the case of direct radiation. While all of these features could have been expected qualitatively, the high degree of similarity of the leaf density shapes (modulo height) across the different light models is remarkable.

Several factors contribute to this phenomenon. Firstly, as described in (51) and (52), respectively, steeper radiation has a greater effect than oblique and flat one because it is stronger by nature. Even more importantly, a relatively larger portion of the latter simply passes through the

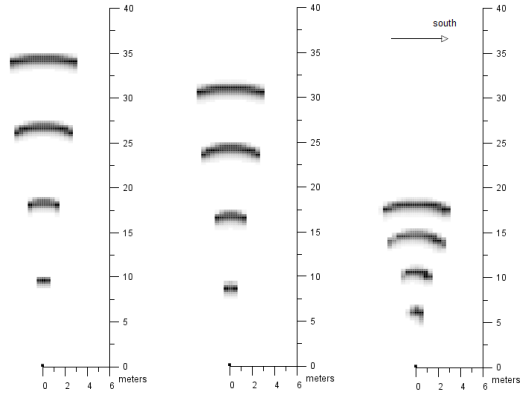

(a) (b) (c)

Figure 23.: Middle vertical cross-section of simulated leaf densities based on (a) vertical radiation (analogous to figure 18), (b) the standard overcast sky model (c) direct radiation as specified in the text at 40, 65, 100 and 140 years. The competition scenario is again based on sub-plot 3, as in figure 18.

horizontally oriented leaves, as opposed to vertical radiation, which is efficiently absorbed and contributes most to the local light gradient. Moreover, especially in the case of the standard overcast sky model, the effects of light coming from opposite directions may to some extend cancel each other out. In addition, the pipe model theory might play a small role in that it decreases the incentive to disproportionately veer away from the crown centre. Lastly, flat radiation is more likely to be intercepted by neighbouring competitors before even reaching a crown than is steep radiation, an effect particularly visible in terms of the non-occurrence of more foliage at the lower southern side of the tree in figure 23c. In particular, this last case demonstrates the high priority of a crown in our model to close light gaps around it (which appear in simulations in terms of a uniform expansion, out from the stem base centre, of the cell assigned to the tree as the result of the gradual mortality- and harvest-induced decrease of stand density, cf. section 3.4.1), no matter the orientation, over a considerably weaker tendency to grow south.

As described above, an equal amount of total incoming radiation does not imply the total amount of intercepted radiation to be the same in the three scenarios. However, a suitable increase in the radiation constant PAR in (51) and (52) results indeed in the adjustment of the heights, yielding an overall similar spatio-temporal pattern as in the case of vertical radiation – and vice versa (not shown). Since realistic light incidence is a consequence of the combination of diffuse

and direct radiation, this suggests that the merged model parameter RUE · PAR in table 2 may have been underestimated.

In summary, this section illustrated the relatively small impact of the choice of the light model on the essential model dynamics. We conclude the simplification of vertical light incidence to have been a reasonable step.

6.5 INCORPORATING WATER DEPENDENCE

In the previous model, biomass production $B(x, n)$ (cf. (48)) was merely light-dependent. In a more general framework, the incorporation of the stand-specific water conditions and their effect on tree growth would be desirable. In this section, we develop a submodel for the determination of light and water-dependent biomass production and subsequently integrate it into the tree growth model presented in the previous section before testing the extended model against a series of sites of even-aged pure beech stands, differing in local water availability.

In the following submodel, we determine transpiration rate E [$\mathrm{kg\,m^{-2}s^{-1}}$] at the local leaf level, and later relate this quantity to annual net biomass production $B(x, n)$ via a water use efficiency parameter. Comparable existing models mostly focus on stomatal conductance g_s instead of leaf transpiration rate E, the two variables being related via

$$E = \alpha \cdot \left(\frac{1}{g_s} + \frac{1}{g_b} \right) \cdot \mathrm{VPD},$$

where g_b denotes the boundary layer conductance to water vapour, VPD the vapor pressure deficit, and α a physical parameter depending on atmospheric pressure, temperature, wind speed and shoot anatomy (Damour et al., 2010). For negligible g_b, as argued, among others, by Monteith (1995), and constant atmospheric conditions, we have indeed

$$E \propto g_s.$$

6.5.1 *Model description*

Models of stomatal conductance g_s at the leaf level commonly postulate a one-sided dependence of g_s on different environmental factors (Damour et al., 2010). In particular the multiplicative approach of Jarvis (1976), expressing g_s as a product of empirical functions of light intensity, leaf temperature, vapour pressure deficit, ambient carbon dioxide concentration and leaf water potential, which we denote by $\Psi(\ell)$, has had a lasting effect. In order to assess water stress more explicitly, follow-up work replaced the response to leaf water potential by a response to soil water deficit (Stewart, 1988), instant pre-dawn

leaf water potential (Misson et al., 2004) as well as pre-dawn leaf water potential aggregated over a period of time (White et al., 1999; MacFarlane et al., 2004), the latter two variables being assumed to be a surrogate for soil water potential.

Hydraulic models take a more mechanistic approach: In their simplest form, stomatal conductance is assumed proportional to the hydraulic conductivity of the soil-to leaf pathway divided by the area of the leaf and the water potential gradient between the soil and the leaf (Oren et al., 1999). Hydraulic conductivity is often deduced from aggregating segments that make up tree architecture (Tyree, 1988; Sperry et al., 1998; Tuzet et al., 2003), a method that has recently benefited from laser scan imagery (Hentschel et al., 2013).

However, the one-sidedness of existing models of expressing stomatal conductance as a decreasing function of leaf water potential $\Psi(\ell)$, which is either a direct argument or pre-calculated based on empirical or hydraulical relationships, neglects the crucial co-regulatory property of leaf water potential and stomatal conductance. Indeed, the response of g_s to $\Psi(\ell)$ is well documented for many species and conditions, and Damour et al. (2010) argue in favour of an underlying mechanistic basis "because it is well demonstrated that stomatal movements result from variations in leaf (or guard cell) water status, which result themselves from variations of evaporation in the substomatal cavity, and thus of the transpiration flux". But there is also a direct mechanistic impact of g_s on $\Psi(\ell)$: By an analogy to Ohm's law, water potential along a soil-to-leaf water column can be expressed in terms of leaf transpiration E, local hydraulic resistances along the pathway, height and soil water potential (see below).

Altogether, other things being equal, E decreases with decreasing $\Psi(\ell)$ while $\Psi(\ell)$ decreases with increasing E. In the following, we determine the equilibrium between these counteracting mechanisms, sometimes denoted hydraulic homeostatis.

The cohesion-tension theory (Tyree and Zimmermann, 2002) states that water ascends from the soil as a result of the transpiration of water from leaves, which induces a water potential gradient along a connected and tense water column from root to leaf, that is embedded in a conducting system of fine capillaries. Increasing transpiration requires faster water flow, implying steeper pressure gradients of water potential. This additionally amplifies with increasing height due to the gravitational pull. An increased tension in the xylem sap increases the risk of cavitation, the rupture of the water column, and the dangerous formation of embolisms. These air-blockings of the vascular system reduce hydraulic conductivity, making even steeper potential gradients in the remaining conductive conduits necessary in order to maintain water flux – a vicious circle that would ultimately result in a fully embolized xylem, null water conductance and catastrophic

turgor loss. By decreasing the aperture of the stomata in the leaves, trees can limit transpirational water loss and hence root-to-leaf water potential gradients and cavitation risk. However, closing the stomata implies a reduced carbon assimilation and production of dry matter. The result of this trade-off is a homeostatic balance which we formally determine in the following.

Let A [m²] denote the surface area of the leaf and E its transpiration rate at a given moment. Let ℓ [m] denote the length of the branch path leading from the soil to the leaf. Under steady-state conditions, the water potential $\Psi(s) \leq 0$ [MPa], $s \in [0, \ell]$, along this path obeys the differential equation

$$\frac{d}{ds}\Psi(s) = -\frac{E \cdot A}{K(s)} - \rho g \cdot \frac{d\,\text{height}}{ds} \tag{53}$$

(Tyree and Zimmermann, 2002), where $\Psi(0)$ and $\Psi(\ell)$ represent soil and leaf water potential respectively. The last term of (53) is due to gravitational force, $\rho = 1000\ \text{kg m}^{-3}$ and $g = 9,81\ \text{m s}^{-2}$ denoting the density of water and the acceleration due to gravity, respectively. $K(s)$ [kg m s^{-1} MPa^{-1}] is the hydraulic conductivity of the branch segment s units away from the roots. (53) is essentially an analogue to Ohm's law for water transport, an idea that historically traces back to Gradmann (1928).

For the hydraulic conductivity, the relation

$$K(s) = a \cdot C^b(s) \tag{54}$$

is empirically documented (Tyree et al., 1991; Yang and Tyree, 1993; Patino et al., 1995; Zotz et al., 1998) where $C(s)$ denotes the branch cross-sectional area at s, and $a, b > 0$ are constants.

Thus, for a given average soil water potential $\Psi(0) = \Psi_0$, (53) solves to

$$\Psi(\ell) = -E \cdot A \cdot \int_0^\ell \frac{1}{a \cdot C^b(s)}\, ds - \rho g \cdot h + \Psi_0, \tag{55}$$

where h denotes the height of the leaf.

Tyree and Zimmermann (2002) asserted a sigmoid relationship of transpiration rate E against leaf water potential $\Psi(\ell)$, in the way that E is maximal for $\Psi(\ell) = 0$ and decreases sigmoidly to 0 as $\Psi(\ell)$ decreases. This corresponds to the closure of stomata in case of low leaf water potential in order to prevent cavitation as described above. Based on the simple algebraic sigmoid function $x \mapsto \frac{x}{1+|x|}$ (which, as opposed to alternative sigmoid function types such as the logistic function used in the regression by Tyree and Zimmermann (2002), will later allow explicit calclulations) let

$$E(\Psi(\ell)) = p_3 \cdot \frac{\Psi(\ell) + p_1}{1 + p_2 \cdot |\Psi(\ell) + p_1|} + \frac{p_3}{p_2} \tag{56}$$

describe this response of E to $\Psi(\ell)$. The parameters p_1, p_2 and p_3 affect horizontal translation, steepness and vertical dilation, respectively. We have $E \geq 0$, $E' > 0$ and $E \to 0$ as $\Psi(\ell) \to -\infty$ as desired.

Inserting (56) into (55) for E results in the following equation for $\Psi(\ell)$:

$$\Psi(\ell) = c_2 + c_1 \cdot \frac{\Psi(\ell) + p_1}{1 + p_2 \cdot |\Psi(\ell) + p_1|}, \tag{57}$$

where for short

$$\begin{aligned} c_1 &:= -A \cdot \int_0^\ell \frac{1}{a \cdot C^b(s)}\, ds \cdot p_3 && \leq 0 \\ c_2 &:= \frac{c_1}{p_2} - \rho g \cdot h + \Psi_0 && \leq 0 \end{aligned}$$

Equation (57) reflects the coupling of transpiration rate E and leaf water potential $\Psi(\ell)$: On the one hand, $\Psi(\ell)$ decreases with increasing E, cf. (55), on the other hand, E decreases with decreasing $\Psi(\ell)$, cf. (56), respectively, other things being equal. The equation's unique non-positive solution describes the balance between these two counteracting mechanisms. It reads

$$\Psi(\ell) = \begin{cases} \dfrac{1}{2p_2} \cdot \left(c_3 - c_1 + 1 - \sqrt{(c_3 - c_1 + 1)^2 + 4p_2^2 c_2 p_1 - c_4} \right) \\ \qquad\qquad\qquad\qquad \text{for } c_2 \leq -p_1 \\ \dfrac{1}{2p_2} \cdot \left(c_3 + c_1 - 1 + \sqrt{(c_3 + c_1 - 1)^2 + 4p_2^2 c_2 p_1 + c_4} \right) \\ \qquad\qquad\qquad\qquad \text{for } c_2 > -p_1 \end{cases} \tag{58}$$

where we abbreviated $c_3 := c_2 p_2 - p_1 p_2$ and $c_4 := 4p_2(c_1 p_1 + c_2)$.

With the balanced value of $\Psi(\ell)$ now at hand, transpiration rate E follows from (56). Altogether, this defines an explicit function

$$E = f_1(\Psi_0) \tag{59}$$

6.5.2 *Properties*

HYDRAULIC LIMITATION OF GROWTH Equation (55) describes that, other things being equal, $\Psi(\ell)$ decreases with height h as well as (ultimately) branch path length ℓ, and thus, as described in (56), so does E. Provided a monotonic correlation between E and leaf net biomass production, the same is true for the latter variable, i.e. increasing height has a decreasing effect on biomass production, other things being equal. This is a quantification of the hydraulic limitation hypothesis (Ryan and Yoder, 1997), which links this very property to the deceleration and eventual limitation of tree height growth.

Despite further supportive evidence (e.g. Hubbard et al., 1999), Ryan et al. (2006) challenged the theory and suggested other causes.

In particular, the authors argue that low leaf water potential affects turgor pressure, thus limiting growth in terms of cell expansion and division. This sink-oriented perspective is conceptually quite different from the more classical source-oriented one that is inherent to the hydraulic limitation hypothesis (as well as to the models in this thesis). Nevertheless, while the debate on the exact biological mechanisms is still ongoing, Fatichi et al. (2014) note that, in practical plant modelling, the two approaches might just amount to the same outcome.

LOCATION OF THE MAIN RESISTANCES The cumulative hydraulic resistance of the soil-to-leaf pathway is given by $\int_0^\ell \frac{1}{a \cdot C^b(s)}$. Our above considerations allow to assess this property theoretically: For illustration, we consider an allometric height h to stem cross-sectional area c relation $h = \mathfrak{a} \cdot c^{\mathfrak{b}}$ and assume, for the sake of the argument, this relation to be scale-invariant, so that the cross-sectional area of a tree of total height H is equal to $C_H(h) = \left(\frac{H-h}{\mathfrak{a}}\right)^{\frac{1}{\mathfrak{b}}}$ at height $h \in [0, H]$. For a leaf located at the tip ot the trunk, $\ell = H$, the cumulative resistance along its pathway up to height $h \in [0, H]$ reads

$$R_H(h) = \int_0^h \frac{1}{a \cdot C_H^b(s)}\, ds = \frac{\mathfrak{a}^{\frac{b}{\mathfrak{b}}}}{a \cdot \left(\frac{b}{\mathfrak{b}} - 1\right)} \cdot \left((H-h)^{1-\frac{b}{\mathfrak{b}}} - H^{1-\frac{b}{\mathfrak{b}}}\right).$$

In the case of European beech (*Fagus sylvatica* L.), we use $\mathfrak{a} = 65.61$ and $\mathfrak{b} = 0.38$ obtained from a height-to-diameter allometry by Bartelink (1997) after replacing the diameter by $\sqrt{2c/\pi}$, as well as $a = 51174.9$ and $b = 1.85$ from fairly concordant results by Cochard et al. (2000) and Cruiziat et al. (2002). Altogether we have $R_H(h) = 3541.48 \cdot \left((H-h)^{-3.87} - H^{-3.87}\right)$. Figure 24 shows $C_H(h)$ and $R_H(h)$ against h for $H = 30$ m; the profiles are virtually identical for different tree heights. This simple calculation illustrates the disproportionately strong impact of the smallest and final parts of the branch path as opposed to a negligible effect of thicker branches and the trunk – which clearly remains true even if the assumption of a scale-invariant allometry is not strictly true.

In other words, the branch path parts that actually matter in the calculation of total hydraulic resistance up to an arbitrary leaf depend very little on the leaf's actual position in the tree, the tree's size or age. This is in agreement with the theoretical considerations by West et al. (1999a), Enquist (2000) and Becker et al. (2000), who demonstrated that an appropriate tapering of the vascular conduits results indeed in a hydraulic resistance that is independent of the path length. Empirical evidence was presented by Yang and Tyree (1993) and Tyree and Zimmermann (2002) (and references therein), who found that the major part of the total water flow resistance was located in the smallest branch parts. In practical applications of our model, this justifies to replace the a priori branch path-dependent term $\int_0^\ell \frac{1}{a \cdot C^b(s)}\, ds$ by a

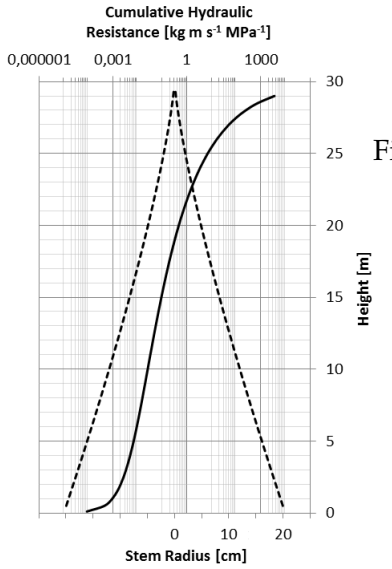

Figure 24.: Total resistance to water flow, $R_H(h)$, up to a given tree height h (solid line, logarithmic scale) and, for comparison, the stem profile $C_H(h)$ (dashed line, linear scale).

constant value – which is a particularly convenient step in a leaf density-based growth model, in which root-to-leaf branch diameters $C(s)$ are not readily available.

HEIGHT AND SOIL WATER POTENTIAL Curiously, in (55) the roles of soil water potential, Ψ_0, and height, in terms of $\rho g \cdot h$, are interchangeable. Provided that the effect of height on $\int_0^\ell \frac{1}{a \cdot C^b}(s)\, ds$ is negligible, which is reasonable as argued in the previous paragraph, this would in theory imply that, if water is the limiting factor to height in the sense of section 6.5.2, an increase of Ψ_0 by 1 Pa enables an increase in height by $\frac{1}{\rho g} \approx 0.1$ mm. Experimental data would be desirable to test this hypothesis.

6.5.3 *Model integration*

In the style of Jarvis (1976) and follow-up work, the dependence of E on Ψ_0 determined in (59), can be straightforwardly extended to other environmental variables such as light intensity, temperature or water pressure deficit in a multiplicative way. Towards an implementation of the above considerations into the tree growth model presented in the previous section, we do this for the light variable, i.e.

$$E(\Psi_0, L) = f_1(\Psi_0) \cdot f_2(L), \tag{60}$$

where now L denotes instantaneous radiation. Here, $f_2 \in [0, 1]$ describes the relative response of E to light intensity at fixed $\Psi(\ell) = 0$ (rescaled such that its supremum equals 1), and where f_1 is as in (59) and describes the response of E to Ψ_0 at maximal radiation $f_2 = 1$. This affects the calculation in section 6.5.1 only in that the constants

c_1, c_2 in (57) change. This is due to the fact that radiation, unlike water potential, is an exogenous variable.

It is important to note that unlike Jarvis (1976) and followers, (60) is not a multiplicative approach in the narrow sense (c.f. Damour et al., 2010) since varying L ultimately also affects $\Psi(\ell)$ by inducing a different E-$\Psi(\ell)$ balance (see also figure 25). The actual response of E to varying L is thus more complex than the term f_2.

We note that due to f_2 being rescaled, we can replace L by

$$L_{\text{rel}}(x,n) = \exp\big(-\int_{x_3}^{\infty} \lambda(x,n) \cdot \clubsuit(x,n)\, dx_3\big),$$

i.e. the relative portion of the total radiation reaching x, under the assumption of a constant average radiation, as done in section 6.1.

We can now use the previous considerations for a light and water-dependent net biomass production function later used in an extension of the previously presented tree growth model. We define

$$B(x,n) = \mu \cdot \clubsuit(x,n) \cdot E(x,n), \tag{61}$$

where $E(x,n) = E(\Psi_0, L(x,n))$ denotes local transpiration rate, and the parameter μ is the product of vegetation period length and water use efficiency, both taken as constant. The latter in particular is assumed constant as observed by Wong et al. (1979), Mott (1988) and Buckley et al. (2003), and derived theoretically in the stomatal optimization theory (Cowan, 1977; Cowan and Farquhar, 1977) independent of light conditions. Biomass production has been computed from transpiration through a water use efficiency coefficient in earlier works, notably by Howell and Musick (1984).

As for the relative response to radiation $f_2 \in [0,1]$, in the style of the original model of section 6.1, we simplify radiation as constant, and describe the response of biomass production to light incidence at fixed $\Psi(\ell) = 0$ in terms of a linear function, hence $f_2 = L_{\text{rel}}$. For given $L_{\text{rel}}(x,n)$ and given soil water potential Ψ_0, we compute local transpiration rate $E(x,n)$. As argued in section 6.5.2, we approximate $\int_0^\ell \frac{1}{a \cdot C^b(s)}\, ds = R$ for a constant total hydraulic resistance independent of x.

The function f_1 can be obtained from data on European beech from Lemoine et al. (2002) on the dependency $\Psi(\ell) \mapsto g_s$ after replacing $E = 0.0166 \cdot g_s$ (fitted with data from Cochard et al., 2000). This provides the three parameters in (57), their values are given in table 4. For this set of parameters, figure 25 illustrates the balanced value of transpiration rate against light intensity as well as, for illustration, total hydraulic resistance in three different height and soil water potential scenarios.

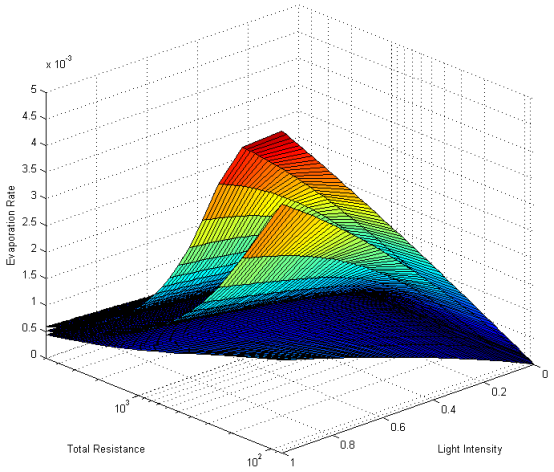

Figure 25.: Balanced transpiration as a function of local relative light incidence L_{rel} as well as (the fixed) total hydraulic resistance R for $\rho g \cdot h + \Psi_0 \in \{0, 1, 1.5\}$ (upper, middle and lower surface, respectively). Although we chose f_2 to be linear, the actual response of E against L is slightly concave due since the immediate increase of E at a higher light incidence results in a decrease in leaf water potential which is responsible for an additional decrease of E.

The modified biomass production function (61) is now in the tree growth model presented in section 6 used in place of (48). To emphasise the teleonomic component of the spatial expansion, we replace the local light gradient $\nabla_x L$, along which produced biomass was translated prior to its allocation, by the productivity gradient $\nabla_x \frac{B(x,n)}{\clubsuit(x,n)}$ – which, in contrast to the original model (there we had $L \propto \frac{B}{\clubsuit}$) is no longer necessarily equivalent to the light gradient. It now points in the direction of the greatest increase in light and productivity with regard to light and water availability. All other previous model mechanisms remain unchanged.

In the simulations presented in the following section, we used a site-specific yet otherwise constant soil water potential Ψ_0. Considering a long-term average instead of a time-dependent soil water potential follows the approaches of White et al. (1999) and MacFarlane et al. (2004) in which stomatal conductance responds to integrated values of pre-dawn water potential (as estimate for soil water potential near roots), arguing that water stress is indeed more relevant in the long rather than short term.

6.5.4 *Simulations*

DATA SET DESCRIPTION We tested our modified model against 24 even-aged pure stands of European beech (*Fagus sylvatica* L.) from eight different sites throughout southern Germany, similar to and including the one described in section 6.2.

In the same way as described in section 6.2, different thinning treatments have been applied on sub-plots 1, 2 and 3 of each site, resulting in high, medium and low stand density, respectively. Table 3 summarizes characteristic stand variables. Additional details can be found in Kennel (1972).

Experimental site	Latitude Mean annual temperature	Longitude Mean annual precipitation	Altitude
Kirchheimbolanden 11	7°93′07″E 7.0 °C	49°63′21″N 660 mm	610 m
Waldbrunn 14	9°80′27″E 8.5 °C	49°72′23″N 710 mm	360 m
Fabrikschleichach 15	10°57′12″E 7.5 °C	49°91′86″N 820 mm	470 m
Elmstein-Nord 20	7°91′86″E 8.0 °C	49°39′08″N 780mm	400 m
Lohr-West 24	9°50′62″E 7.5 °C	49°99′10″N 960 mm	430 m
Mittelsinn 25	9°51′54″E 7.0 °C	50°19′50″N 1020 mm	505 m
Rothenburg 26	9°44′69″E 7.0 °C	49°97′42″N 1050 mm	475 m
Hain 27	9°33′47″E 7.0 °C	49°99′25″N 1080 mm	420 m

Table 3.: Details of the experimental sites. Stand densities over time, affected by harvest and natural mortality, are qualitatively similar to those shown in figure 15 and can be found in Kennel (1972).

Standard deviation values for tree height and trunk diameter at breast height were not available for the sites Kirchheimbolanden 11, Waldbrunn 14, Lord-West 24 and Rothenburg 26. In figure 26, to give a rough impression, we thus used estimates based on a fairly reasonable linear regression of standard deviation against mean value derived from the remaining sites.

6.5.4.1 *Comparison to long-term data*

The simulation procedure is identical to the one described in section 6.2. Parameters not related to the modified computation of biomass

production are the same as in table 2. Newly added species-specific parameters are summarised in table 4. Site-specific average soil water potentials were not available by measurement and were thus estimated by model inversion (table 5). The range of values is realistic as plants are known to function within -0.006 MPa to -1.6 MPa (Horn et al., 2010). Table 5 also shows empirically measured site-specific top tree heights (averaged over the three stand densities), which are a good indicator for soil water conditions (Martin Nickel, personal communication). Indeed, we note a strong positive correlation with the estimated site-specific soil water potentials, as desired.

Parameter	Value	Reference
p_1	357	Lemoine et al. (2002)
p_2	1.8	Lemoine et al. (2002)
p_3	3	Lemoine et al. (2002)
A [m²]	0.0015	Barna (2004), Meier and Leuschner (2008)
R [m^{-1} s^{-1}]	800	
μ [y]	0.041	

Table 4.: Model parameters. Unreferenced parameters were estimated. Additional ones are the same as in table 2.

Site	Ψ_0 [MPa]	Top height [m]
Kirchheimbolanden 11	-0.05	29.0
Waldbrunn 14	-0.2	26.8
Fabrikschleichach 15	-0.15	28.4
Elmstein-Nord 20	0	29.7
Lohr-West 24	-0.6	25.7
Rothenburg 26	-0.05	29.3
Hain 27	0	31.8
Mittelsinn 25	-0.8	23.1

Table 5.: Site-specific average soil water potentials Ψ_0, estimated to the nearest twentieth. The values are well positively correlated ($r > 0.9$) with the empirical stand-specific top heights.

The spatial leaf density dynamics in all cases are virtually the same as in the light-only case shown in figures 18 and 19. Figure 26 illustrates model simulations against the empirical data. Overall, our results correspond well to observations across the different sites as well as, as before, across the different stand densities.

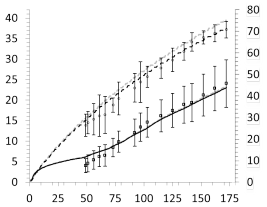

(a) Hain 27, sub-plot 1

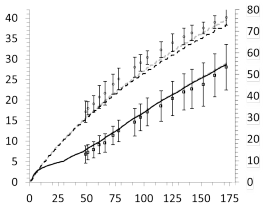

(b) Hain 27, sub-plot 2

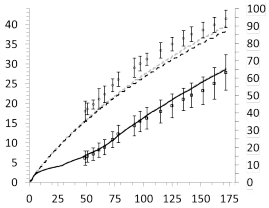

(c) Hain 27, sub-plot 3

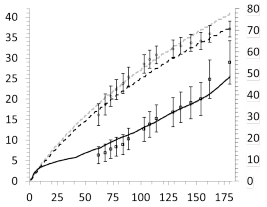

(d) Elmstein-Nord 20, sub-plot 1

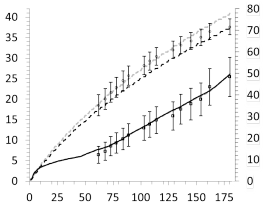

(e) Elmstein-Nord 20, sub-plot 2

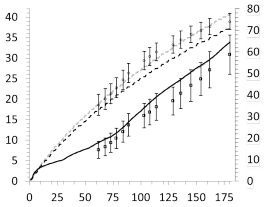

(f) Elmstein-Nord 20, sub-plot 3

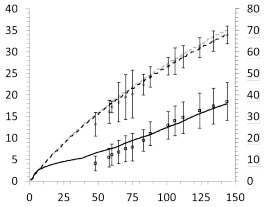

(g) Rothenburg 26, sub-plot 1

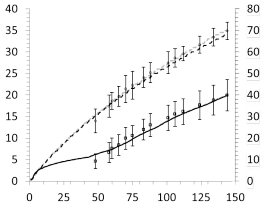

(h) Rothenburg 26, sub-plot 2

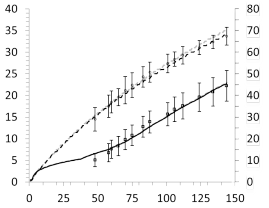

(i) Rothenburg 26, sub-plot 3

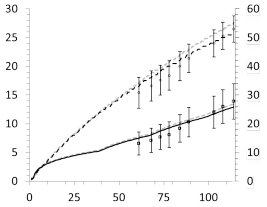

(j) Kirchheimbolanden 11, sub-plot 1

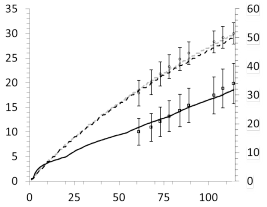

(k) Kirchheimbolanden 11, sub-plot 2

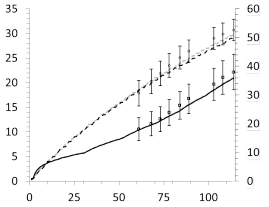

(l) Kirchheimbolanden 11, sub-plot 3

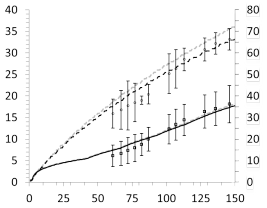

(m) Fabrikschleichach 15, sub-plot 1

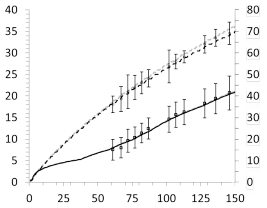

(n) Fabrikschleichach 15, sub-plot 2

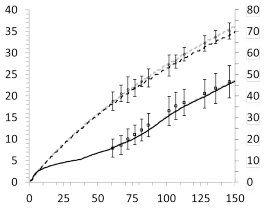

(o) Fabrikschleichach 15, sub-plot 3

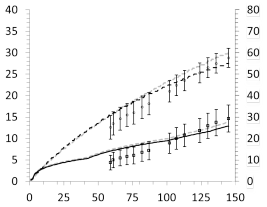

(p) Waldbrunn 14, sub-plot 1

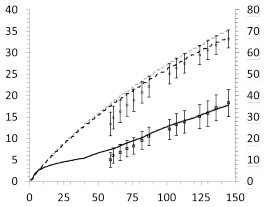

(q) Waldbrunn 14, sub-plot 2

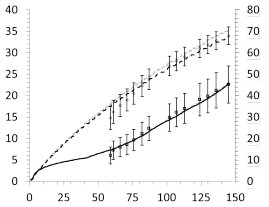

(r) Waldbrunn 14, sub-plot 3

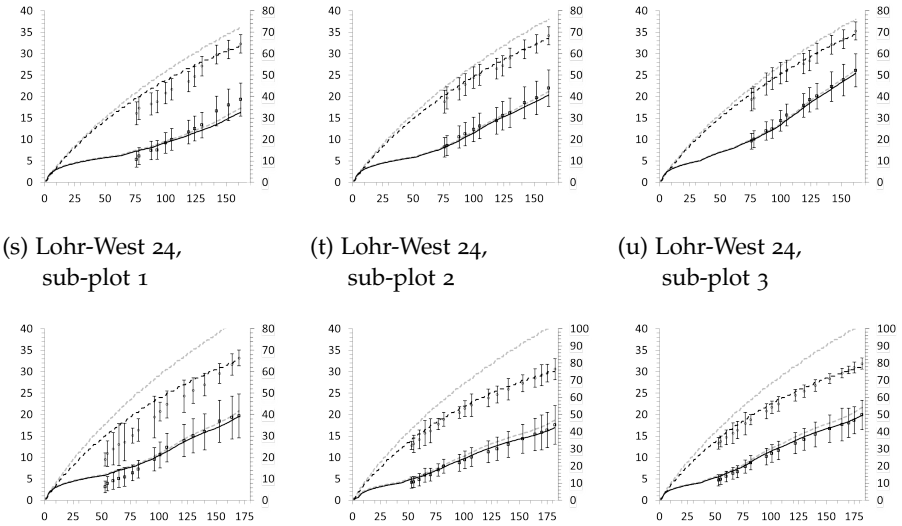

(s) Lohr-West 24, sub-plot 1

(t) Lohr-West 24, sub-plot 2

(u) Lohr-West 24, sub-plot 3

(v) Mittelsinn 25, sub-plot 1

(w) Mittelsinn 25, sub-plot 2

(x) Mittelsinn 25, sub-plot 3

Figure 26.: Comparison of simulated to empirical stand average and standard deviation (partially estimated, see text) data of tree height [m] (dashed line, circles, left axis) and diameter at breast height [cm] (solid line, circles, right axis) over time [years] and three sub-plots differing in stand density. Transparent lines illustrate the case of leaf water potential $\Psi(\ell)$ artificially being set to 0, thus nullifying the effect of the hydraulic submodel, see text.

Incorporating water availability and hydraulic effects into our tree growth model in the way described hitherto has a curious impact: If we artificially set $\Psi(\ell)$ to 0 for comparison (figure 26, transparent lines), thus running simulations for the case of perfectly unconstrained water supply and effectively reducing the model to the previous version in which biomass production and spatial expansion depended merely on light, reveals an almost unchanged trunk diameter growth, as well as, as could be expected, an increase in height growth. We address the latter property before turning to the more striking former one.

Under equal light and local leaf density conditions, local biomass production decreases with increasing height due to a resulting lower leaf water potential and consequently transpiration rate. Hence, the third entry of the productivity gradient decreases in magnitude with increasing height. Height growth in the first place both in the modified and the original model in section 6.1 is a consequence of the local attempt to avoid inter-individual and, at least to an equal extent, intra-individual competition for light (recall the concept of modularity). The incentive to do so by growing in height is lessened by the above-described impact of hydraulic limitation on the vertical component of the productivity gradient governing the crown's vertical expansion.

The upward motion of a leaf density under water constraints will thus continuously decelerate, compared to the scenario of a light-only dependency.

This observation is also essential as to why trunk diameter growth is relatively less affected by water conditions in our simulations: A crown – or more precisely, a canopy, since, surrounding competitors are affected and respond in an identical way, which is crucial – settling for a smaller height, due to the above-described mechanism of a mitigated incentive to escape competition for light, can use a larger portion of produced biomass for the allocation to foliage as opposed to supporting sapwood in terms of the pipe model theory (recall that the partitioning coefficient $p(x)$ in (14) decreases with height). Other things being equal, this induces an increased future production of a lower compared to a higher located and otherwise similar crown. It appears that this effect compensates to a considerable extend for the inherently lower biomass production of a water-constrained crown in comparison to its unconstrained counterpart where $\Psi(\ell) \equiv 0$, other things being equal, altogether bringing about a similar trunk diameter growth.

It is striking that with the exception of the very dry sites Lohr-West 24 and Mittelsinn 25, the difference in simulation output of the complete model and the one where the hydraulic mechanism is overridden, i.e. essentially the model from section 6.1, is marginal. In these cases, soil water potential Ψ_0 is not low enough to bring leaf water potentials close to the inflexion point of the function (56), close and below which hydraulic limitations become more pronounced. Above all, this strongly confirms the predictive power of the only light-dependent model of section 6.1 in overall moist conditions.

6.5.5 *Discussion*

We have demonstrated that the relationship between leaf water potential and transpiration is not unilateral as tacitly assumed by existing models, but interactive, given that transpiration levels affect the speed at which a soil-to-leaf water column moves and thereby that the water potential gradient along it, as well as ultimately the end value $\Psi(\ell)$.

The possibility of including additional environmental parameters in this framework remains unaffected. We illustrated this by incorporating the effect of light incidence in terms of a semi-multiplicative approach, in which the ultimate effect of the arguments is more complex than their response term as such. This is notably in response to one of the major criticisms of the widely-used multiplicative approaches, namely the supposedly independent action of the different factors (Damour et al., 2010).

Our model is based on several simplifications which suggested it to be applied in a long-term and large-scale scenario. We did this by integrating it into our previously developed tree growth model and running simulations for a stand-average tree over a long period of time.

Adapting our model to small-scale and short-term processes and relaxing these simplifications begins with including other environmental, in particular atmospheric parameters. Moreover, the steady-state assumption of the tree's water balance is an idealisation, given that water storage in trees underlies diurnal fluctuations (Tyree and Zimmermann, 2002). Nevertheless, in the long term, it may be a reasonable simplification. Linked to this is the non-consideration of the horizontal transport of water (see Tyree and Zimmermann, 2002) within the tree in our model. Although this is an important process, it plays a considerably smaller role than vertical movement – an observation that gave rise to the concept of hydraulic branch autonomy (Sprugel et al., 1991). We tacitly assumed the establishment of an E-$\Psi(\ell)$ equilibrium for given environmental conditions, such as light L and soil water potential Ψ_0 in our model, to occur infinitely fast. Indeed, it has been shown that stomata open and close very quick (Saliendra et al., 1995; Salleo et al., 2000, 2001). Still, applying the model to a much smaller time scale would call for a modifications e.g. in terms of a smooth change in stomata aperture in response to changing environmental conditions as well as a delay in its interaction with water potential. The balancing between the probability for embolism formation, which, in so-called vulnerability curves, is described as a function of water potential, and the repair of embolisms (see Tyree and Zimmermann, 2002) is only implicitly accounted for in our model, and could be addressed from a more mechanistic point of view. Lastly, our assumption of average, spatially and temporally constant soil water potentials leaves room for refinement, although such values are tedious to trace experimentally.

In our model, soil water potential is a given, exogenous parameters, whereas in reality it is subject to the functioning of the individual tree and the larger stand community. While in this thesis, we focus on above-ground functional-structural dynamics, a possible next step would be to couple our crown models with a suitable root growth model – e.g. in the style of density-based approaches mentioned in section 1.2.3 – and incorporate the below-ground local competition for water and its impact on local soil water potentials.

In this thesis, we have incorporated root growth in terms of simplifying assumptions in conjunction with the pipe model theory (see section 3.5.1). In general, the partitioning of available biomass between shoots and roots is a complex modelling domain (Wilson, 1988). In accordance with the basic idea of the teleonomic root models mentioned in section 3.5, here, we sketch a perspective for a teleonomic

generalization of the water-dependent tree growth model presented in this section. Based on a formalisation of the positive correlation between the average soil water potential that a tree has access to and its root mass, the partitioning of biomass between shoots and roots can be seen as an optimization problem: There is a trade-off between allocating biomass to the shoots, which increases biomass production by means of higher leaf area, and allocating biomass to roots, which increases biomass production by means of a higher soil water potential. A suitable model would determine the optimal balance between these two alternatives.

7

ASSIGNING A BRANCH STRUCTURE

The non-consideration of branch topology in the previous chapters has facilitated the efficient modelling of the spatial dynamics of the leaf distribution. However, an important aspect of the tree's morphology is currently not part of the spatial output of the tree models presented in chapters 5 and 6. Thus, in this chapter, we investigate in what way the provided leaf density can be used to derive a complete description of the tree's geometry, namely a realistic branch system.

The problem we address is a static one: We aim at assigning a branch structure merely to the leaf density output at a given fixed point in time, $\clubsuit = \clubsuit(x)$, without it having an impact on future model dynamics. In particular, a branch structure determined for a leaf density at some time t_1 is a priori not required to be consistent with a branch structure determined at a time $t_2 > t_1$; this would already imply a topological approach.

In a first step, the subsequent method determines for a given finite set of points (leaf positions) a set of lines connecting those down to the stem base. In the context of leaf density $\clubsuit$, the points can be regarded as realizations of the probability distribution on $\mathbb{R}^3$

$$x \mapsto \frac{\clubsuit(x)}{\int_{\mathbb{R}^3} \clubsuit(\xi)\, d\xi}. \tag{62}$$

We address the issue of an infinite number of points in section 7.2.

Approaches that are related to the one presented in this chapter have appeared in the domains of computer graphics as well as photograph-based reconstructions of tree structures. In the model by Runions et al. (2007), the constructed branch system is composed of adjacent particles that are iteratively strung together in order to gradually pass through a set of points that is evenly distributed in a given crown envelope. The approach focusses on the space filling of the crown, and conceptually appears to be not straightforwardly generalizable to a given distribution of leaves, which is our target set. In the model by Neubert et al. (2007), a branch structure is formed by the paths of points starting at the leaf positions and being transported down to the stem base along a vector field that is defined based on an a priori given trunk and primary branch structure. On the same basis, Sakaguchi (1998) uses L-systems to generate a more detailed branch skeleton

that fills a given crown envelope. The last two models thus require a rudimentary skeleton as input, whereas our model constructs the latter from scratch.

7.1 MODEL DESCRIPTION

In his trailblazing article for the systematization of tree structure, Leopold (1971) wrote "By analogy [to river systems] it seems possible that the branching patterns of trees and of other biologic forms are governed by [...] tendencies which are analogous to minimum energy expenditure [...]. In the case of trees it might be supposed that [this] involves minimizing the total length of all branches and stems." and hypothesized that "the form which is most probable also tends to minimize the total length of all paths within the applicable constraints". Leopold's point of view is clearly a teleonomic one: For a given distribution of leaves, he assumes the minimization of the total length of the branch network and thus of wood mass, implying a maximization of leaf mass and hence future biomass production.

The following algorithm is strongly based on Leopold's hypothesis. We construct a set S of possible branch systems that connect the leaf positions to the stem base via line segments and bifurcations, and which is essentially formed only under the constraint of given branching angles. S covers a very large, if not exhaustive set of skeletons, of which, in the end, we identify the system with the shortest total length.

Let $x_1, \dots, x_m \subset \mathbb{R}^2 \times \mathbb{R}_+$ denote leaf positions of a tree with a vertical trunk rooting in $(0,0,0)$. This last assumption is made without loss of generality and can be readily relaxed. For the sake of convenience we assume that $x_1 = (0,0,h)$ where h denotes the height of the tree.

For later use, let $\mathbb{L}^n$ denote the set of ordered lists of length n, composed of natural numbers. For lists $a = a_1 a_2 \dots a_n \in \mathbb{L}^n$ and $b = b_1 b_2 \dots b_m \in \mathbb{L}^m$, with $a_i, b_i, n, m \in \mathbb{N}$, we define the *concatenation* of a and b by

$$a.b = a_1 \dots a_n b_1 \dots b_n \in \mathbb{L}^{n+m}.$$

a is by definition *contained in* b, $a \subset_{\mathbb{L}} b$, if a is the tail of b, i.e. if

$$m \geq n \quad \text{and} \quad a_i = b_{m-n+i} \quad \text{for } i = 1, \dots, n.$$

a and b are called *compatible*, $a \sim_{\mathbb{L}} b$, if either $a_i \neq b_j$ for all i, j, or

$$\exists i_0 \geq 0 : \; a_{n-i} = b_{m-i} \text{ for all } i = 0, \dots, i_0 \\ \text{and } \{a_1, \dots, a_{n-i_0-1}\} \cap \{b_1, \dots, b_{m-i_0-1}\} = \varnothing.$$

Compatibility is a symmetric and reflexive but not transitive relation.

For two points $x, y \in \mathbb{R}^3$ denote by xy and $\overline{xy}$ the line and line segment through x and y, respectively. With

$$P_{y,z}(x) = z + (x - z) \cdot (y - z) \cdot \frac{y - z}{\|y - z\|^2}$$

denoting the orthogonal projection of x onto the line through y and z, let

$$P^{\varphi}_{y,z}(x) = P_{y,z}(x) - \frac{y-z}{\|y-z\|} \cdot \|P_{y,z}(x) - x\| \cdot \tan(\varphi)$$

be the oblique projection, where the angle that $x\, P^{\varphi}_{y,z}(x)$ draws with yz is φ.

We follow Honda (1971) in that branches are straight, and a ramification comprises the bifurcation of one mother branch into two daughter ones. A necessary input for the subsequent algorithm are the branching angles, i.e. the angle between a mother and daughter branch. We assume these to be only dependent on branching order. This is an assumption common in many topological models (e.g. Takenaka, 1994; Perttunen et al., 1996) and, in a particular case, empirically confirmed by Mäkelä and Vanninen (1998). It can principally be relaxed, e.g. by introducing a dependence on the ratio of height and crown diameter of the given leaf density as a global proxy for competition. Denote by φ_n the bifurcation of an order n branch from an order $n-1$ branch in the botanical (or Hack's) ordering system (e.g Borchert and Slade, 1981), which is the appropriate one here.

The starting point of the following procedure is a given line segment representing the trunk. Iteratively, we construct new line segments leading from the leaves to branching points on line segments formed in the previous step; starting by connecting all leaves to the trunk in the first step, then looking for connections between the leaves and these branches, and so forth.

Next, we describe the method in detail. Although the basic ideas are generally intuitive, the formalism is at times rather cumbersome. Parallel to its development, boxes throughout the text aim to illustrate the specific steps for an exemplary set of given leaf positions.

In the following we consider the sets G^i_n and T^i_n, formally defined in (63) and illustrated in the box below. We denote by $G^i_n \subset \mathbb{R}^3$ all possible points where an order n branch directed and terminating at x_i bifurcates from an order $n-1$ branch, where the latter is given by a line segment through a different leaf position x_j and one of its appropriate order $n-1$ branching points. In order for $P^{\varphi_{n+1}}_{(G^j_n)_k, x_j}(x_i)$ – i.e. the oblique projection of x_i onto the line through x_j and the kth element of G^j_n – to be indeed added to the set G^i_{n+1}, it must satisfy the two conditions (64) of lying indeed on the line segment (not just the line), and (65) of a daughter branch not being longer than the remaining mother branch, reflecting the concept of apical dominance which we assume here.

A particular branching point in G^i_{n+1} associated to leaf position x_i is thus defined by a different leaf position x_j, $j \neq i$ as well as one of the branching points associated to x_j, each of which is, on its part,

associated to a leaf position x_k, $k \neq j$, and so on. The set $T_n^i \subset \mathbb{L}^{n+1}$ captures this topological history of bifurcations for branches of order n terminating at x_i. In particular $|G_n^i| = |T_n^i|$. Formally,

$$T_1^1 = \{1\}\,,\ T_1^i = \varnothing \text{ for } i > 1 \quad G_1^1 = \{(0,0,0)\}\,,\ G_1^i = \varnothing \text{ for } i > 1$$

$$T_{n+1}^i = \bigcup_{\substack{j=1 \\ j\neq i}}^{m} \bigcup_{\sigma_{i,j,k,n}}^{k=1} \left\{ i.(T_n^j)_k \right\} \qquad G_{n+1}^i = \bigcup_{\substack{j=1 \\ j\neq i}}^{m} \bigcup_{\sigma_{i,j,k,n}}^{k=1} \left\{ P^{\varphi_{n+1}}_{(G_n^j)_k, x_j}(x_i) \right\} \tag{63}$$

where $\sigma_{i,j,k,n}$ is by definition `true` if and only if

$$\begin{cases} \max\left(\left\| P^{\varphi_{n+1}}_{(G_n^j)_k, x_j}(x_i) - x_i \right\|, \left\| P^{\varphi_{n+1}}_{(G_n^j)_k, x_j}(x_i) - (G_n^j)_k \right\| \right) < \left\| x_j - (G_n^j)_k \right\| & (64) \\ \left\| P^{\varphi_{n+1}}_{(G_n^j)_k, x_j}(x_i) - x_i \right\| < \left\| P^{\varphi_{n+1}}_{(G_n^j)_k, x_j}(x_i) - x_j \right\| & (65) \end{cases}$$

One might want to specify additionally restrictive criteria, e.g. regarding the angle potential branches defined by an end point x_i and a potential branching point $P^{\varphi_{n+1}}_{(G_n^j)_k, x_j}(x_i)$ draw with the horizontal plane, i.e.

$$\left| \arctan\left(\frac{\left| \left(P^{\varphi_{n+1}}_{(G_n^j)_k, x_j}(x_i) \right)_3 - x_3 \right|}{\sqrt{\left(\left(P^{\varphi_{n+1}}_{(G_n^j)_k, x_j}(x_i) \right)_1 - x_1 \right)^2 + \left(\left(P^{\varphi_{n+1}}_{(G_n^j)_k, x_j}(x_i) \right)_2 - x_2 \right)^2}} \right) \right| \leq \phi$$

for some upper limit ϕ, which seems reasonable in the case of many plagiotropic species. This and other possible criteria referring to branching angles (e.g. Honda, 1971; Honda et al., 1982) or the branch length ratio, i.e. the length ratio of mother and daughter branch (publicised by Whitney, 1976, Oohata and Shidei, 1971 and Leopold, 1971, but questioned by Borchert and Slade, 1981), which could be restricted to a suitable interval

$$\frac{\left\| P^{\varphi_{n+1}}_{(G_n^j)_k, x_j}(x_i) - x_i \right\|}{\left\| x_j - (G_n^j)_k \right\|} \in \left[\underline{R_b}, \overline{R_b} \right]$$

have not been accounted for in the following, in view of the supposedly little restricted plasticity of our target species beech.

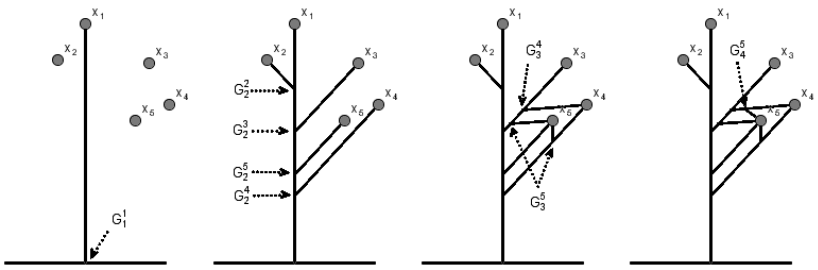

$T_1^1 = \{1\}$	$T_2^1 = \varnothing$	$T_3^1 = \varnothing$	$T_4^1 = \varnothing$
$T_1^2 = \varnothing$	$T_2^2 = \{21\}$	$T_3^2 = \varnothing$	$T_4^2 = \varnothing$
$T_1^3 = \varnothing$	$T_2^3 = \{31\}$	$T_3^3 = \varnothing$	$T_4^3 = \varnothing$
$T_1^4 = \varnothing$	$T_2^4 = \{41\}$	$T_3^4 = \{431\}$	$T_4^4 = \varnothing$
$T_1^5 = \varnothing$	$T_2^5 = \{51\}$	$T_3^5 = \{531, 541\}$	$T_4^5 = \{5431\}$

2D example of the iterative construction of branch segments. In step $n > 1$, leaves are connected to branch structures established in the previous step in accordance with the criteria (64) and (65). We used $\varphi_n = 137.5°$ for all n. Below the figure: Topologies corresponding to the branching points G_n^i. For instance, in step 3, a branch connection from x_4 is drawn to a branch leading to x_3 which, on its part, had been connected to a branch to x_1 in the previous step. Hence $431 \in T_3^4$. For $n \geq 5$, $T_n^i = \varnothing$ for all i.

Let N be the smallest number for which $G_{N+1}^i = \varnothing$ for all i, and define

$$G^i = \bigcup_{n=1}^{N} G_n^i \quad \text{and} \quad T^i = \bigcup_{n=1}^{N} T_n^i \,,$$

i.e. the sets of branching points for x_i of arbitrary order, and the appropriate topological information. For some $t \in T^1 \times \ldots \times T^m$, t_k gives a topological history of bifurcations leading to the leaf position x_k- However, not all the different histories in t may be compatible. Thus we define

$$T = \left\{ (t_1, \ldots, t_m) \in T^1 \times \ldots \times T^m : \; t_i \sim_{\mathbb{L}} t_j \text{ for all } i, j \right\}$$

In the above example $T = \big\{(1,21,31,41,51), (1,21,31,41,531), (1,21,31,41,541), (1,21,31,41,51), (1,21,31,431,51), (1,21,31,431,531), (1,21,31,431,5431)\big\}$.

and for the index set

$$K = \left\{ (k_1, \ldots, k_m) : \; \exists t \in T : \; t = (T_{k_1}^1, \ldots, T_{k_m}^m) \right\}$$

let

$$G = \left\{ (g_1, \ldots, g_m) \in (G^1)_{k_1} \times \ldots \times (G^m)_{k_m} \right\}_{(k_1, \ldots, k_m) \in K}$$

be the set of branching points whose topologies correspond to elements of the set of compatible topologies T.

The set of all admissible skeletons for the leaves $x_1, \ldots, x_m$, expressed in terms of line segments, is now given by

$$S = \{\overline{x_1 g_1} \cup \ldots \cup \overline{x_m g_m}\}_{(g_1,\ldots,g_m)\in G}$$

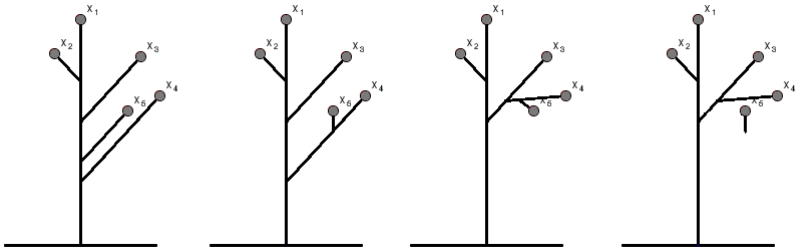

Left: Three (of total six) admissible skeletons. The second skeleton in the first box is admissible as well. Right: An inadmissible skeleton. Its topology reads $(1, 21, 31, 431, 541) \notin T$; the last two entries are incompatible.

For reasonably distributed x_i, S will be non-empty. According to Leopold's hypothesis, we choose the one with the shortest total length:

$$s^* = \arg\min_{s\in S} \sum_{i=1}^{m} |s_i| \ .$$

BRANCH THICKNESSES Prior to the introduction of the conceptual pipe model theory, Shinozaki et al. (1964) empirically established a proportionality between the total cross-sectional area of branches above crown break to the amount of foliage they support. As previously done e.g. by Runions et al. (2007), we can assign cross-sectional areas to the previously determined branch segments above crown break under this assumption. Let $t \in T$ and $g \in G$ denote the topology and set of branching points that correspond to some $s \in S$. The subset

$$t' = \left\{t_i \in t : \ \nexists j : \ t_i^* \subset_{\mathbb{L}} t_j\right\}$$

strips t of redundant information.

For $s = s^*$: $t = \{1, 21, 31, 431, 5431\}$ and $t' = \{21, 5431\}$. In particular t'_2 covers all the information of t_1, t_3, t_4 and t_5.

The branches, characterised as a set of the appropriate indices of the leaves they terminate at, that bifurcate from branch i are

$$b_i = \{t'_j \in t' : \ t'_{j+1} = i\}.$$

For $s = s^*$: $b_1 = \{2,3\}$, $b_2 = \varnothing$, $b_3 = \{4\}$, $b_4 = \{5\}$, $b_5 = \varnothing$.

The number of leaves supported by branch i is thus

$$l_i = 1 + \sum_{j=1}^{|t'|} \left(\mathrm{ind}_{t'_j}(i) - 1 \right) ,$$

where $\mathrm{ind}_{t'_j}(i)$ returns the index of i in t'_j if $i \in t'_j$ and 0 else.

For $s = s^*$: $l_1 = 1+1+3 = 5$, $l_2 = 1+0+0 = 1$, $l_3 = 1+0+2 = 3$, $l_4 = 1+0+1 = 2$, $l_5 = 1+0+0 = 1$.

Without loss of generality, let $g^i_1, \ldots, g^i_{|b_i|}$ denote the branching points on branch i ordered such that

$$\|g^i_1 - x_i\| \leq \ldots \leq \|g^i_{|b_i|} - x_i\|$$

The number of pipes that join branch i at the branching point g^i_k is l_k. Denoting the end points of branch i by $g^i_0 := x_i$ and $g^i_{|b_i|+1} := g_i$, the number of leaves L^i_k supported be the branch segment $\overline{g^i_k g^i_{k+1}}$ equals

$$L^i_k = 1 + \sum_{\kappa=1}^{k} l_\kappa \qquad \text{for } k = 0, \ldots, |b_i| \ .$$

For $s = s^*$: The trunk (branch 1) in particular is devided into 3 segments, supporting – from leaf to stem base – 1, 2 and 5 leaves respectively.

Assuming a proportionality of branch cross-sectional area to the number of leaves supported by it, the cross-sectional area of branch segment $\overline{g^i_k g^i_{k+1}}$ is given by $P \cdot L^i_k$ where P, denotes petiole cross-sectional area. Shinozaki et al. (1964) claims this to be true with the exception of the below-crown trunk segment, i.e. $\overline{(0,0,0), g^1_{|b_1|}}$, which needs to be considered separately. Among other approaches, Oohata and Shinozaki (1979) proposed a straightforward to apply model for below-crown trunk tapering, depending merely on species-specific parameters as well as the cross-sectional area at crown break and the above-crown tree mass, both of which are provided by the presented algorithm.

7.2 SIMULATIONS AND DISCUSSION

All subsequent results are based on leaf positions given by realizations of the probability distribution associated to the simulated leaf density shown in figure 21 according to (62). In practice, the algorithm quickly

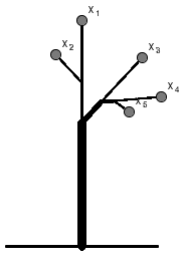

The final skeleton s^* with the appropriate segment thicknesses (not considering trunk tapering).

generates a number of complex combinatorial structures that drastically slow down computational speed to the point where a number of leaves beyond the order of twenty becomes to intensive. Testing lists for compatibility is a particular bottleneck in this process. Figure 27 illustrates the fast increase of computational time against the number of given leaf positions.

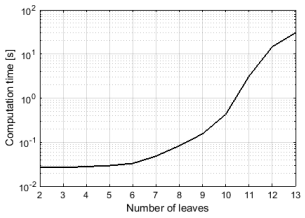

Figure 27.: Computational time averaged over 100 randomly chosen sets of leaf positions for each given number of leaves.

Nevertheless, the method yields realistic results for the system of main branches as exemplified in figure 28. In particular, it can thus complement the above-mentioned reconstruction models by Sakaguchi (1998) and Neubert et al. (2007), which require this very structure as an input based on which more complex skeletons are generated.

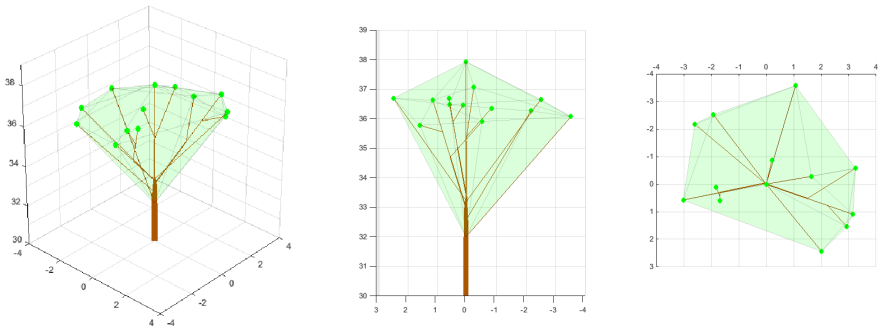

Figure 28.: Oblique top and side view of an example of a skeleton generated from thirteen randomly chosen leaf positions (green points). We used $\varphi_n = 138.5°$ (cf. Bayer et al., 2013) for all n. The transparent surface represents the crown's convex hull.

Formally, a leaf density, whose support has a non-empty interior, is an infinite set of points. The task of assigning a branch network to

such a structure may thus be assumed linked to fractal geometry, a field that has traditionally been stimulated by and interacting with plant modelling (e.g. Mandelbrot, 1983; Smith, 1984; Palmer, 1988; Zeide, 1991). In particular, West et al. (1999b) elaborated on the idea of two-dimensional foliage being arranged in a fractal way such as to virtually fill a three-dimensional space.

Theoretically, the iteration step of the algorithm presented here can be reasonably generalized to an infinite set of points. However, in general the existence of $N \in \mathbb{N}$ such that for all $n > N$ we have $G_n^i = T_n^i = \varnothing$ cannot be expected. Meanwhile, the question whether the skeleton converges in a reasonable sense, e.g. in the way that $s^*(n)$ and $s^*(n+1)$ share the same branch system up to order m where m grows beyond all bounds as n becomes large, $s^*(n)$ denoting the shortest of all admissible skeletons up to iteration step n, remains open.

8

CONCLUSION AND PERSPECTIVES

The aim of this thesis was to introduce, explore and apply leaf area density ♣ and horizontal leaf area density ♠ as means to characterise the local distribution of foliage and thus crown morphology in dynamic plant growth models. This has indeed proven an efficient middle-way between computationally expensive small-scale models with a topological architecture and large-scale models based on a description of crown shape in terms of rigid structures such as envelopes. In an intentionally concise framework, our applied models managed to generate a series of empirically documented, complex emergent phenomena, and motivated biological hypotheses on the drivers of spatial growth. In the spirit of teleonomic modelling, the approach of a spatial expansion along the local productivity gradient allowed to set aside the otherwise complex modelling of branching processes at a lower hierarchical level, and instead describe goal-directed crown expansion in a direct way. This mechanism accounted for a spontaneous adaptation to competition for light and captured the resulting reduction in growth rate – a property well reflected in the comparison to empirical data sets from density experiments. Across different plant types from crops to forest stands, as well as against diverse data types from long-term biometrical observations to 3D spatial data, our approaches allowed realistic simulations of growth dynamics, plasticity and spontaneous local adaptability to different competitive conditions with only few parameters – key challenges for present day functional-structural plant models.

The deliberate simplicity of our models leaves room for refinements in terms of additional ecophysiological parameters and processes. Monteith's radiation use efficiency concept is a powerful and reasonable simplification at large time scales, but could be replaced by more sophisticated models for photosynthesis and biomass production in response to light incidence (cf. Marcelis et al., 1998; Farquhar et al., 2001; Yin and Struik, 2009; Ye, 2010). These could additionally account for soil nutrients as well as atmospheric variables, such as temperature, vapour pressure deficit or carbon dioxide concentration, which we tacitly assumed as constant. Perspectives for introducing more detail in our hydraulic model have been itemised in section 6.5.5.

In this thesis, we have made do with the assertions of the pipe model theory. Criticism concerning not only the postulated constancy of the ratio of leaf mass to supportive sapwood cross-sectional area, but also with regard to the simplified transformation of sapwood to heartwood as well as the implicit neglect of maintenance respiration leave room for improvement in the appropriate model mechanisms. Empirical and conceptual contributions to these questions are part of an in-depth survey on the pipe model theory and follow-up articles, which has been conducted in parallel to this thesis (Beyer, R., Lehnebach, R., Letort, V., Heuret, P., unpublished manuscript).

Spatial leaf distributions obtained in the simulations throughout this thesis featured a high degree of regularity. In section 2.1, we argued this to be a realistic property in consideration of the high irregularity of the underlying branch network, and in section 6.2.2 we demonstrated that our simulated crowns can indeed approximate a population's average. Nevertheless, our simulations clearly represent a generic ideal type (cf. also figure 18) which contrasts with a typical individual crown that commonly features a more heterogeneous leaf distribution. At this scale, the limits of our approach of unconstrained plasticity and teleonomy, and namely the assumption of the negligibility of the effects of branch topology and its dynamics, become visible. From a modelling point of view, the possibility of a hybrid approach, introducing a simple trunk and main branches topology, coupled to and somewhat constraining and channelling the expansion of leaf density, raises serious conceptual problems that we will not address in detail here. A more promising perspective for the generation of heterogeneous patterns appears to be the introduction of stochasticity in the deterministic models presented here, e.g. with regard to the magnitude or direction of the mobility coefficient of the transport gradient, or the leaf angle distribution. Light gaps resulting from such a mechanism could induce an expansion of leaf density in an atypical direction at the next time step.

In section 3.2, we showed that horizontal leaf density provides the same amount of information on biomass production based on radiation use efficiency as does leaf density ♣, under the assumption of vertical light incidence, which in section 6.4 we justified in our particular modelling framework by comparing it to alternative light models. If information on 3D crown shape is not of interest in a specific scenario, these considerations motivate to approach the modelling of homogeneous, even-aged forests in terms of a horizontal leaf density-based model. In section 4.4, we argued that in this case, vertical profiles are of considerably less importance for inter-individual competition (among other reasons because they can be expected to be similar) than the horizontal occupation of space, suggesting the use of ♠ with the

objective of computationally efficient simulations at the landscape scale. Due to $\nabla_x \exp(-\lambda \cdot \spadesuit(x)) = -\lambda \cdot \exp(-\lambda \cdot \spadesuit(x)) \cdot \nabla_x \spadesuit(x)$, equations describing phototropism in the case of horizontal leaf density are merely quasi-linear (and potentially even more simple if the magnitude coefficient $\exp(-\lambda \cdot \spadesuit(x))$ is additionally simplified). This opens up exciting opportunities in terms of theoretical analysis and simplification up to partial solvability, and thereby additional computational speed-up (as exemplified in section 4.2), not exclusively but particularly in a sensible continuous-time setting, i.e. in the form of a reaction-diffusion equation – potentially based on the two-dimensional adaptation of an approach presented in chapter 5.

9

APPENDIX

9.1 NUMERICAL DETAILS

This section discusses selected details for the numerical implementations of the models presented in the preceding chapters. Being technically very related to the time-continuous tree models of chapter 5 addressed in the following, we omit numerical particulars of the two-dimensional crop model of chapter 4. For the sake of clarity and generality, we omit the time variable unless it is essential.

Models in chapters 4, 5 and 6 were implemented in a finite volume scheme (e.g. Toro, 2009), in which we consider the cell-specific leaf density

$$\overline{\clubsuit}_{ijk} = \frac{1}{(\Delta x)^3} \int_{\Sigma_{ijk}} \clubsuit(x)\, dx$$

on a regular mesh with cells

$$\Sigma_{ijk} = [i \cdot \Delta x, (i+1) \cdot \Delta x[\times [j \cdot \Delta x, (j+1) \cdot \Delta x[\times [k \cdot \Delta x, (k+1) \cdot \Delta x[$$

for $i, j \in \mathbb{Z}$, $k \in \mathbb{N}_0$ and small Δx. For a given $\overline{\clubsuit}$, the local light incidence $\overline{L}_{ijk}$ in Σ_{ijk} in the case of vertical radiation, i.e. (4), reads

$$\overline{L}_{ijk} = \text{PAR} \cdot \exp\left(-\lambda \cdot \sum_{\kappa \geq k} \overline{\clubsuit}_{ij\kappa} \cdot \Delta x\right).$$

The general case of light incidence from an arbitrary direction $v \in S^2_+$ is conceptually similar and only technically more extensive: For a given v, the sum in the above exponential term ranges over all cells $\Sigma_{i'j'k'}$ whose intersection with the line through the centre of Σ_{ijk} and pointing in the direction v is non-empty. Δx is replaced by the length of this intersection (which is at most $\sqrt{3} \cdot \Delta x$), and λ is adjusted depending on v as detailed in section 3.1. In this case, the potential interception of radiation by competitors before it reaches the simulated tree is accounted for by means of periodic boundary conditions. Based on a given total light incidence, cell-specific biomass production is computed straightforwardly.

Numerically, the flux vector field $J = \clubsuit \cdot \nabla_x L$ used in the continuous-time models of section 5 (cf. (35) and (39)) is defined at the faces of the grid cells, namely

$$\begin{aligned}
\overline{\phi}^{(1)}_{ijk} &= \frac{\overline{\clubsuit}_{i+1jk} + \overline{\clubsuit}_{ijk}}{2} \cdot \frac{\overline{L}_{i+1jk} - \overline{L}_{ijk}}{\Delta x} \\
\overline{\phi}^{(2)}_{ijk} &= \frac{\overline{\clubsuit}_{ij+1k} + \overline{\clubsuit}_{ijk}}{2} \cdot \frac{\overline{L}_{ij+1k} - \overline{L}_{ijk}}{\Delta x} \\
\overline{\phi}^{(3)}_{ijk} &= \frac{\overline{\clubsuit}_{ijk+1} + \overline{\clubsuit}_{ijk}}{2} \cdot \frac{\overline{L}_{ijk+1} - \overline{L}_{ijk}}{\Delta x}
\end{aligned}$$

at the borders of Σ_{ijk} and Σ_{i+1jk}, Σ_{ij+1k}, Σ_{ijk+1}, respectively. The numerical analogon of $\nabla_x \cdot J$ in (34), and similarly in(44), reads

$$\frac{\overline{\phi}^{(1)}_{ijk} - \overline{\phi}^{(1)}_{i-1jk}}{\Delta x} + \frac{\overline{\phi}^{(2)}_{ijk} - \overline{\phi}^{(2)}_{ij-1k}}{\Delta x} + \frac{\overline{\phi}^{(3)}_{ijk} - \overline{\phi}^{(3)}_{ijk-1}}{\Delta x}$$

For a given $\overline{\clubsuit}_{ijk}(t)$, the leaf density $\overline{\clubsuit}_{ijk}(t + \Delta t)$ at the next time step, with Δt small, is then inferred by means of a standard Runge Kutta scheme.

In the time-discrete case of chapter 6, we formally considered the translation of the biomass produced in a point x to the point $x + \nabla_x L(x, n)$ (analogous for the water-dependent case). In a finite volume framework, this process is accounted for as follows: Having computed the biomass $\overline{B_{ijk}}$ produced in the cell Σ_{ijk}, we assign vectors to its vertices, representing the local light gradients in these positions. These vertex-specific gradients are defined based on the gradients at the adjacent cell faces (see above). For short, we denote

$$\begin{aligned}
\frac{\Delta L_{ijk}}{\Delta x_1} &= \frac{\overline{L}_{i+1jk} - \overline{L}_{ijk}}{\Delta x} \\
\frac{\Delta L_{ijk}}{\Delta x_2} &= \frac{\overline{L}_{ij+1k} - \overline{L}_{ijk}}{\Delta x} \\
\frac{\Delta L_{ijk}}{\Delta x_3} &= \frac{\overline{L}_{ijk+1} - \overline{L}_{ijk}}{\Delta x}
\end{aligned}$$

In the following we consider the upper rear right vertex of Σ_{ijk}, i.e. $\big((i+1) \cdot \Delta x, (j+1) \cdot \Delta x, (k+1) \cdot \Delta x\big)$. The most sensible definition of the light gradient in this point is given by the average over the appropriate four adjacent difference quotients, yielding

$$\frac{1}{4} \cdot \begin{pmatrix}
\frac{\Delta L_{ijk}}{\Delta x_1} + \frac{\Delta L_{ij+1k}}{\Delta x_1} + \frac{\Delta L_{ijk+1}}{\Delta x_1} + \frac{\Delta L_{ij+1k+1}}{\Delta x_1} \\
\frac{\Delta L_{ijk}}{\Delta x_2} + \frac{\Delta L_{i+1jk}}{\Delta x_2} + \frac{\Delta L_{ij+1k}}{\Delta x_2} + \frac{\Delta L_{i+1j+1k}}{\Delta x_2} \\
\frac{\Delta L_{ijk}}{\Delta x_3} + \frac{\Delta L_{i+1jk}}{\Delta x_3} + \frac{\Delta L_{ijk+1}}{\Delta x_3} + \frac{\Delta L_{i+1jk+1}}{\Delta x_3}
\end{pmatrix} \tag{66}$$

Figure 29a illustrates this for the third entry of (66).

Translating all vertices of Σ_{ijk} by the appropriate vectors analogous to (66) results in eight points $v_{ijk}, \ldots, v_{i+1j+1k+1}$ defining a polytope

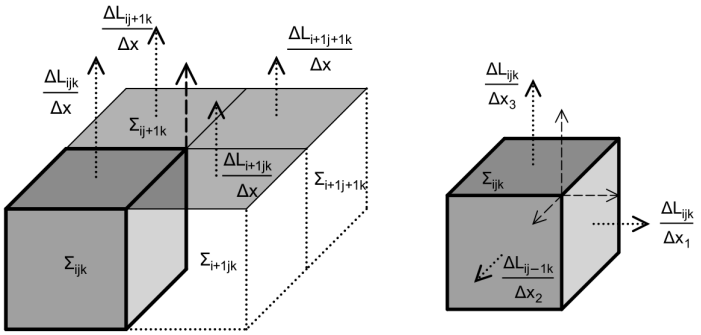

(a) (b)

Figure 29.: (a) The vertical entry of the light gradient in the upper rear right vertex of Σ_{ijk} (dashed line) is defined as the average over the those of the adjacent cells (dotted lines). (b) The three entries of the translation vector at the vertex shown correspond to the appropriate difference quotients at the three adjacent faces of Σ_{ijk}.

P_{ijk}. Let V_{ijk} denote its total , and $V_{ijk}^{i'j'k'} \in \left[0, (\Delta x)^3\right]$ the volume of its intersection with an arbitrary cell $\Sigma_{i'j'k'}$ (hence $\sum_{i',j',k'} V_{ijk}^{i'j'k'} = V_{ijk}$). Then $B_{ijk} \cdot \frac{V_{ijk}^{i'j'k'}}{V_{ijk}}$ is the amount of biomass produced in and transported from Σ_{ijk} to the cell $\Sigma_{i'j'k'}$. Hence, the numerical analogue of (49), i.e. the biomass available for allocation in an arbitrary cell Σ_{ijk}, reads

$$\overline{\mathcal{B}}_{ijk} = \sum_{i',j',k'} B_{i'j'k'} \cdot \frac{V_{i'j'k'}^{ijk}}{V_{i'j'k'}}$$

The computational bottleneck of this procedure is the determination of the intersection volumes $V_{ijk}^{i'j'k'}$, which can be complex polytopes. A considerably faster way consists of defining the three entries of the vertex-specific light gradient as the appropriate difference quotients of the adjacent faces of the cell as illustrated in figure 29b. Hence the third entries of the gradients corresponding to the four top vertices are all equal to $\frac{L_{ijk}}{\Delta x_3}$, etc. In particular, in place of (66) we have

$$\begin{pmatrix} \frac{\Delta L_{ijk}}{\Delta x_1} \\ \frac{\Delta L_{ijk}}{\Delta x_2} \\ \frac{\Delta L_{ijk}}{\Delta x_3} \end{pmatrix} \tag{67}$$

for the gradient at the upper rear right vertex of Σ_{ijk}. This approach has the advantage that the resulting polytope is a cuboid, and hence so are the intersections with the cells $\Sigma_{i'j'k'}$, cf. figure 30, speeding up the computations of the $V_{ijk}^{i'j'k'}$ significantly. A conceptual downside of this approximation is the fact that the images of the faces shared

by adjacent cells (e.g. the top face of Σ_{ijk} and the bottom face of Σ_{ijk+1}) under the above-described translational motion are no longer necessarily the same. However, the error is negligible for sufficiently small Δx since the appropriate gradients of adjacent cells converge to one another as $\Delta x \to 0$, e.g. (67) converges to (66).

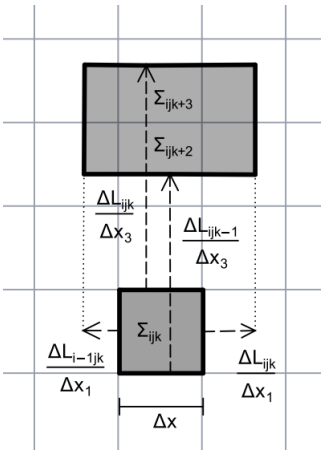

Figure 30.: Illustration of the procedure (projected onto the x_2-plane). Dashed lines indicate the different face-specific difference quotients which define the translational motion of the vertices of Σ_{ijk}.

With the exception of the algorithm presented in chapter 7, which was written in Matlab, the models in this thesis have been implemented in PYGMALION, a C++ platform offering a generic framework for the development, analysis and evaluation of dynamical plant growth models (see Cournède et al., 2013, for details). In this thesis, we used the generalized least squares method for parameter estimation as well as the standardized regression coefficients method for sensitivity analysis, which are part of PYGMALION's built-in toolbox.

BIBLIOGRAPHY

J.D. Aber. A method for estimating foliage-height profiles in broad-leaved forests. *The Journal of Ecology*, 67:35–40, 1979.

L.H. Allen. Model of light penetration into a wide-row crop. *Agronomy Journal*, 66:41–47, 1974.

M.T. Allen, P. Prusinkiewicz, and T.M. Dejong. Using L-systems for modeling source-sink interactions, architecture and physiology of growing trees, the L-peach model. *New Phytologist*, 166:869–880, 2005.

B. Andrieu, J.M. Allirand, and K.W. Jaggard. Ground cover and leaf area index of maize and sugar beet crops. *Agronomie*, 17:315–321, 1997.

P. Balandier, A. Lacointe, X. Le Roux, H. Sinoquet, P. Cruiziat, and S. Le Dizs. Simwal: A structural-functional model simulating single walnut tree growth in response to climate and pruning. *Annals of Forest Science*, 57:571–585, 2000.

D.D. Baldocchi, J.J. Finnigan, K.W. Wilson, Paw. K.T., and E. Falge. On measuring net ecosystem carbon exchange in complex terrain over tall vegetation. *Boundary Layer Meteorology*, 96:257–291, 2000.

V.C. Jr. Baldwin, K.D. Peterson, H.E. Burkhart, R.L. Amateis, and P.M. Dougherty. Equations for estimating loblolly pine branch and foliage weight and surface area distributions. *Canadian Journal of Forest Research*, 27:918–927, 1997.

C.L. Ballaré. Light gaps: Sensing the light opportunities in highly dynamic canopy environments. In *Exploitation of Environmental Heterogeneity by Plants*. Academic Press, 1994.

M. Barna. Adaptation of European beech (Fagus sylvatica L.) to different ecological conditions: leaf size variation. *Polish Journal of Ecology*, 52:35–45, 2004.

H.H. Bartelink. Allometric relationships for biomass and leaf area of beech (Fagus sylvatica L). *Annals of Forest Science*, 54:39–50, 1997.

H.H. Bartelink, K. Kramer, and G.M.J. Morhen. Applicability of the radiation-use efficiency concept for simulating growth of forest stands. *Agricultural and Forest Meteorology*, 88:169–179, 1997.

D. Barthélémy and Y. Caraglio. Plant architecture: a dynamic, multilevel and comprehensive approach to plant form, structure and ontogeny. *Annals of Botany*, 99:375–407, 2007.

D. Bayer, S. Seifert, and H. Pretzsch. Structural crown properties of Norway spruce (Picea abies [L.] Karst.) and European beech (Fagus sylvatica [L.]) in mixed versus pure stands revealed by terrestrial laser scanning. *Trees*, 27:1035–1047, 2013.

P. Becker, R.J. Gribben, and C.M. Lim. Tapered conduits can buffer hydraulic conductance from path-length effects. *Tree Physiology*, 20: 965–967, 2000.

R. Beyer, V. Letort, and P.-H. Cournède. Modeling Tree Crown Dynamics with 3D Partial Differential Equations. *Frontiers in Plant Science*, 5:329, 2014.

R. Beyer, O. Etard, P.-H. Cournède, and P. Laurent-Gengoux. Modeling spatial competition for light in plant populations with the porous medium equation. *Journal of Mathematical Biology*, 70:533–547, 2015a.

R. Beyer, V. Letort, D. Bayer, H. Pretzsch, and P.-H. Cournède. Spatial leaf density-based modeling of phototropic crown dynamics and application to European Beech. *submitted*, 2015b.

R. Borchert and N. Slade. Bifurcation ratios and the adaptative geometry of trees. *Botanical Gazette*, 142:394–401, 1981.

H. Bossel. TREEDYN3 forest simulation model. *Ecological Modelling*, 90:187–227, 1996.

O. Bouriaud, K. Soudani, and N. Bréda. Leaf area index from litter collection: impact of specific leaf area variability within a beech stand. *Canadian Journal of Remote Sensing*, 29:371–380, 2003.

O. Bouriaud, , N. Bréda, G. Le Moguédec, and G. Nepveu. Modelling variability of wood density in beech as affected by ring age, radial growth and climate. *Trees*, 18:264–276, 2004.

N.J.J. Bréda. Ground-based measurements of leaf area index: a review of methods, instruments and current controversies. *Journal of Experimental Botany*, 54:2403–2417, 2003.

N. Brisson, F. Bussiere, H. Ozier-Lafontaine, R. Tournebize, and H. Sinoquet. Adaptation of the crop model STICS to intercropping. Theoretical basis and parameterisation. *Agronomie*, 24:409–421, 2004.

R. Brouwer. Distribution of dry matter in the plant. *Netherlands Journal of Agricultural Science*, 10:361–376, 1962.

T.N. Buckley, K.A. Mott, and G.D. Farquhar. A hydromechanical and biochemical model of stomatal conductance. *Plant, Cell & Environment*, 26:1767–1785, 2003.

H. Bugmann. A review of forest gap models. *Climatic Change*, 51: 259–305, 2001.

H.E. Burkhart and M. Tomé. *Modeling Forest Trees and Stands*. Springer, 2012.

M.G.R. Canell and R.C. Dewar. Carbon allocation in trees: a review of concepts for modeling. In *Advances in ecological research*, volume 25. Academic Press, 1994.

R.S. Cantrell. *Spatial Ecology via Reaction-Diffusion Equations*. Wiley, 2013.

A. Cescatti. Modelling the radiative transfer in discontinuous canopies of asymmetric crowns. I. Model structure and algorithms. *Ecological Modelling*, 101:263–274, 1997.

J. Chason, D. Baldocchi, and M. Hutson. A comparison of direct and indirect methods for estimating forest leaf area. *Agricultural and Forest Meteorology.*, 57:107–112, 1991.

Y. Chen and P.-H. Cournède. Data assimilation to reduce uncertainty of crop model prediction with convolution particle filtering. *Ecological Modelling*, 290:165–177, 2014.

H. Cochard, D. Lemoine, and E. Dreyer. The effects of acclimation to sunlight on the xylem vulnerability to embolism in Fagus sylvatica L. *Plant, Cell & Environment*, 1999:101–108, 2000.

S. Cohen and M. Fuchs. The distribution of leaf area, radiation, photosynthesis and transpiration in a Shamouti Orange hedgerow orchard 1. Leaf area and radiation. *Agricultural and Forest Meteorology*, 40:123–144, 1987.

L. Coll, P. Balandier, and C. Picon-Cochard. Morphological and physiological responses of beech (Fagus sylvatica) seedlings to grass-induced belowground competition. *Tree Physiology*, 24:45–54, 2004.

C.F. Cooper. Pattern in ponderosa pine forests. *Ecology*, 42:493499, 1961.

P.-H. Cournède, M.Z. Kang, A. Mathieu, J.-F. Barczi, H.P. Yan, B.G. Hu, and P. de Reffye. Structural factorization of plants to compute their functional and architectural growth. *Simulation*, 82:427–438, 2006.

P.-H. Cournède, A. Mathieu, F. Houllier, D. Barthélémy, and P. de Reffye. Computing competition for light in the GreenLab model of plant growth: a contribution to the study of the effects

of density on resource acquisition and architectural development. *Annals of Botany*, 101:1207–1219, 2008.

P.-H. Cournède, Y. Chen, Q. Wu, C. Baey, and B. Bayol. Development and Evaluation of Plant Growth Models: Methodology and Implementation in the PYGMALION platform. *Mathematical Modelling of Natural Phenomena*, 8:112–130, 2013.

I.R. Cowan. Stomatal behaviour and environment. *Advances in Botanical Research*, 4:117–228, 1977.

I.R. Cowan and G.D. Farquhar. Stomatal function in relation to leaf metabolism and environment: stomatal function in the regulation of gas exchange. In D.H. Jennings, editor, *Integration of Activity in the Higher Plant*. Cambridge University Press, 1977.

P. Cruiziat, H. Cochard, and T. Amégio. Hydraulic architecture of trees: main concepts and results. *Annals of Forest Science*, 59:723–752, 2002.

G. Damour, T. Simonneau, H. Cochard, and L. Urban. An overview of models of stomatal conductance at the leaf level. *Plant, Cell & Environment*, 33:1419–1438, 2010.

J. Dauzat. Simulated plants and radiative transfer simulations. In *Crop Structure and Light Microclimate. Characterization and Applications*. INRA, 1993.

A. Davidson, D. Da Silva, B. Quintana, and T.M. DeJong. The phyllochron of Prunus persica shoots is relatively constant under controlled growth conditions but seasonally increases in the field in ways unrelated to patterns of temperature or radiation. *Scientia Horticulturae*, 184:106–113, 2015.

R.L. Davidson. Effect of root/leaf temperature differentials on root/shoot ratios in some pasture grasses and clover. *Annals of Botany*, 3:561–569, 1969.

P. de Reffye, C. Edelin, J. Françon, M. Jaeger, and C. Puech. *Plant models faithful to botanical structure and development*, volume 22. ACM, 1988.

P. de Reffye, T. Fourcaud, F. Blaise, D. Barthélémy, and F. Houllier. A functional model of tree growth and tree architecture. *Silva Fennica*, 31:297–311, 1997.

R.C. Dewar. Maximum entropy production and plant optimization theories. *Philosophical Transactions of the Royal Society B: Biological Sciences*, 365:1429–1435, 2010.

R.C. Dewar, O. Franklin, A. Mäkelä, R.E. McMurtrie, and H.T. Valentine. Optimal function explains forest responses to global change. *BioScience*, 59:127–139, 2008.

J. Dieler and H. Pretzsch. Morphological plasticity of European beech (Fagus sylvatica L.) in pure and mixed-species stands. *Forest Ecology and Management*, 295:97–108, 2013.

E. Dufrêne and N. Bréda. Estimation of deciduous forest leaf area index using direct and indirect methods. *Oecologia*, 104:156–162, 1995.

L. Dupuy, T. Fourcaud, A. Stokes, and F. Danjon. A density-based approach for the modelling of root architecture: application to Maritime pine (Pinus pinaster Ait.) root systems. *Journal of Theoretical Biology*, 236:323–334, 2005.

L. Dupuy, P.J. Gregory, and A.G. Bengough. Root growth models: towards a new generation of continuous approaches. *Journal of Experimental Botany*, 61:2131–2143, 2010.

A. El Hamidi, M. Garbeyb, and N. Alia. A PDE model of clonal plant competition with nonlinear diffusion. *Ecological Modelling*, 234:83–92, 2008.

H. Ellenberg. *Vegetation Mitteleuropas mit den Alpen in kologischer, dynamischer und historischer Sicht*. Ulmer, 1996.

B.J. Enquist. Quarter-power allometric scaling in vascular plants: functional basis and ecological consequences. In J.H. Brown and G.B. West, editors, *Scaling in Biology*. Oxford University Press, 2000.

K.D. Farnsworth and K.J. Niklas. Theories of optimization, form and function in branching architecture in plants. *Functional Ecology*, 9: 355–363, 1995.

G.D. Farquhar, S. von Caemmerer, and J.A. Berry. Models of photosynthesis. *Plant Physiology*, 125:42–45, 2001.

K.S. Fassnacht, S.T. Gower, J.M. Norman, and R.E. McMurtrie. A comparison of optical and direct methods for estimating foliage surface area index in forests. *Agricultural and Forest Meteorology*, 71: 183–207, 1994.

S. Fatichi, S. Leuzinger, and C. Koerner. Moving beyond photosynthesis: from carbon source to sink-driven vegetation modeling. *New Phytologist*, 201:1086–1095, 2014.

J.B. Fisher. How predictive are computer simulations of tree architecture? *International Journal of Plant Sciences*, 3:137–146, 1992.

S. Fleck. *Integrated analysis of relationships between 3D-structure, leaf photosynthesis, and branch transpiration of mature Fagus sylvatica and Quercus petraea trees in a mixed forest stand*. PhD thesis, Universität Bayreuth, 2001.

E. D. Ford. Competition and stand structure in some evenaged plant monocultures. *J . Ecol.*, 63:311–333, 1975.

O. Franklin, J. Johansson, R.C. Dewar, U. Dieckmann, R.E. McMurtrie, Å. Brännström, and R. Dybzinski. Modeling carbon allocation in trees: a search for principles. *Tree Physiology*, 2012. doi: 10.1093/treephys/tpr138.

F. Franz, H. Röhle, and F. Meyer. Wachstumsgang und Ertragsleistung der Buche. *Allgemeine Forstzeitung*, 48:262–267, 1995.

S. Fukai and R.S. Loomis. Leaf display and light environments in row-planted cotton communities. *Agricultural Meteorology*, 17:353–379, 1976.

S.C. Gao, G. Chen, Z.L. Fu, and P.X. Liu. A functional-structural model of virtual plant based on the labeling algorithm and the growth state chain. 543:2075–2083, 2014.

T.J. Givnish. Adaptation to sun vs. shade: A whole-plant perspective. *Australian Journal of Plant Physiology*, 15:63–92, 1988.

C. Godin. Representing and encoding plant architecture: A review. *Annals of Forest Science*, 57:413–438, 2000.

C. Godin and H. Sinoquet. Functional-strucutural plant modelling. *New Phytologist*, 166:705–708, 2005.

H. Gradmann. Untersuchungen über die Wasserverhältnisse des Bodens als Grundlage des Pflanzenwachstums. *Jahrbücher wissenschaftlicher Botanik*, 69:1–100, 1928.

R. Grote and H. Pretzsch. A Model for Individual Tree Development Based on Physiological Processes. *Plant Biology*, 4:167–180, 2002.

M. Guerif and C. Duke. Calibration of the SUCROS emergence and early growth module for sugar beet using optical remote sensing data assimilation. *European Journal of Agronomy*, 9:127–136, 1998.

O. Gutmann. Durchforstungsversuche in Fichtenbeständen. *Mitteilungen der Staatlichen Forstverwaltung Bayerns*, 17:1–92, 1926.

F. Hallé, R.A.A. Oldeman, and P.B. Tomlinson. *Tropical trees and forests, An architectural analysis*. Springer-Verlag, New York, 1978.

J. Hanan and P. Prusinkiewicz. Foreword: studying plants with functional-structural models. *Functional Plant Biology*, 35:i–iii, 2008.

M. Hauhs, A. Kastner-Maresch, and K. Rost-Siebert. A model relating forest growth to ecosystem-scale budgets of energy and nutrients. *Ecological Modelling*, 83:229–243, 1995.

R. Hemmerling, O. Kniemeyer, D. Lanwert, G. Buck-Sorlin, and W. Kurth. The rule based language xl and the modeling environment gro imp illustrated with simulated tree competition. *Functional Plant Biology*, 35:739–750, 2008.

R. Hentschel, S. Bittner, M. Janott, C. Biernath, J. Holst, J.P. Ferrio, A. Gessler, and E. Priesack. Simulation of stand transpiration based on a xylem water flow model for individual trees. *Agricultural and Forest Meteorology*, 182:31–42, 2013.

T. Higashide. Light interception by tomato plants (solanum lycopersicum) grown on a sloped field. *Agricultural and Forest Meteoreology*, 149:756–762, 2009.

D. Hodáňová. Structure and development of sugar beet canopy. I. Leaf angle relations. *Photosynthetica*, (6):401–409, 1972.

Preuten T. Hohm, T. and and C. Fankhauser. Phototropism: translating light into directional growth. *Americal Journal of Botany*, 100, 2013.

D.Y. Hollinger. Canopy organization and foliage photosynthetic capacity in a broad-leaved evergreen montane forest. *Functional Ecology*, 3:53–62, 1989.

H. Honda. Description of the form of trees by the parameters of tree-like body: Effects of the branching angle and the branche length on the shape of the tree-like body. *Journal of Theoretical Biology*, 31: 331–338, 1971.

H. Honda, P.B. Tomlinson, and J.B. Fisher. Two geometrical models of branching of botanical trees. *Annals of Botany*, 49:1–11, 1982.

T. Horie. Vertical distribution of photosynthetic intensity within a sunflower community. In *Photosynthesis and utilization of solar energy. Level III. Experiments*, pages 85–90. Jap. nat. Subcomm. for PP (JPP), 1969.

R. Horn, G.W. Brümmer, E. Kandeler, I. Kögel-Knabner, R. Kretzschmar, K. Stahr, and B.-M. Wilke. *Scheffer/Schachtschabel: Lehrbuch der bodenkunde*. Springer, 2010.

T.A. Howell and J.T. Musick. Relationship of dry matter production of field crops to water. In Riou C. Perrier, A., editor, *Les besoins en eau des cultures, Paris*. INRA, 1984.

R.M. Hubbard, B.J. Bond, and M.G. Ryan. Evidence that hydraulic conductance limits photosynthesis in old pinus ponderosa trees. *Tree Physiology*, 19:165–172, 1999.

M. Iino. Phototropism: mechanisms and ecological implications. *Plant, Cell & Environment*, 13:633–650, 1990.

J.D. Ingle Jr and S.R. Crouch. Spectrochemical analysis. 1988.

IPCC. *Special report on land use, land use change, and forestry*. Cambridge University Press, 2000.

IPCC. *IPCC WGI fourth assessment report to climate change: the physical science basis; summary for policymakers*. IPCC Secretariat, 2007.

P.G. Jarvis. The interpretation of the variations in leaf water potential and stomatal conductance found in canopies in the field. *Philosophical Transactions of the Royal Society of London. Series B*, 273:593–610, 1976.

M. Jerez, T.J. Dean, Q.V. Cao, and S.D. Roberts. Describing leaf area distribution in loblolly pine trees with Johnsons Sb function. *Forest Science*, 51:93–101, 2005.

R. Kato, Y. Tadaki, and H. Ogawa. Plant biomass and growth increment studies in Pasoh Forest. *Malayan Nature Journal*, 30:211–224, 1978.

S. Kellomäki and H. Strandman. A model for the structural growth of young scots pine crowns based on light interception by shoots. *Ecological Modelling*, 80:237–250, 1995.

N.C. Kenkel. Pattern of self-thinning in jack pine: testing the random mortality hypothesis. *Ecology*, 69:10171024, 1988.

R. Kennel. *Die Buchendurchforstungsversuche in Bayern von 1870 bis 1970*. Forstliche Forschungsanstalt München, 1972.

K. Kikuzawa and K. Umeki. Effect of Canopy Structure on Degree of Asymmetry of Competition in Two Forest Stands in Northern Japan. *Annals of Botany*, 77:565–571, 1996.

D. King. The adaptive significance of tree height. *The American Naturalist*, 135:809–828, 1990.

M. Kleunen and M. Fischer. Constraints on the evolution of adaptive phenotypic plasticity in plants. *New Phytologist*, 166:49–66, 2005.

J. Krahl-Urban. Buchen-Nachkommenschaften. *Allgemeine Forst- und Jagdzeitung*, 133:29–38, 1962.

H. Kratzer. Die schönste Buche der Welt ist tot. *Süddeutsche Zeitung*, 3.11.2013, 2013.

T. Kubo and T. Kohyama. Abies population dynamics simulated using a functional-structural tree model. In *Forest Ecosystems and Environments*, pages 15–29. 2005.

W. Kurth. Morphological models of plant growth: Possibilities and ecological relevance. *Ecological Modelling*, 75:299–308, 1994.

W. Kurth. Some new formalisms for modelling the interactions between plant architecture, competition and carbon allocation. In *4th workshop on individual-based structural and functional models in ecology*. Bayreuther Forum Ökologie, 1996.

W. Kurth and B. Sloboda. Growth grammars simulating trees-an extension of L-systems incorporating local variables and sensitivity. *Silva Fennica*, 31:285–295, 1997.

R. Küssner and R. Mosandl. Comparison of direct and indirect estimation of leaf area index in mature Norway spruce stands of eastern Germany. *Canadian Journal of Forest Research*, 30:440–447, 2000.

J. Kvet and J.K. Marshall. Assesment of leaf area and other assimilating plant surfaces. In Z. Sestak, J. Catsky, and P.G. Jarvis, editors, *Plant photosynthetic production*. Dr Junk, 1971.

A. Lacointe. Carbon allocation among tree organs : A review of basic processes and representation in functional-structural models. *Annals of Forest Sciences*, 57:521–533, 2000.

C.T. Lai, G. Katul, D. Ellsworth, and R. Oren. Modelling vegetationatmosphere CO2 exchange by a coupled EulerianLagrangian approach. *Boundary-Layer Meteorology*, 95:91–122, 2000.

J.J. Landsberg. *Physiological Ecology of Forest Production*. Academic Press, 1986.

J.J. Landsberg and S.T. Gower. *Applications of Physiological Ecology to Forest Management*. Academic Press, 1997.

R.L. Lanner. On the intensitivity of height growth to spacing. *Forest Ecology and Management*, 13:143–148, 1985.

B. Law, F.M. Kelliher, D.D. Baldocchi, P.M. Anthoni, J. Irvine, D. Moore, and S. Van Tuyl. Spatial and temporal variation in respiration in a young ponderosa pine forest during a summer drought. *Agricultural and Forest Meteorology*, 110:27–43, 2001.

X. Le Roux, A. Lacointe, A. Escobar-Gutirrez, and S. Le Dizs. Carbon-based models of individual tree growth: A critical appraisal. *Annals of Forest Sciences*, 58:469–506, 2001.

E.G. Leigh. The golden section and spiral leaf-arrangement. *Transactions of the Connecticut Academy of Arts and Sciences*, 44:163–176, 1972.

S. Lemaire, F. Maupas, P.-H. Cournède, J.-M. Allirand, P. de Reffye, and B. Ney. Analysis of the density effects on the source-sink dynamics in Sugar-Beet growth. In B.-G. Li, M. Jaeger, and Y. Guo, editors, *3rd international symposium on Plant Growth and Applications (PMA09)*. IEEE Computer Society, 2009.

D. Lemoine, H. Cochard, and A. Granier. Within crown variation in hydraulic architecture in beech (Fagus sylvatica L): evidence for a stomatal control of xylem embolism. *Annals of Forest Sciences*, 59: 19–27, 2002.

L.B. Leopold. Trees and Streams: The Efficiency of Branching Patterns. *Journal of Theoretical Biology*, 31:339–354, 1971.

V. Letort, P.-H. Cournède, A. Mathieu, P. de Reffye, and T. Constant. Parametric identification of a functional-structural tree growth model and application to beech trees (Fagus sylvatica). *Functional Plant Biology*, 35:1243–1254, 2008.

A. Lindenmayer. Mathematical models for cellular interactions in development I. Filaments with one-sided inputs. *Journal of Theoretical Biology*, 18:280–299, 1968a.

A. Lindenmayer. Mathematical models for cellular interactions in development II. Simple and Branching Filaments with Two-sided Inputs. *Journal of Theoretical Biology*, 18:300–315, 1968b.

A. Lintunen, R. Sievänen, P. Kaitaniemi, and J. Perttunen. Corrigendum: Models of 3D crown structure for Scots pine (Pinus sylvestris) and silver birch (Betula pendula) grown in mixed forest. *Canadian Journal of Forest Research*, 42:2153–2153, 2012.

M. Lu, P. Nygren, J. Perttunen, S.G. Pallardy, and D.R. Larsen. Application of the functional-structural tree model LIGNUM to growth simulation of short-rotation eastern cottonwood. *Silva Fennica*, 45: 431–474, 2011.

Y. Ma, M.P. Wen, Y. Guo, B.G. Li, P.-H. Cournède, and P. de Reffye. Parameter optimization and field validation of the functional-structural model GreenLab for maize at different population densities. *Annals of Botany*, 101, 2008.

R.H. MacArthur and H.S. Horn. Foliage profile by vertical measurements. *Ecology*, 50:802–804, 1969.

C. MacFarlane, D.A. White, and M.A. Adams. The apparent feedforward response to vapour pressure deficit of stomata in droughted, field-grown Eucalyptus globulus Labill. *Plant, Cell & Environment*, 27:1268–1280, 2004.

D.A. Maguire and W.S. Bennett. Patterns in vertical distribution of foliage in young coastal douglas-fir. *Canadian Journal of Forest Research*, 26:1991–2005, 1996.

A. Mäkelä. Implications of the pipe model theory on dry matter partitioning and height growth in trees. *Journal of Theoretical Biology*, 123:103–120, 1986.

A. Mäkelä and P. Vanninen. Impacts of size and competition on tree form and distribution of aboveground biomass in Scots pine. *Canadian Journal of Forest Research*, 28:216–227, 1998.

A. Mäkelä, T.J. Givnish, F. Berninger, T.N. Buckley, G.D. Farquhar, and P. Hari. Challenges and opportunities of the optimality approach in plant ecology. *Silva Fennica*, 36:605–614, 2002.

B.B. Mandelbrot. *The fractal geometry of nature*. Macmillan, 1983.

L.F.M. Marcelis. A simulation model for dry matter partitioning in cucumber. *Annals of botany*, 74(1):43–52, 1994.

L.F.M. Marcelis, E. Heuvelink, and J. Goudriaan. Modelling of biomass production and yield of horticultural crops: a review. *Scientia Horticulturae*, 74:83–111, 1998.

M.J. Mariscal, S.N. Martens, S.L. Ustin, J. Chen, S.B. Weiss, and D.A. Roberts. Light-transmission profiles in an old-growth forest canopy: simulations of photosynthetically active radiation by using spatially explicit radiative transfer models. *Ecosystems*, 7(5):454–467, 2004.

A. Mathieu, P.-H. Cournde, D. Barthlmy, and P. de Reffye. Rhythms and alternating patterns in plants as emergent properties of a model of interaction between development and functioning. *Annals of Botany*, 101(8), 2008.

A. Mathieu, P.-H. Cournède, V. Letort, D. Barthlmy, and P. de Reffye. A dynamic model of plant growth with interactions between development and functional mechanisms to study plant structural plasticity related to trophic competition. *Annals of Botany*, 103:1173–1186, 2009.

J.C. Mawson, J.W. Thomas, , and R.M. DeGraaf. Program HTVOL: the determination of tree crown volume by layers. Technical report, Upper Darby, PA: U.S. Department of Agriculture, Forest Service, Northeastern Forest Experiment Station, 1976. Res. Pap. NE-354.

R.E. McMurtrie and R.C. Dewar. New insights into carbon allocation by trees from the hypothesis that annual wood production is maximized. *New Phytologist*, 199:981990, 2013.

A.L.C. McWilliam, J.M. Roberts, O.M.R. Cabral, M.V.B.R. Leitao, A.C.L. de Costa, G.T. Maitelli, and C.A.G.P. Zamparoni. Leaf area index

and above-ground biomass of terra firme rain forest and adjacent clearings in amazonia. *Functional Ecology*, 7:310–317, 1993.

R. Mech and P. Prusinkiewicz. Visual models of plant interacting with their environment. In *Computer Graphics proceedings, Annual Conference Series, SIGGRAPH 96*, 1996.

B.E. Medlyn. Physiological basis of the light use efficiency model. *Tree Physiology*, 18:167–176, 1998.

I.C. Meier and C. Leuschner. Leaf size and leaf area index in Fagus sylvatica forests: competing effects of precipitation, temperature, and nitrogen availability. *Ecosystems*, 11:655–669, 2008.

P. Meir, J. Grace, and A.C. Miranda. Photographic method to measure the vertical distribution of leaf area density in forests. *Agricultural and Forest Meteorology*, 102:105–111, 2000.

M. Mencuccini and J. Grace. Climate influences the leaf area/sapwood area ratio in Scots pine. *Tree Physiology*, 15:1–10, 1995.

L. Misson, J.A. Panek, and A.H. Goldstein. A comparison of three approaches to modeling leaf gas exchange in annually drought-stressed ponderosa pine forest. *Tree Physiology*, 24:529–541, 2004.

K. Mokany, R.E. McMurtrie, B.J. Atwell, and H. Keith. Interaction between sapwood and foliage area in alpine ash (eucalyptus delegatensis) trees of different heights. *Tree Physiology*, 23:949–958, 2003.

J. Monod. *Chance and necessity*. Collins Fontana Books, 1972.

M. Monsi and T. Saeki. On the factor light in plant communities and its importance for matter production. *Annals Of Botany*, 95:549–567 (originally published in German in 1953 in: *Japanese Journal of Botany* 14:22–52), 2005.

J.L. Monteith. Solar radiation and productivity in tropical ecosystems. *Journal of Applied Ecology*, 2:747766, 1972.

J.L. Monteith. Climate and the efficiency of crop production in Britian. *Proceedings of the Royal Society of London B*, 281:277–294, 1977.

J.L. Monteith. A reinterpretation of stomatal responses to humidity. *Plant, Cell & Environment*, 22:567–582, 1995.

P. Moon and D.E. Spencer. Illumination from a non-uniform sky. *Illuminating Engineering*, 37:707–726, 1942.

S. Mori, , and A Hagihara. Crown profile of foliage area characterized with the Weibull distribution in a hinoki (Chamaecyparis obtusa) stand. *Trees*, 5:149–152, 1991.

K.A. Mott. Do stomata respond to CO2 concentrations other than intercellular? *Plant Physiology*, 88:200–203, 1988.

R.B. Myneni, G. Asrar, Z.T. Kanemasu, D.J. Lawlor, and I. Impens. Canopy architecture, irradiance distribution on leaf surfaces and consequent photosynthetic efficiences in heterogeneous plant canopies. l. theoretical considerations. *Agricultural and Forest Meteorology*, 37: 189–204, 1986.

S. Najla, G. Vercambre, L. Pagès, D. Grasselly, H. Gautier, and M. Génard. Tomato plant architecture as affected by salinity: descriptive analysis and integration in a 3-D simulation model. *Botany*, 87:893–904, 2009.

A.S. Nelson, A.R. Weiskitte, and R.G. Wagner. Development of branch, crown, and vertical distribution leaf area models for contrasting hardwood species in maine, usa. *Trees*, 28:17–30, 2014.

B. Neubert, T. Franken, and O. Deussen. Approximate image-based tree-modeling using particle flows. *ACM Transactions on Graphics (TOG)*, 26:88, 2007.

E. Nikinmaa. Analysis of the growth of Scots pine; matching structure with function. *Acta Forestalia Fennica*, 235:1–68, 1992.

E. Nikinmaa, R. Sievänen, and T. Hölttä. Dynamics of leaf gas exchange, xylem and phloem transport, water potential and carbohydrate concentration in a realistic 3-D model tree crown. *Annals of Botany*, 114:653–666, 2014.

T. Nilson. A theoretical analysis of the frequency of gaps in plant stands. *Agricultural and Forest Meteorology*, 8:25–38, 1971.

R.J. Norby, K. Ogle, P.S. Curtis, F.-W. Badeck, A. Huth, G.C. Hurtt, T. Kohyama, and J. Peñuelas. Aboveground growth and competition in forest gap models: an analysis for studies of climatic change. *Climatic Change*, 51:415–447, 2001.

A. Okubo and S.A. Levin. *Diffusion and Ecological Problems, Modern Perspectives*. Springer, 2002.

S. Oohata and T. Shidei. Studies of the branching structure of trees. 1. Bifurcation ratio of trees in Horton's law. *Japanese Journal of Ecology*, 21:7–14, 1971.

S. Oohata and K. Shinozaki. A statistical model of plant form-further analysis of the pipe model theory. *Jap. J. Ecol*, 29:323–35, 1979.

R. Oren, J.S. Sperry, G.G. Katul, D.E. Pataki, F.W. Ewers, N. Phillips, and K.V.R. Schäfer. Survey and synthesis of intra- and interspecific variation in stomatal sensitivity to vapour pressure deficit. *Plant, Cell & Environment*, 22:1515–1526, 1999.

M.W. Palmer. Fractal geometry: a tool for describing spatial patterns of plant communities. *Vegetatio*, 75:91–102, 1988.

S. Patino, M.T. Tyree, and E.A. Herre. A comparison of the hydraulic architecture of woody plants of differing phylogeny and growth form with special reference to free-standing and hemiepiphytic Ficus species from Panama. *New Phytologist*, 129:125–134, 1995.

J. Perttunen, R. Sievänen, E. Nikinmaa, H. Salminen, H. Saarenmaa, and J. Väkevä. LIGNUM: a tree model based on simple structural units. *Annals of Botany*, 77:87–98, 1996.

J. Perttunen, R. Sievänen, and E. Nikinmaa. LIGNUM: a model combining the structure and the functioning of trees. *Ecological Modelling*, 108:189–198, 1998.

R. Peters. Growth and form: Beech versus other dominant tree species. *Geobotany*, 24:58–88, 1997.

G. Petit and T. Anfodillo. Plant physiology in theory and practice: an analysis of the WBE model for vascular plants. *Journal of Theoretical Biology*, 259:1–4, 2009.

M. Pierre. Global Existence in Reaction-Diffusion Systems with Control of Mass: a Survey. *Milan Journal of Mathematics*, 78:417–455, 2010.

A. Porté, A. Bosc, I. Chamption, and D. Loustau. Estimating the foliage area of Maritime pine (Pinus pinaster A it.) branches and crowns with application to modelling the foliage area distribution in the crown. *Annals of Forest Science*, 57:73–86, 2000.

I.C. Prentice, M.T. Sykes, and W. Cramer. A simulation model for the transient effects of climate change on forest landscapes. *Ecological Modelling*, 65:51–70, 1993.

R. Preßler. *Das Gesetz des Stammbildung*. Arnoldische Buchhandlung, 1865.

H. Pretzsch. Species-specific allometric scaling under self-thinning. Evidence from long-tern plots in forest stands. *Oecologia*, 146:572–583, 2006.

H. Pretzsch. *Forest Dynamics, Growth and Yield*. Springer, 2009.

H. Pretzsch. Re-Evaluation of Allometry: State-of-the-Art and Perspective Regarding Individuals and Stands of Woody Plants. *Progress in Botany*, 71:339–369, 2010.

H. Pretzsch. Canopy space filling and tree crown morphology in mixed-species stands compared with monocultures. *Forest Ecology and Management*, 327:251–264, 2014.

H. Pretzsch and J. Dieler. Evidence of variant intra- and interspecific scaling of tree crown structure and relevance for allometric theory. *Oecologia*, 169:637–649, 2012.

H. Pretzsch, H. Röhle, and W. Foerster. Exkursionsführer Buchen-Durchforstungsversuch Fabrikschleichach 015. Technical report, LMU München, 1994. MWW-EF 35-6.

H. Pretzsch, P. Biber, J. Dursky, and R. Sodtke. The individual-tree-based stand simulator SILVA. In *Sustainable Forest Management*. Springer, 2006.

Seifert S. Huang P. Pretzsch, H. Beitrag des terrestrischen Laserscannings zur Erfassung der Struktur von Baumkronen. *Schweizerische Zeitschrift fr Forstwesen*, 162:186–194, 2011.

P. Prusinkiewicz and A. Lindenmayer. *The Algorithmic Beauty of Plants*. Springer, 1990.

H. Qu and Y. Wang. A self-assembling approach to simulation of phototropism. *International Journal of Digital Content Technology and its Applications*, 5:55–62, 2011.

D.C. Rapaport. *The art of molecular dynamics simulation*. Cambridge university press, 2004.

H.M. Rauscher, J.G. Isebrands, G.E. Host, R.E. Dickson, Dickmann D.I., Crow T.R., and Michael D.A. ECOPHYS: An ecophysiological growth process model for juvenile poplar. *Tree Physiology*, 7:255–281, June 1990.

V.R. Reddy and Y.A. Pachepsky. Testing a Convective-dispersive Model of Two-dimensional Root Growth and Proliferation in a Greenhouse Experiment with Maize Plants. *Annals of Botany*, 87:759–768, 2001.

J.P. Richter. *The Notebooks of Leonardo da Vinci, vol. 1*. New Yorker (unabridged edition of the work originally published in London in 1883), 1970.

J.N. Ridley. Packing efficiency in sunower heads. *Mathematical Biosciences*, 58:129–139, 1982.

A. Roloff. *Baumkronen. Verständnis und praktische Bedeutung eines komplexen Naturphänomens*. Ulmer, 2001.

P.M. Room, L. Maillette, and J.S. Hanan. Module and metamer dynamics and virtual plants. *Advances in Ecological Research*, 25:105–157, 1994.

J. Ross. *The radiation regime and architecture of plant stands*. Dr. W. Junk Publishers, 1981.

T. Rötzer, M. Leuchner, and A.J. Nunn. Simulating stand climate, phenology, and photosynthesis of a forest stand with a process-based growth model. *International Journal of Biometeorology*, 54:449–464, 2010.

A. Runions, B. Lane, and P. Prusinkiewicz. Modeling trees with a space colonization algorithm. *NPH*, 7:63–70, 2007.

M.G. Ryan and B.J. Yoder. Hydraulic Limits to Tree Height and Tree Growth. *BioScience*, 47:235–242, 1997.

M.G. Ryan, N. Phillips, and B.J. Bond. The hydraulic limitation hypothesis revisited. *Plant, Cell & Environment*, 29:367–381, 2006.

Tatsumi Sakaguchi. Botanical tree structure modeling based on real image set. In *ACM SIGGRAPH 98 Conference abstracts and applications*. ACM, 1998.

N.Z. Saliendra, J.S. Sperry, and J.P. Comstock. Influence of leaf water status on stomatal response to humidity, hydraulic conductance, and soil drought in Betula occientalis. *Planta*, 196:357–366, 1995.

S. Salleo, A. Nardini, F. Pitt, and M.A. LoGullo. Xylem cavitation and hydraulic control of stomatal conductance in laurel (Laurus nobilis L.). *Plant Cell & Environment*, 23:71–79, 2000.

S. Salleo, M.A. LoGullo, F. Raimondo, and A. Nardini. Vulnerability to cavitation of leaf minor veins: any impact on gas exchange? *Plant Cell & Environment*, 24:851–859, 2001.

V. Sarlikioti, P.H.B. de Visser, and L.F.M. Marcelis. Exploring the spatial distribution of light interception and photosynthesis of canopies by means of a functionalstructural plant model. *Annals of Botany*, 107: 875–883, 2011.

K. Shinozaki, K. Yoda, K. Hozumi, and T. Kira. A quantitative analysis of plant form - the pipe model theory I. Basic Analysis. *Japanese Journal of Ecology.*, 14:97–105, 1964.

R. Sievänen, E. Nikinmaa, P. Nygren, H. Ozier-Lafontaine, J. Perttunen, and H. Hakula. Components of a functional-structural tree model. *Annals of Forest Sciences*, 57:399–412, 2000.

R. Sievänen, J. Perttunen, E. Nikinmaa, and P. Kaitaniemi. Toward extension of a single tree functional-structural model of Scots pine to stand level: effect of the canopy of randomly distributed, identical trees on development of tree structure. *Functional Plant Biology*, 35: 964–975, 2008.

R. Sievanen, C. Godin, T.M. DeJong, and E. Nikinmaa. Functional-structural plant models: a growing paradigm for plant studies. *Annals of Botany*, 114:599–603, 2014.

H. Sinoquet and B. Andrieu. The geometrical structure of plant canopies: characterization and direct measurement methods. In C. Varlet-Grancher, R. Bonhomme, and H. Sinoquet, editors, *Crop structure and light microclimate: characterization and applications*. INRA, 1993.

H. Sinoquet, B. Moulia, and R. Bonhomme. Estimating the three-dimensional geometry of a maize crop as an input of radiation models: comparison between three-dimensional digitizing and plant profiles. *Agricultural and Forest Meteorology*, 55:233–249, 1991.

H. Sinoquet, G. Sonohat, J. Phattaralerphong, and C. Godin. Foliage randomness and light interception in 3-D digitized trees: an analysis from multiscale discretization of the canopy. *Plant, Cell & Environment*, 28:1158–1170, 2005.

A.R. Smith. Plants, fractals, and formal languages. *ACM SIGGRAPH Computer Graphics*, 18:1–10, 1984.

F.W. Smith, A.D. Sampson, and N.J. Long. Comparison of leaf area index estimates from tree allometrics and measured light interception. *Forest Science*, 37:1682–1688, 1991.

M. Sonntag. Effect of morphological plasticity on leaf area distribution, single tree, and forest stand dynamics. *Bayreuther Forum Ökologie*, 52:205–222, 1996.

K.A. Sorrensen-Cothern, E.D. Ford, and D.G. Sprugel. A model of competition incorporating plasticity through modular foliage and crown development. *Ecological Monographs*, 63:277–304, 1993.

J.S. Sperry, F.R. Adler, G.S. Campbell, and J.P. Comstock. Limitation of plant water use by rhizosphere and xylem conductance: results from a model. *Plant, Cell & Environment*, 21:347–359, 1998.

D.G. Sprugel, T.M. Hinckley, and W. Schaap. The theory and practice of branch autonomy. *Annual Review of Ecology and Systematics*, 22: 309–334, 1991.

P. Stenberg, T. Kuuluvainen, S. Kellomiki, J.C. Grace, E.J. Jokela, and H.L. Gholz. Crown structure, light interception and productivity of pine trees and stands. *Ecological Bulletins*, 43:20–34, 1994.

F.J. Sterck and F. Schieving. 3D growth patterns of trees: effects of carbon economy, meristem activity and selection. *Ecological Monographs*, 77:405–420, 2007.

F.J. Sterck, F. Schieving, A. Lemmens, and T.L. Pons. Performance of trees in forest canopies: explorations with a bottom-up functional-structural plant growth model. *New Phytologist*, 166:827–843, 2005.

J.B. Stewart. Modelling surface conductance of pine forest. *Agricultural and Forest Meteorology*, 43:19–35, 1988.

P. Stoll and B. Schmid. Plant foraging and dynamic competition between branches of Pinus sylvestris in contrasting light environments. *Journal of Ecology*, 86:934–945, 1998.

N. Strigul, D. Pristinski, D. Purves, J. Dushoff, and S. Pacala. Scaling from trees to forests: Tractable macroscopic equations for forest dynamics. *Ecological Monographs*, 78:523–545, 2008.

A. Takenaka. A simulation model of tree architecture development based on growth response to local light environment. *Journal of Plant Research*, 107:321–330, 1994.

J.H.M. Thornley and I.R. Johnson. *Plant and Crop Modeling: A Mathematical Approach to Plant and Crop Physiology*. The Blackburn Press, 2000.

J.H.M. Thornley and A.J. Parsons. Allocation of new growth between shoot, root and mycorrhiza in relation to carbon, nitrogen and phosphate supply: teleonomy with maximum growth rate. *Journal of Theoretical Biology*, 342:1–14, 2014.

E. Toro. *Riemann Solvers and Numerical Methods for Fluid Dynamic*. Springer, 2009.

A. Tuzet, A. Perrier, and R. Leuning. A coupled model of stomatal conductance, photosynthesis and transpiration. *Plant, Cell & Environment*, 26:1097–1116, 2003.

MT. Tyree. A dynamic model for water flow in a single tree: evidence that models must account for hydraulic architecture. *Tree Physiology*, 4:195–217, 1988.

M.T. Tyree and M.H. Zimmermann. *Xylem Structure and the Ascent of Sap*. Springer Series in Wood Science, 2002.

M.T. Tyree, D.A. Synderman, T.R. Wilmot, and J.L. Machado. Water relations and hydraulic architecture of a tropical tree (Schefflera morototoni). Data, models and a comparison with two temperate species (Acer saccharum and Thuja occidentalis). *Plant Physiology*, 96:1105–1113, 1991.

T. Udagawa, Z. Uchijima, T. Horie, and K. Kobayashi. Canopy structure of corn plant. In *Photosynthesis and utilization of solar energy. Level III. Experiments*, pages 20–24. Jap. nat. Subcomm. for PP (JPP), Tokyo, 1968.

H.T. Valentine. Tree-growth Models: Derivations Employing the Pipe-model Theory. *Journal of Theoretical Biology*, 117:579–585, 1985.

H.T. Valentine. A Carbon-balance Model of Stand Growth: a Derivation Employing Pipe-model Theory and the Self-thinning Rule. *Annals of Botany*, 62:389–396, 1988.

M. Van Leeuwen and M. Nieuwenhuis. Retrieval of forest structural parameters using LiDAR remote sensing. *European Journal of Forest Research*, 129:749–770, 2010.

J.L. Vazquez. *The Porous Medium equation: Mathematical Theory*. Oxford University Press, 2007.

Verein der deutschen Forstlichen Versuchsanstalten. Anleitung zur Ausführung von Durchforstungen und Lichtungsversuchen. *Allgemeine Forst- und Jagdzeitung*, page 422, 1902.

J. Vos, L.F.M. Marcelis, and J.B. Evers. Functional-structural plant modelling in crop production. In J. Vos, L.F.M. Marcelis, P.H.B. de Visser, P.C. Struik, and J.B. Evers, editors, *Functional-structural plant modelling in crop production*. Springer, 2007.

J. Vos, J.B. Evers, G.H. Buck-Sorlin, B. Andrieu, M. Chelle, and P.H.B. de Visser. Functional-structural plant modelling: a new versatile tool in crop science. *Journal of Experimental Botany*, 61:2101–2115, 2010.

J.M. Vose and W.T. Swank. Assessing seasonal leaf area dynamics and vertical leaf area distribution in eastern white pine (Pinus strobus L.) with a portable light meter. *Tree Physiology*, 7:125–134, 1990.

J.M. Vose, N.H. Sullivan, B.D. Clinton, and P.V. Bolstad. Vertical leaf area distribution, light transmittance, and application of the Beer-Lambert law in four mature hardwood stands in the southern Appalachians. *Canadian Journal of Forest Research*, 25:1036–1043, 1995.

F. Wang, V. Letort, Q. Lu, X. Bai, Y. Guo, P. de Reffye, and B. Li. A functional and structural Mongolian scots pine (Pinus sylvestris var. mongolica) model integrating architecture, biomass and effects of precipitation. *PLoS ONE*, 7:e43531, 2012.

Q. Wang, J. Tenhunen, A. Granier, O. Reichstein, M. Bouriaud, D. Nguyen, and N. Breda. Long-term variations in leaf area index and light extinction in a Fagus sylvatica stand as estimated from global radiation profiles. *Theoretical and Applied Climatology*, 79: 225–238, 2004.

W.-M. Wang, Z.-L. Li, and H.-B. Su. Comparison of leaf angle distribution functions: Effects on extinction coefficient and fraction of sunlit foliage. *Agricultural and Forest Meteorology*, 143:106–122, 2007.

Y.P. Wang and P.G. Jarvis. Description and validation of an array model MAESTRO. *Agricultural and Forest Meteorology*, 51:257–280, 1990.

Y.P. Wang, P.G. Jarvis, and M.L. Benson. Two-dimensional needle-area density distribution within the crowns of Pinus radiata. *For. Ecol. Manage.*, 32:217–237, 1990.

R.H. Waring. Estimating forest growth and efficiency in relation to canopy leaf area. *Advances in Ecological Research*, 13:327–354, 1983.

D.J. Watson. Comparative physiological studieson the growth offield crops. 1. Variation in net assimilation rate and leaf area between species and varieties, and within and between years. *Annals of Botany*, 11:41–76, 1947.

A.R. Weiskittel, J.A. Kershaw Jr, P.V. Hofmeyer, and R.S. Seymour. Species differences in total and vertical distribution of branch and tree-level leaf area for the five primary conifer species in Maine, USA. *Forest Ecology and Management*, 258:1695–1703, 2009.

G.B. West, J.H. Brown, and B.J. Enquist. A general model for the origin of allometric scaling laws in biology. *Science*, 276:122–126, 1997.

G.B. West, J.H. Brown, and B.J. Enquist. A general model for the structure and allometry of plant vascular systems. *Nature*, 400: 664–667, 1999a.

G.B. West, J.H. Brown, and B.J. Enquist. The fourth dimension of life: fractal geometry and allometric scaling of organisms. *Science*, 284: 1677–1679, 1999b.

P.W. West. Model of above-ground assimilate partitioning and growth of individual trees in even aged forest monoculture. *Journal of Theoretical Biology*, 161:369–394, 1993.

C.W. Whippo. Phototropism: Bending towards enlightenment. *The Plant Cell*, 18:1110–1119, 2006.

D. White, C. Beadle, D. Worledge, J. Honeysett, and M. Cherry. The influence of drought on the relationship between leaf and conducting sapwood area in eucalyptus globulus and eucalyptus nitens. *Trees*, 12:406–414, 1998.

D.A. White, C. Beadle, P.J. Sands, D. Worledge, and J.L. Honeysett. Quantifying the effect of cumulative water stress on stomatal conductance of Eucalyptus globulus and Eucalyptus nitens: a phenomenological approach. *Australian Journal of Plant Physiology*, 26: 17–27, 1999.

G.G. Whitney. The bifurcation ratio as an indicator of adaptive strategy in woody plant species. *Bulletin of the Torrey Botanical Club*, pages 67–72, 1976.

M. Williams, E.B. Rastetter, D.N. Fernandes, M.L. Goulden, S.C. Wofsy, G.R. Shaver, J.M. Melillo, J.W. Munger, S.M. Fan, and K.J. Nadelhoffer. Modelling the soil-plant-atmosphere continuum in a Quercus-Acer stand at Harvard forest: The regulation of stomatal conductance by light, nitrogen and soil/plant hydraulic properties. *Plant Cell & Environment*, 19:911–927, 1996.

J.B. Wilson. A review of evidence on the control of shoot:root ratio, in relation to models. *Annals of Botany*, 61:433–449, 1988.

S.C. Wong, I.R. Cowan, and G.D. Farquhar. Leaf conductance to assimilation in Eucalyptus pauciflora Sieb. ex Spreng. *Plant Physiology*, 62:670–674, 1979.

H.P. Yan, M.Z. Kang, P. De Reffye, and M. Dingkuhn. A dynamic, architectural plant model simulating resource-dependent growth. *Annals of Botany*, 93:591–602, 2004.

Y. Yang and M.T. Tyree. Hydraulic resistance in the shoots of Acer saccharum and its influence on leaf water potential and transpiration. *Tree Physiology*, 12:231–242, 1993.

Z.-P. Ye. A review on modeling of responses of photosynthesis to light and CO2. *Chinese Journal of Plant Ecology*, 34:727–740, 2010.

X. Yin and P.C. Struik. C 3 and c 4 photosynthesis models: an overview from the perspective of crop modelling. *NJAS-Wageningen Journal of Life Sciences*, 57:27–38, 2009.

B. Zeide. Fractal geometry in forestry applications. *Forest Ecology and Management*, 46:179–188, 1991.

G. Zotz, M.T. Tyree, S. Patino, and M.R. Carlton. Hydraulic architecture and water use of selected species from a lower montane forest in Panama. *Trees*, 12:302–309, 1998.